Energy-Efficient Coordination Schemes for Underwater Acoustic Sensor Networks

by

©Ruoyu Su, B. Eng., M. Eng.

A thesis submitted to the School of Graduate Studies

in partial fulfilment of the requirements for the

Degree of Doctor of Philosophy

Faculty of Engineering and Applied Science

Memorial University of Newfoundland

May 2015

St. John's Newfoundland Canada

Abstract

Underwater acoustic sensor networks (UWSNs) have attracted much research interest in recent years due to the wide range of their potential applications, such as environmental monitoring, natural resources development, and geological oceanography. While much research effort has been devoted to the improvement of acoustic signal reception and processing, the increase of throughput, and the reduction of packet delay, not really studies focus on reducing and balancing energy consumption among sensor nodes in long-term marine monitoring applications. In this dissertation, through a comprehensive understanding of underwater acoustic channels, we propose a series of solutions to achieve energy-efficient data transmission in UWSNs by considering both battery energies of sensor nodes and network connectivity.

We first review different approaches to modelling the underwater acoustic channels to obtain a comprehensive understanding of the underwater acoustic communication environment. We propose an asynchronous wake-up scheme based on combinatorial designs to minimize the working duty cycle of sensor nodes for UWSNs in long-term marine monitoring applications. Network connectivity can be maintained using such a design, even with a reduced duty cycle. We conduct simulation experiments to evaluate performance of the proposed scheme. It is shown through our results that the proposed asynchronous wake-up scheme can effectively reduce the energy consumption for idle listening and can outperform other cyclic difference set (CDS)-based wake-up schemes. It is worth noting that all these are achieved without

sacrificing the network connectivity among sensor nodes.

We investigate the deployment strategy of UWSNs with a square grid topology to balance the network robustness and the energy consumption of sensor nodes. We propose a relay node selection scheme for such network applications. We evaluate its performance in different network sizes and using different initial battery energy to balance the network lifetime. Simulation results show that the proposed relay node selection scheme can effectively balance and prolong the network lifetime. Compared to routing algorithms solely based on the minimum hops, the performance of the proposed scheme is closer to the optimal theoretical value obtained by solving the linear programming problem. The network lifetime is further increased if sensor nodes are allowed to have different initial energy values based on their traffic load conditions.

Finally, we propose an effective coordination scheme for data collection when an autonomous underwater vehicle (AUV) is used as a mobile data sink in UWSNs. We demonstrate the effectiveness of the proposed scheme when time synchronization is not available between the AUV and the sensor nodes. Based on the features available in existing acoustic modems, we introduce transmitting power control to further reduce energy consumption. Simulation results show that the proposed scheme with power control leads to lower energy consumption than without power control during underwater communication.

The proposed schemes have been demonstrated to work well for underwater networks with a square grid topology. It can be also extended for other network topologies and more sophisticated modems.

Acknowledgements

I deeply express my appreciation and respect to my supervisors Dr. Ramachandran Venkatesan and Dr. Cheng Li. Their solid academic foundation and their accurate comments have made my time at the Memorial University of Newfoundland both a pleasure and a rich learning experience. I would like to extend my acknowledgement to Dr. Vlastimil Masek, Dr. Howard M. Heys, Dr. Ralf Bachmayer, and Dr. Paul Gillard, who made effort to support me, review my thesis, and give valuable suggestions. I offer my sincere gratitude to Dr. Yuanzhu Chen, who encourages me to think and supports me in spirit. I also like to thank the School of Graduate Studies and the SEAformatics Group at the Memorial University of Newfoundland for their financial support during my Ph.D. program.

It is my great honor to know and get along with many good colleagues, including Dr. Chen Wang, Zehua Wang, Fan Jiang, Yi Zhang, and Jingwen Zhu. Thanks for their support and encouragement. I am grateful to my landlords Claude S. Quigley and Jessie M. A. Chisholm, with whom I have lived since 2012. They accommodate me with a comfortable and carefree home so that I concentrate on my work at the university. I also extend my thanks to my friends, Yue Zhang and Yu Zhou, who support me during my tough period.

Finally, I would like to mention that there is no way to fully appreciate my parents Xiaohui Su and Xiaozuo Wu for their selfless love and support. There is also no way to erase my regret not able to accompany them over the years as the only child of them. I dedicate my thesis to them.

Contents

List of Abbreviations

ALAN	Acoustic Local Area Network
BER	Bit Error Rate
CDS	Cyclic Difference Set
CTS	Clear To Send
CUMAC	Cooperative Underwater Multichannel MAC
DACAP	Distance Aware Collision Avoidance Protocol
DAG	Directed Acyclic Graph
DTN	Delay Tolerant Network
EACDS	Exponential Adaptive CDS-based protocol
FBR	Focused Beam Routing protocol
FH/FSK	Frequency-Hopping Frequency Shift Keying
KAM	Kauai AComms Multidisciplinary University Research Initiative
LCDR	Linear Coded Digraph Routing Scheme
LDPC	Low-Density Parity-Check
LP	Linear Programming

MACDS	Multiplicative Adaptive CDS-based protocol
MACE	Mobile Acoustic Communications Experiment
PL	Path Length of the AUV in the transmission range of a sensor node
QEC	Quorum-based Energy Conserving Protocol
QELAR	Q-learning-based Adaptive Routing protocol
RANO	Reservation Aloha for No Overhearing
RFID	Radio Frequency Identification
RSSI	Receive Signal Strength Indication
RTS	Request To Send
S-MAC	Sensor-MAC
S2C	Sweep-Spread Carrier
SPACE	Surface Processes and Acoustic Communications Experiment
T-Lohi	Tone-Lohi
T-MAC	Timeout-MAC
TSP	Traveling Salesperson Problem
UAN	Underwater Acoustic Network
UWAN-MAC	Underwater Wireless Acoustic Networks MAC Protocol
UWSN	Underwater Acoustics Sensor Network
VBF	Vector Based Forwarding protocol
WHOI	Woods Hole Oceanographic Institution
WSN	Wireless Sensor Networks

List of Symbols

$a(f)$	Absorption coefficient of acoustic signals
$B(\cdot)$	Benefit by adopting a given amount of sleeping time in one cycle period
$c^{(u,v)}$	Cost of (u, v)
$C(\cdot)$	Cost using a given amount of sleeping time in one cycle period
d_c	Shortest distance between two adjacent nodes in meters
d_e	Depth of seawater in meters
d_{sr}	Distance between a sound source and a receiver in meters
DI	Directivity index
DT	Detection threshold in dB re 1 μ Pa^2
E	Set of edges or links
$\mathcal{E}_t$	Energy consumption for transmitting a data packet in Joule
$\mathcal{E}_0^{(u)}$	Initial energy of node u in Joule
$\mathcal{E}_r^{(u)}$	Residual energy of node u in Joule
f	Center frequency of a sound source in Hz
$\mathcal{F}$	Scoring function in Chapter 5
G	Graph
H_u	Set of next-hop candidates of node u
$\mathcal{H}$	Distance between the upper and lower boundaries in meters
$i^{(u)}$	Injection rate of node u or traffic intensity in packets per day

I	Sound intensity in watts per square meters
I_{ref}	Reference intensity of acoustic signals in watts per square meters
$\mathcal{K}$	Coefficient used in the Semi-empirical formula
L_d	Size of a data packet in bits
N	Size of a UWSN with a square grid topology
N_c	Number of cyclic shifts
$N_{hop}(\cdot)$	For all sensor nodes, the total number of hops (from sensor nodes to the sink node)
N_s	Number of sink nodes
N_{tp}	Number of transmitting power levels
NL	Noise level in dB re 1 μ Pa^2
$\mathcal{N}(\mu, \sigma^2)$	Gaussian distribution with the mean value of μ and the standard deviation of σ
$\mathbb{N}$	Natural number
p_l	Idle listening power of a sound source in watts
p_r	Receiving power of a sound source in watts
p_s	Sleeping power of a sound source in watts
p_t	Transmitting power of a sound source in watts
p_{cy}	Power at the cylindrical surface in watts
p_{sp}	Power at the spherical surface in watts
P_j	Pressure of each eigenray j
$\mathcal{P}_j$	One path from source node j to the sink node
$\mathfrak{P}_m^{(X_0,Y_0)}$	Set of all paths from a source node located at (X_0, Y_0) to the sink node using m hops
PL	Path length of the AUV within the communication range of a sensor node in meters
q	Prime power
$\mathcal{Q}$	Marcum Q-function
r	Transmission range of a sensor node in meters
$r^{(u,v)}$	Transmit rate from node u to v in packets per day

R_d	Data rate of an acoustic modem in bits per second
R_u	Set of previous-hop candidates of node u
$\mathcal{R}$	Network robustness
s	Salinity in parts per thousand
SL	Sound source level in dB re 1 μ Pa^2
T_a	Transmission time of an ACK packet in seconds
T_A	Duration of one cycle period of an AUV in seconds
T_A^l	Listening duration of an AUV in one cycle period in seconds
T_b	Transmission time of a beacon message in seconds
T_{day}	Duration of one day in seconds
T_n	Duration of one cycle period of a sensor node in seconds
T_n^w	Wake period of a sensor node in one cycle period in seconds
T_R	Transmission time of a data request packet in seconds
T_{slot}	Duration of each slot (active or inactive slot) in seconds
T_n^s	Sleeping period of a sensor node in one cycle period in seconds
$T_n^{s^*}$	Optimized sleeping period of a sensor node in one cycle period in seconds
T_u	Lifetime of node u in days or in number of received data packets
T	Network lifetime in days or in number of received data packets
$\hat{T}_n^s$	Supposed amount of sleeping time of every sensor node in seconds
TL	Transmission loss
T	Water temperature in degrees Celsius
$\mathbb{T}(i)$	Maximum amount of sleeping time of node i in seconds
u_0	Sink node
(u, v)	Link between node u and node v
$U(\cdot)$	Utility function
$\mathcal{U}$	Utilization ratio of the sink node

v_A	Velocity of an AUV in meters per second
v_s	Velocity of sound in seawater in meters per second
V	Set of vertices or nodes
$(\mathcal{V}, k, \lambda)$	Triplet in balanced incomplete block design
w_e	Weight of energy in Chapter 6
w_E	Weights for the energy consumption of sensor nodes in Chapter 5
w_p	Weight of power levels (transmitting and receiving power levels)
$w_{\mathcal{R}}$	Weights for the network robustness
$W(\theta)$	Shading function to weight the amplitude of a ray
$(X, \mathcal{A})$	Pair in balanced incomplete block design
(X_a, Y_a)	Coordinate of node a
z	Depth of a sound source in the ocean
$\mathbb{Z}^+$	Positive integers
α	Ratio of r to d_c
β	Weight coefficient in $U(\cdot)$
ϵ	Step of transmission range in meters
η	Confidence interval
ξ	Transducer efficiency
τ	Transmission time of a data packet in seconds

List of Tables

List of Figures

Chapter 1

Introduction

1.1 Overview

Underwater acoustic sensor networks (UWSNs) have attracted much research interest in recent years due to their wide range of potential applications such as marine environmental monitoring, undersea resource explorations, disaster prevention and monitoring, assisted location and navigation, military surveillance, and security monitoring [1, 2, 3]. Early generation of UWSNs include the Acoustic Local Area Network (ALAN), which was deployed by the Woods Hole Oceanographic Institution (WHOI) in 1994 off the coast of Monterey, California [4]. ALAN, aiming at long-term data acquisition and ocean monitoring, consists of a number of sensor nodes placed on the seafloor and one surface node attached to a buoy. The sensor nodes located on the seafloor transmit data to the surface node via acoustic links. Data was transmitted to the onshore base station via a radio frequency link. Another example of UWSNs is Seaweb 2000 [5], which was one of the first multi-hop underwater acoustic networks. This project advanced the underwater communication technology to achieve near-real-time, synoptic observation of the underwater environment. In Seaweb 2000, fourteen sensor nodes (to sense, collect, and relay data) were placed on the seafloor and three gateway nodes with buoys (to collect data from sensor nodes and transmit data the onshore station) were deployed on the sea surface [5, 6]. During data transmission, the researchers tested packet forwarding through multiple nodes using Request To Send (RTS) / Clear To Send (CTS) handshaking. New acoustic modems (i.e., ATM-885) [7] were tested in Seaweb 2000, which can provide powerful acoustic communications and large memory for data storage. Figure 1.1 presents an example of UWSNs, where regular sensor nodes and sink nodes are deployed on the seafloor. Sink nodes are in charge of gathering data from regular sensor nodes and reporting the collected data to the surface nodes using acoustic signals. The surface nodes then transmit the data to the satellites via radio signals and these data can be downloaded by onshore base stations.

The advancement of UWSNs is later augmented by the recent increase in engineering activities in the design and deployment of autonomous underwater vehicles (AUVs). This technology has allowed UWSNs to incorporate mobility characteristics [8, 9]. The Underwater Acoustic Network (UAN) [10, 11, 12] project reports one of the first cases of successful deployment of mobile UWSNs. In this project, four fixed sensor nodes, two autonomous underwater vehicles (AUVs) and one sensor node mounted on a surface ship (acting as a mobile node) were deployed in seawater to evaluate the performance of UWSNs and to verify

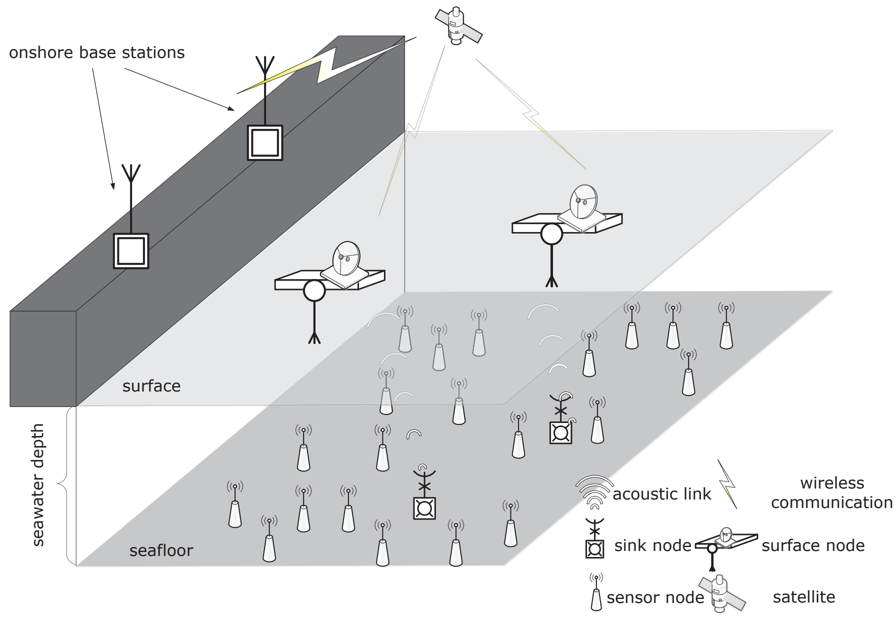

Figure 1.1: Illustration of underwater acoustic sensor networks

the variation of the underwater acoustic channel. Their experimental results indicate that underwater communication capability degrades quickly in low SNR conditions. The authors also investigated the factors that affect the packet delay in UWSNs. Noise, packet collision, and signal fading are the main contributing factors for packet retransmission, which, lead to an increased delay of data packets. The delay in signalling packets is often caused by queue blocking and the operations of network protocols. In general, the performance of underwater acoustic networks is strongly related to the underwater acoustic channel conditions. Figure 1.2 shows an example of UWSNs where AUVs are deployed to collect data from regular sensor nodes located on the seafloor. Upon returning to the surface ships, the collected data will be reported to the onshore base stations via satellites, or kept there for later processing.

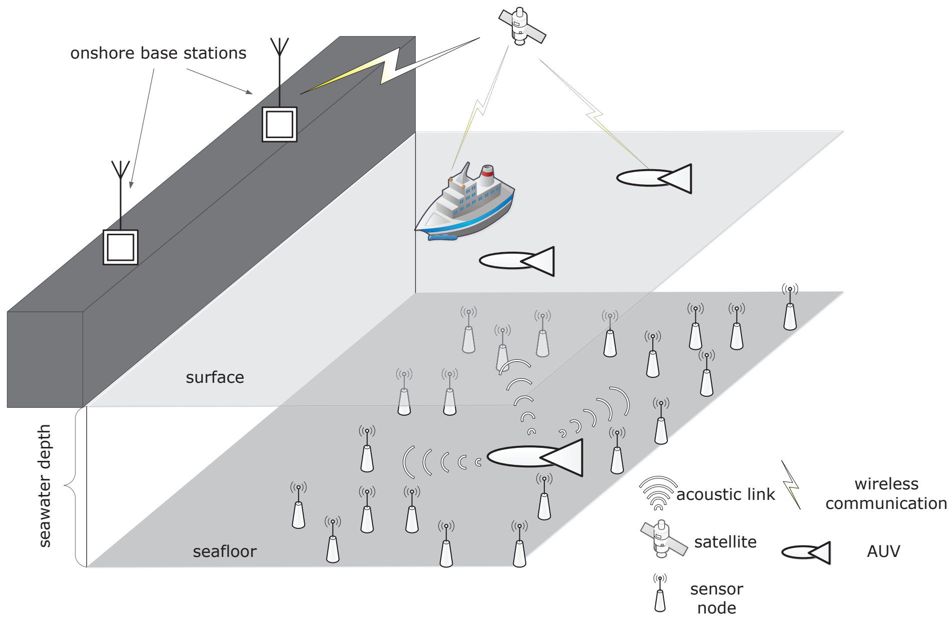

Figure 1.2: Illustration of underwater acoustic sensor networks with AUVs

The propagation velocity and the absorption loss of electromagnetic signals are functions of carrier frequency in seawater [13, 14]. Due to the high absorption loss in seawater, electromagnetic signals do not travel long distances [13, 15]. Optical waves are another potential option for underwater communications. However, the performance of underwater optical communications is affected by scattering and the precision in pointing laser beams. In general, optical waves can only reach a few hundred meters with directional transmission [16, 17, 18]. Compared to electromagnetic signals and optical signals, acoustic signals emerge as a better choice for underwater communications in terms of communication distance (a few thousands of meters or more) and communication quality (relatively low attenuation) [19, 20, 21]. Table 1.1 compares the communication characteristics of electromagnetic, optical and acoustic signals in seawater.

Table 1.1: Comparison of propagation properties of electromagnetic, optical, and acoustic signals in seawater

	Electromagnetic signals	Optical signals	Acoustic signals
Frequency band	MHz to GHz	$10^{14} - 10^{15}$ Hz	Hz to kHz
Data rate	Mb/s	Gb/s	kb/s
Wave speed	3×10^8 m/s	3×10^8 m/s	1.5×10^3 m/s
Effective range	m	m	km
Power loss	~ 122 dB (1 km and 1 MHz)[22]	$\propto$ turbidity	> 30 dB (1 km and 1kHz)[19]

There are several challenging issues of underwater acoustic communications. First, energy availability is limited in underwater acoustic communications because of the unchangeable and non-chargeable battery in the sensor nodes. Frequently replacing sensor nodes is not realistic in long-term marine monitoring applications. Second, the link quality in underwater acoustic communications is lower than that in terrestrial wireless sensor networks (WSNs) due to multi-path propagation and temporal / spatial-variation of the underwater acoustic channels [23]. Furthermore, the data rate of underwater acoustic communications (i.e., kb/s to tens of kb/s) is much lower than that of radio frequency (RF) communications due to the low bandwidth of acoustic signals [23, 24]. The data rate increases when the transmission distance becomes shorter, necessitating more sensor nodes to satisfy a certain requirement of coverage and connectivity. Larger-scale and high-density UWSNs bring additional challenges because of the higher cost of underwater acoustic devices and non-trivial deployment costs. In Section 2.2.1, we summarize the parameters and costs of underwater acoustic modems that are widely used for academic and commercial purposes in Table 2.2.

As shown in Figure 1.2, several earlier works reported in the literature [25, 26] employ AUVs to gather data from regular sensor nodes located on the seabed using optical communications, instead of acoustic communications, in order to achieve a high data rate. However, because short communication distance and accurate positioning often become a must in underwater optical communications, controlling and navigating AUVs to reach the preferred or correct positions becomes a critical issue.

A large number of studies have addressed the above issues from the physical layer to the network layer of UWSNs. For the physical layer, to mitigate the long delay spread and the time-varying phase distortion, frequency shift keying modulation (FSK) and non-coherent detection are employed [27]. These techniques can provide robust underwater acoustic communications at low bit rates (on the order of 100 b/s) without efficiently utilizing the bandwidth [27, 28, 29]. The Micro-modem designed by WHOI [30] and the Telesonar series manufactured by Teledyne-Benthos [31] are two commercial modems using these techniques. After coherent detection demonstrated feasible on underwater acoustic channels [32], greater bandwidth utilization can be achieved by phase shift keying modulation (PSK) and quadrature amplitude modulation (QAM) [33, 34]. Moreover, the adaptive equalization and synchronization for single-carrier wideband systems are introduced to achieve a high-speed underwater acoustic communication (i.e., the bit rate can be in the order of kb/s over horizontal and vertical acoustic links in seawater) [35, 36]. Furthermore, as reported in [37, 38], higher bit rates can be achieved by multi-carrier modulation/detection if a multi-input multi-output (MIMO) system is employed.

For the medium access control (MAC) (i.e., link layer), the performance of ALOHA, slotted ALOHA, and carrier-sense multiple access / collision avoidance (CSMA/CA) in UWSNs are evaluated [39, 40, 41]. These protocols, commonly used in terrestrial networks, aim at reducing packet collision and increasing network throughput without considering the context of underwater acoustic communications. Distance-aware collision avoidance protocol (DACAP) [42] is specifically designed for UWSNs by taking into account the underwater propagation delay and its impact on packet collision and detection. The RTS/CTS handshake is used for reserving the acoustic channel for packet transfer. As a further improvement, the optimized data packet size selection [43] is proposed for CSMA/CA and DACAP. The optimum packet size which relies on the protocol characteristics, the data rate, and the bit error rate (BER), can achieve a balance between the network throughput and the energy consumption of sensor nodes. An example is the Tone-Lohi (T-Lohi) protocol [44], which allows sensor nodes to work on a low duty cycle to reduce energy consumption for idle listening. Sensor nodes also can detect potential packet collision using tone with low power consumption.

Network deployment strategy is also an important issue in UWSNs due to the high cost of sensor nodes and the non-trivial deployment cost. Two-dimensional (2D) and three-dimensional (3D) architectures have been widely used in UWSNs [3, 45, 46]. In 2D-UWSNs, sensor nodes are placed on the seafloor with a regular topology such as ring, star, and grid. The position information of sensor nodes often is known *a priori*. Randomly distributed UWSNs are also investigated in [47, 48], where the connectivity among sensor nodes and the network coverage are guaranteed under a certain operation frequency and a transmitting power. In 3D-UWSNs, a number of sensor nodes are deployed in different layers of seawater (suspended in seawater) to forward data packets (collected by sensor nodes located on the seafloor) to the surface nodes [45, 49]. Algorithms for calculating the optimal position of sensor nodes in different layers are studied to improve the robustness of UWSNs [50].

The routing problem of UWSNs has been reported by several researchers, for example, in [51, 52, 53, 54, 55]. For delay-sensitive and delay-insensitive applications, the routing protocols in [51] allow sensor nodes to select next-hop nodes by jointly considering the link reliability and packet delay. A set of geographic routing protocols is presented in [52]. By fully utilizing the position information of sensor nodes, routing decisions can be made to minimize the energy consumption of total paths used for data transmission [52]. Other routing approaches, such as the depth-aware routing and the pressure-aware routing, make routing decisions based on the depth of sensor nodes or the sensed pressure [53, 54]. The variation of depth and pressure can be obtained by using additional equipment. The location information of sensor nodes can also be used in multipath routing protocols to enhance the link reliability and increase the network throughput [55].

This dissertation addresses the issue of energy efficiency for UWSNs in long-term marine monitoring applications. Through a comprehensive understanding of underwater acoustic channels and network topologies, the schemes proposed in this dissertation jointly consider energy consumption of sensor nodes and network connectivity, and can be utilized for data collection in UWSNs.

1.2 Motivation for the Research

Much of the research effort in the past decade has been devoted to the improvement of acoustic signal reception and processing, the increase of the network throughput, and the reduction of packet delay and packet error rate. In contrast, little work has been done to reduce and balance energy consumption of sensor nodes during data transmission in UWSNs. In long-term marine monitoring applications under energy-constrained conditions, transmitting data using an energy-efficient approach becomes more important than improving the network throughput.

In this dissertation, we examine several different aspects related to the energy efficiency issue in 2D UWSNs. Link quality, energy consumption of sensor nodes, and network operations in UWSNs are closely related to the propagation properties of acoustic signals in seawater. The time-varying and space-varying underwater acoustic channel often leads to unreliable communication links. The performance of UWSNs degrades if networking protocols originally designed for WSNs are directly adopted. In the past 50 years, the normal mode model and the ray-theoretical model have been utilized for the underwater acoustic channel estimation. These models calculate transmission loss of acoustic signals within their scope of applicability [19, 21]. However, there are several challenging issues: 1) in the ray-theoretical model, the amplitude of the sound line (i.e., ray) should vary slower than the phase, which is not always true in practice; 2) it is difficult to obtain accurate marine environment parameters such as sound speed profile and bathymetry data. Due to the high expenses of sea trials, researchers strive to use models that better resemble the realistic channels when designing upper layer protocols for UWSNs. The semi-empirical formula [21, 52] is a convenient approach for estimating underwater acoustic channels. The differences between these two underwater acoustic channel models and the semi-empirical formula should be studied under different environmental conditions.

Wake-up coordination schemes provide an effective technique for reducing energy consumption for idle listening during data transmission. Wake-up coordination schemes fall into three categories: on-demand, synchronous, and asynchronous [56]. An on-demand wake-up scheme relies on a low-power module embedded on the transmitter. This module is used to wake up all circuits at any time determined by the requirements of applications. However, the majority of commercial acoustic modems are not equipped with such a module [30, 57]. Synchronous wake-up schemes allow sensor nodes to enter a sleep mode in order to reduce energy consumption during idle listening. A sensor node alternates between the wake-up mode and sleep mode according to a selected duty cycle pattern. Synchronous wake-up schemes require clock synchronization among all sensor nodes to guarantee data exchange. Protocols such as the sensor medium access control protocol (S-MAC) and the time-out medium access control protocol (T-MAC) follow this approach [58, 59] . However, transmitting and receiving power dominate the energy consumption in UWSNs (which will be discussed in Section 2.2.1). Energy consumption for signalling packet exchange during the process of clock synchronization increases energy overhead and shortens the network lifetime when the number of sensor nodes becomes large [60, 61]. In asynchronous wake-up schemes, sensor nodes use different predetermined wake-up and sleep patterns for each cycle of operation to achieve good energy efficiency and guarantee network connectivity. These patterns are often based on certain properties in linear algebra and optimization and no time synchronization is required. These asynchronous wake-up schemes are suitable for applications where the cost of time synchronization is prohibitive. Several asynchronous wake-up schemes are proposed for delay tolerant networks (DTNs) and ad hoc networks [62, 63, 64]. However, when applied to a network with dynamic topology change and considerably large delay and delay spread, these schemes have to utilize frequent signalling packet exchange to keep the connectivity of the network. This will inevitably lead to unnecessary energy consumption and deteriorate the network performance when applied to UWSNs [62, 65].

Randomly-distributed network topology is widely used in WSNs. However, in practice, the random topology is not quite realistic for UWSNs. The number of sensor nodes in UWSNs is often much smaller than that in WSNs due to the high cost of acoustic devices and the non-trivial deployment cost. The common starting price of a commercial acoustic modem is more than $8000 [7, 66, 67, 68]. The predetermined and regular topologies are more suitable for UWSNs than WSNs. Regular topologies include: linear, ring, star, and grid. [45, 50]. The deployment error caused by location accuracy and marine environmental factors should be studied in UWSNs with a regular topology. Moreover, the relationship between energy consumption of sensor nodes and network robustness should be considered.

For end-to-end data transmissions, multi-hop communication is an alternative mechanism in UWSNs because communication over a long distance in seawater requires a fairly high transmitting power level [2, 21]. Transmitting and receiving power levels dominate the energy consumption of sensor nodes. For example, for a particular model of the Micro-modem [30], the power consumption for transmitting, receiving, idle listening and sleeping are 20 W, 3 W, 0.08 W, and 0 W, respectively. The transmitting power level of 20 W can reach a transmission range of 1,000 m (we discuss these parameters in Chapter 4). Several routing protocols reported in previous studies merely concentrate on increasing the network throughput and decreasing the packet delay in UWSNs [51, 69]. To the best of our knowledge, few routing protocols address the energy consumption issue in UWSNs. In contrast, in WSNs, there are many different routing protocols aimed at prolonging network lifetime [70, 71]. The appropriateness of these protocols should be considered in the context of underwater environments and applications.

AUVs can work as mobile sinks to collect data from UWSNs. However, AUVs also introduce new challenges of synchronization, route planning, and coordination estimation. Due to different requirements of UWSNs and operations of AUVs, the data collection schemes using mobile sinks for WSNs may not be directly applicable to UWSNs with AUVs. Moreover, unlike sensor nodes with nonchargeable and unchangeable batteries, the AUV can return to the surface ship to recharge its batteries. However, energy conservation remains the main objective when designing a scheme for data collection using AUVs equipped with limited-energy supply so that the duration of data collection can be extended. Designing schemes without prior clock synchronization that facilitate AUV coordination with sensor nodes for efficient data gathering is a particular goal.

1.3 Thesis Organization

The thesis organization is shown in Figure 1.3 for an easy illustration. In this dissertation, the main goal is to improve energy efficiency in UWSNs. The power parameters of acoustic modems, e.g., transmitting power, receiving power and idle listening power, are the essential parts of the energy consumption calculation. Power consumption parameters that are used in the thesis are obtained from both underwater channel models and specifications provided by the manufacturers of commercial acoustic modems. The power parameters of the Micro-modem manufactured by WHOI [30] and the underwater acoustic channel models with the semi-empirical formula (discuss in Chapter 3) are used in Chapters 4, 5, and 7. The power parameters of the S2CR-18/34-modem developed by Evologics [68] and the underwater acoustic channel models with the semi-empirical formula are adopted in Chapter 6. The manufacturers of the Micro-modem and the S2CR-18/34 modem provide complete sets of the power consumption parameters, such as transmitting, receiving, sleeping and listening power levels, which can be used in our research. On the other hand, unlike the Micro-modem, the S2CR-18/34 modem provide three transmitting power levels corresponding to three transmitting ranges. The power consumption parameters of the S2CR-18/34 modem are used in Chapter 6 when considering relay node selection in UWSNs.

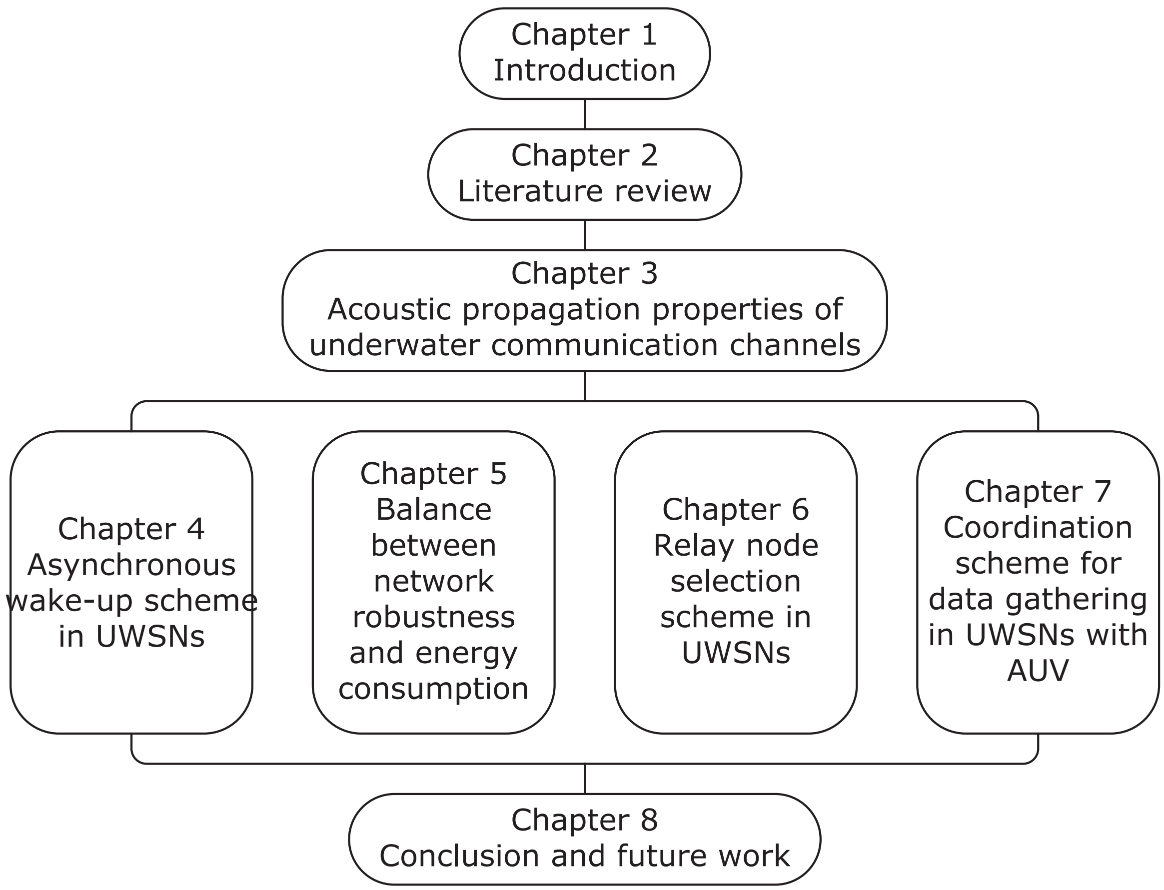

Figure 1.3: Thesis organization

Chapter 2 presents a literature survey of statistical underwater acoustic channel models with sea trials. Underwater acoustic modems commonly used in commercial and academic areas and the wake-up coordination schemes in both WSNs and UWSNs are described. Different routing protocols in UWSNs are categorized based on the architecture of the network. In particular, routing protocols designed specifically for energy efficiency and network lifetime prolonging are closely examined.

In Chapter 3, we study the propagation characteristics of the acoustic signal in seawater. We compare the ray-theoretical model to the normal mode model. We describe three different kinds of transmission loss based on the ray-theoretical model and compare them with the semi-empirical formula. Finally, we evaluate the transmission loss using different environment parameters.

Chapter 4 describes asynchronous wake-up coordination schemes for multi-hop UWSNs for long-term marine monitoring applications. We present the network topology and basic operations of the wake-up schemes in UWSNs. We then propose an asynchronous wake-up coordination scheme based on the combinatorial designs to reduce the working duty cycle of sensor nodes while maintaining the network connectivity. Furthermore, we conduct theoretical analysis to investigate the utilization ratio of the sink node and the scalability of the proposed scheme in large sized networks. Performance evaluation of the proposed scheme is studied in different network sizes, under different traffic loads, and by different numbers of sink nodes.

In Chapter 5, we study the deployment strategy of UWSNs. We present a mathematical model to study the deployment error of UWSNs. According to the model, we introduce the ratio, α, of the transmission range of a sensor node to the distance between two closest adjacent sensor nodes, to balance the network robustness and the energy consumption of sensor nodes. We report optimal values of α that correspond to this balance for different sizes of UWSNs in performance evaluation.

Chapter 6 addresses the relay node selection problem in UWSNs. First, we formulate the relay node selection problem as a linear programming problem, where the objective is network lifetime maximization. Then, we propose a routing metric that reflects both the transmitting power level and the residual energy of the two-end nodes of each acoustic link. We evaluate the performance of the proposed relay node selection scheme in different network sizes and by assigning different initial energy levels based on their traffic loads. Also, the performance of the proposed relay node selection scheme is compared to that of a shortest path routing protocol and the theoretical results values obtained from the linear programme.

Chapter 7 proposes a coordination scheme between an AUV and sensor nodes in order to effectively collect data from UWSNs. First, the asynchronous coordination scheme between an AUV and a single sensor node is studied. The amount of the sleeping time of a sensor node is optimized by taking into account the energy consumption and the number of sensor nodes successfully transmitting data packets. Furthermore, power control is introduced to further reduce energy consumption of sensor nodes.

The dissertation is concluded in Chapter 8. Possible directions of future research are discussed.

Chapter 2

Literature Review

In this chapter, we review previous studies on underwater acoustic channel models for shallow and deep water to gain a better understanding of protocol designs for UWSNs. We also summarize several sea trials in terms of their objectives, network sizes, and the type of underwater acoustic modems used. As an essential part of underwater acoustic communication, the performance of different acoustic modems are presented and compared. WSNs and UWSNs share some common features, which are reviewed in this chapter. Different coordination wake-up schemes are discussed for both WSNs and UWSNs. Also, we survey routing protocols for UWSNs and energy-efficient routing protocols for WSNs, and we summarize data collection schemes reported in the literature using mobile sinks for WSNs and UWSNs.

2.1 Underwater Acoustic Channel Models and Sea Trials

Acoustic signals suffer severe attenuation, absorption, Doppler spread, and time-varying multipath propagation in seawater. It is necessary to obtain a comprehensive understanding of underwater acoustic channel models when designing protocols for upper layers, such as the MAC layer and the network layer. Unlike terrestrial radio channel models, there is no consensus on the statistical characterization of the underwater acoustic channel model due to its temporal and spatial variability. In this section, we investigate several statistical underwater acoustic channel models obtained from sea trials and field measurements. As well, the results from several sea trials are summarized and compared in terms of their objectives, number of transceivers, communication range and other factors.

2.1.1 Statistical Shallow Water Acoustic Channels

Chitre [72] investigated the shallow warm-water acoustic channel, which is a common underwater communication environment in most tropical coastal regions. Extensive time-varying multipath and non-Gaussian ambient noise are two main characteristics of the shallow warm-water acoustic channel. The channel model derived in [72] closely agrees with the experimental data obtained from the sea trial conducted in February 2004 in Singapore [73]. The channel model in [72] captures the multipath arrival structure and the statistical effects of acoustic signals, such as fading and arrival-time jitter. Rayleigh fading was present in the 15 m deep underwater channel and was verified at different horizontal communication ranges, including 50 m, 100 m, and 1,020 m, respectively. As well, the author concludes that the time-correlation of the arrival-time jitter does not affect short distance communications in seawater when the arrival time of the acoustic signal does not vary over the transmission time of one data packet.

Non-Rayleigh or non-Rician distribution characteristics can be observed from the experimental data collected by the TREX04 sea trial, conducted in April 2004 off the coast of New Jersey [74, 75]. In this trial, the depth of seawater was 70 m, the source and the receiver were located at 35 m depth, and the data packets were transmitted within a horizontal communication range of 3.4 km. As well, the center frequency of the sound source varied from 15 kHz to 19 kHz. Several conventional channel models assume that the fading statistics are valid for all time scales, which is why these models fail to present non-Rayleigh or non-Rician distribution characteristics [75]. As an improvement, Yang *et al.* [75] categorize the time-scale fading phenomena into two types: long-term and short-term, which was based on a 0.2 s time scale obtained from the experimental data from the TREX04. A lognormal distribution was used to model the long-term fading statistics, and a Rayleigh distribution was used to model the short-term fading statistics. The K-distribution was observed through a joint consideration of the long-term and short term fading.

Qarabaqi and Stojanovic [24] studied the random channel variations and proposed statistical underwater acoustic channel models by taking into account the frequency-dependent attenuation and bottom/surface reflections. In their work, random channel variations are classified into small scale and large scale based on the size of wavelengths. The small-scale channel model includes scattering and motion-induced Doppler shifting, which is used to estimate the fast variations of the instantaneous channel response. An autoregressive Gaussian displacement of scattering points leads to the exponential time-correlation function of small-scale fading coefficients. In the large-scale model, the channel gain, is modeled as a lognormal distribution. The location uncertainty and the variation of environmental conditions are also considered in the large-scale model. In [24], the authors utilize data from the Surface Processes and Acoustic Communications Experiment (SPACE), the Mobile Acoustic Communications Experiment (MACE), and the Kauai AComms Multidisciplinary University Research Initiative (KAM) to verify the proposed channel models. These three sea trials are conducted at different depths, i.e., 10 m, 60 m, and 100 m, respectively. Both small-scale and large-scale models present a good match with the data from SPACE, MACE, and KAM experiments.

2.1.2 Propagation Properties of Acoustic Signals in Deep Water

Several sea trials studying acoustic propagation properties in deep water have been conducted in the past 10 years. In [76], the authors concentrated on the effect of the sea-bottom reflection on the acoustic propagation within a horizontal communication range of 50 km. In this study, the depth of seawater was 1.4 km. Using the experimental data collected in the long-range ocean acoustic propagation experiment [76], the authors found that the sea-reflected acoustic signal was sensitive to the seafloor topography and its properties. Within the transmission range of bottom-reflected and surface-reflected acoustic signals, bottom-reflected acoustic signals interfere with refracted acoustic signals. The parabolic equation method was used to achieve an acceptable model-data fit by taking into account the range-dependent bathymetry data. Furthermore, the seafloor was modeled as a fluid layer without scattering.

To evaluate the performance of multiuser communication in deep water, another oceanic experiment was conducted at a depth of 5,000 m in Japan in 2010 [77]. The sound sources were deployed at depths of 2,000 m, 2,500 m, and 3,000 m, respectively. The receiver array was placed at around the sound channel axis (around 1,000 m depth). Adaptive time reversal with a single channel decision feedback equalizer is used to mitigate the potential data packets collision at the base station. In [77], the authors reported that the aggregate data rate of 300 b/s can be achieved for up to three users when the horizontal range between the source and the receiver is 150 km and 180 km. Moreover, two users separated by a horizontal distance of 3 km at 1,000 m depth can transmit data simultaneously to the base station at an aggregate data rate of 200 b/s. The horizontal distance between the base station and any one of the two users was 500 km.

A glider can be used for data collection and acoustic communication in deep water. In a sea trial conducted in Kauai, Hawaii in 2006, a glider equipped with an acoustic modem was deployed at a depth of 1,000 m [78]. The experimental data reveals that the glider can collect a large amount of data during a single dive even when the SNR is fairly low. The combination of spatial and temporal diversity is utilized for acoustic communication, which can bring larger coverage and more reliable acoustic communication. Upon surfacing, the glider can forward data to the onshore base station by radio frequency signals.

2.1.3 Sea Trials

The SPACE experiment [79] was conducted at the Air-Sea Interaction Tower in October 2008, which aimed to evaluate the performance of the MIMO-OFDM technology in underwater acoustic communications. The researchers assessed the impact of the time variation and other environmental factors on the MIMO-OFDM communication system. The transmitter and receiver arrays were located on the seafloor. The depth of seawater was 15 m and the maximum horizontal communication range was 1,000 m. The experimental data showed that the performance variation of the MIMO-OFDM underwater communication system is correlated with environmental conditions, such as wave height. The experimental signals were processed by linear equalization in the frequency domain. The corresponding weights for the equalizer were calculated by the inter-carrier-interference coefficients [80]. In the MIMO-OFDM underwater communication system, the inter-carrier-interference equalization can provide performance gains using simple gain combining, which indicates that the MIMO-OFDM underwater communication system can offer reliable data transmission over time-varying and band-limited underwater acoustic channels.

The KAM experiment [81, 82] was conducted in the western side of Kauai, Hawaii, at the Pacific Missile Range Facility in June and July of 2008, respectively. The objective of KAM was to gather marine environmental data for studying oceanography and underwater acoustic communication. An acoustic source and a linear array receiver were deployed in seawater. The depth of seawater was about 100 m and the maximum horizontal distance between the source and the receiver was 8 km. The researchers investigated the impact of the fluctuating marine environment on the waveguide of the acoustic impulse response between the source and the receiver. The experimental data showed that the OFDM underwater acoustic communication system can achieve a high-rate data transmission (10 kb/s) when the iterative sparse channel estimation with the low-density parity-check (LDPC) is implemented on the receiver [81].

Another multi-university research initiative experiment was conducted at the same place as KAM in 2011 [83]. The depth of seawater was about 106 m and the horizontal distance between the sound source and the receiver array was 3 km. The experimental results showed that the single-carrier communication with 32-QAM can achieve a data rate of up to 60 kb/s. The data rate of multi-carrier communication can achieve 32 kb/s with QPSK. Moreover, the researchers indicated that single-carrier system can utilize the spectral efficiency with low computational complexity and that the increase of communication diversity can be obtained by multi-carrier communication. The authors in [84] noted that a smaller symbol duration with a high signaling rate led to better channel tracking because the underwater acoustic channel remained coherent over a large number of symbols at the cost of higher computational complexity. However, the authors in [83] explained that it was difficult to draw this definitive conclusion since the source power allocation, transmitted symbol energy, and noise spectral density over the bandwidth were not fully specified in [84]. For example, noise affected the received SNR for different signalling rates if the noise spectral density was not flat over the bandwidth, which was reported in the experimental results of KAM in 2011 [83].

The MACE experiment [85] was carried out in the Cape Cod in the southern Atlantic Ocean in July 2010. The objective of MACE was to evaluate the performance of the mobile MIMO underwater acoustic communication system. The transmitter was towed by a ship (moving at speeds of 1 m/s or 2 m/s) and the receivers were fixed on buoys. The maximum horizontal distance between the transmitter and the receivers was 7 km. The depth of seawater was about 100 m. The experimental results illustrated that the OFDM communication system consumes less energy and mitigates various channel distortions, such as motion-induced Doppler distortion.

In Table 2.1, we summarize the sea trials that were discussed in Section 2.1 in terms of objective, horizontal communication range, depth of seawater, number of nodes (source and receiver), type of underwater acoustic modem used, and power consumption parameters. We use "N/A" to denote the parameters not specified in the literature. According to the summary of sea trials, we observe that, in practice, the number of sensor nodes deployed on the seafloor is much fewer than that in WSNs because of the high cost of underwater devices and the non-trivial deployment cost. Therefore, for UWSNs, regular topologies such as linear, ring, and grid, are the preferred network structures than a randomly distributed topology. In Chapters 4, 5, and 6, we adopt the square grid topology for UWSNs and the proposed schemes can be extended to other regular topologies.

Table 2.1: Summary of sea trials

	Seaweb 2000 [6]	SPACE[79]	KAM[81, 83]	MACE [85]	UAN [10, 12]
Objective	marine environment observation	MIMO-OFDM evaluation	gather marine data; OFDM evaluation	mobile MIMO evaluation	UWSNs evaluation; channel variation
Communication range (m)	2,000	1,000	8,000/3,000	7,000	900
Depth of seawater (m)	50	15	100	100	100
Number of nodes	17	6	≤4	≤4	7
Acoustic modem	Teledyne Benthos ATM-885[7]	ITC-1007[86]	ITC-1001/2015[67]	ITC-1007[86]	cNODE mini transponder[87]
Power consumption parameters[1]	N/A	N/A	N/A	N/A	190 dB re 1 μPa[2]

[1] Most literature on these sea trials does not specify the power consumption parameters.

[2] The authors in [10, 12] choose 190 dB re 1 μPa as the transmitting power without specifying other power consumption parameters.

2.2 Underwater Modems

2.2.1 Underwater Acoustic Modems

Underwater acoustic modems are used for commercial and academic applications such as oil and gas exploration, ocean observations, and network protocols verification. The Micro-modem is a compact and low-power acoustic modem manufactured by WHOI [30]. It supports the programmability to implement additional features, such as Ping, a mini-packet that can be utilized by a node to communicate with any other node. The Micro-modem employs two different modulations: frequency-hopping frequency shift keying (FH/FSK) and PSK. FH/FSK is used for shallow water with low data rate (80 b/s) whereas PSK can achieve a higher data rate of 5000 b/s in deep water [30, 66]. The price of the Micro-modem starts at $ 8,000.

EvoLogics, a German technology enterprise, supplies at least six types of acoustic modems based on their patented technology, namely, the sweep-spread carrier (S2C) [68, 88]. S2C technology aims at mitigating the multipath effect in seawater by imitating the sound patterns generated by dolphins and by continuously spreading the signal energy over a wide range of communication frequencies. S2C-series acoustic modems provide self-adaptive algorithms for reliable underwater acoustic communications and support addressing and networking to easily build relay chains and underwater networks. High data rate can be achieved in a short horizontal range with low power consumption. The starting price of the Evologic acoustic modem is $14,000.

The AquaComm is an underwater acoustic modem for the short range underwater communication, and is produced by DSPComm [89]. It can achieve a communication range of 3 km with a low data rate of 100 or 480 b/s. The operation bandwidth is from 16 kHz to 30 kHz. For underwater communication protocols, the number of retransmitted data packets can be configured by users when packet collision occurs. The price of the AquaComm acoustic modem starts at $6,600.

A prototype underwater acoustic modem has been developed by the University of Southern California for the Sensor Networks for Underwater Seismic Experimentation (SNUSE) project [90, 91]. Low production cost and low power consumption are the main objectives of the acoustic modem designed in the SNUSE project. An inexpensive, ultra-low power wake-up module is implemented on the acoustic modem with 0.5 W for idle listening. Additionally, channel estimation is achieved by the received signal strength indicator (RSSI).

2.2.2 Underwater Optical Modems

Although optical waves suffer severely from scattering caused by current and suspended particles in seawater, it can provide a higher data rate in a very short communication range. The BlueComm, an underwater optical modem, is a high-speed underwater communication device produced by Sonardyne [92]. BlueComm modem utilizes an array of high power light emitting diodes (LEDs) to modulate optical signals and transmit data. The highly sensitive receivers can detect optical signals with a lower energy consumption in daylight operation. For shallow water, the BlueComm optical modem can reach a communication range of 20 m with 5 Mb/s. In dark, deep water (over 350 m deep), the BlueComm modem can transmit data with up to 20 Mb/s in a maximum horizontal range of 200 m. The BlueComm modem can be utilized for collection of large amounts of data and supports real-time data transmission, such as high definition video and images.

Table 2.2 compares the underwater acoustic and optical modems in terms of their modulation, data rate, power consumption, communication range, operation frequency, power control, and price. The S2CR18/34 modem provides different transmitting power levels with different transmission ranges in their specification. From Table 2.2, we observe that the transmitting and receiving power levels dominate the energy consumption during data transfer. Therefore, it makes a lot of sense that the sending node communicate with the corresponding receiving node via fewest hops when a modem only support a single transmitting power level, which is discussed in Chapter 4 and 5. In Chapter 6, we discuss the relay node selection scheme for modems that allow multiple transmitting power levels to prolong the network lifetime.

Table 2.2: Comparison of underwater acoustic and optical modems

	Micro-modem	AquaComm	S2CR18/34	SNUSE	BlueComm(optical)
Manufacturer	WHOI	DspComm	EvoLogics	USC	Sonardyne
Modulation	FH-FSK/PSK	DSSS/OFDM	Sweep-Spread Carrier	FSK	N/A
Data rate (b/s)	80/5,000	100/480	19,200/31,200	N/A	1×10^6~20×10^6
Transmitting Power (W)	<50	N/A	2.8/8/35	2	40
Receiving Power (W)	3	N/A	1.1	0.02	8
Idle-listening Power (W)	0.08	N/A	0.005~0.284	0.2	N/A
Communication Range (m)	N/A	N/A	<3500	<500	<200
Power control	N/A[1]	N/A	√	√[2]	N/A
Price ($)	>8,000	>6,600	>14,000	N/A	>51,000 short range[3] >110,000 long range[4]

[1] The Micro-modem 2 provides power control [93], which does not specify the steps of power and communication range.

[2] The SNUSE modem supports four discrete power levels for transmission from 15 dBm to 33dBm at a 6 dBm step without specifying the corresponding transmission ranges [91].

[3,4] The starting price of BlueComm includes a pair of optical modems (a transmitter and a receiver).

2.3 Coordination Schemes in WSNs and UWSNs

In both WSNs and UWSNs, energy efficiency is a fundamental issue when designing network protocols because sensor nodes rely on a limited amount of battery energy for sensing, data collection, and communication. In long-term monitoring applications of UWSNs, it is not realistic to recharge or replace the batteries of sensor nodes frequently. An effective approach to energy saving is the wake-up coordination scheme, which can be categorized into on-demand, synchronous, and asynchronous coordination schemes. In the wake-up coordination scheme, each sensor node has two modes of operations: wake-up mode and sleep mode. In the wake-up mode, the transceiver is turned on for data transfer and channel detection, whereas it remains off during the sleep mode so that energy consumption can be reduced. In this section, we survey different coordination schemes in WSNs and UWSNs.

2.3.1 On-Demand Coordination Schemes

In on-demand coordination schemes, a sensor node is equipped with a low power radio module that is able to wake up the node for tasks such as sensing and communication. The wake-up time can be determined according to application requirements, current network data traffic and so on.

2.3.1.1 Radio Frequency Identification (RFID)

RFID is the wireless technique used for automatically identifying and tracking the tags attached to objects. The tag contains user information, which is powered by batteries.

Due to its low energy consumption (i.e., power lower by three orders of magnitude than the common radio), this technique is used in WSNs for energy-efficient data transmission [94, 95].

Jurdak, Ruzzelli, and O'Hare proposed an adaptive radio low-power sleep scheme for WSNs [96]. They studied a comprehensive energy consumption model of sensor nodes. This model included energy consumption components for radio switching, transmission, reception, idle listening, sleeping, and microcontroller operations (determined by different circuit boards). They then proposed the RFIDImpluse [96], which is a low-power radio wake-up scheme for WSNs using RFID readers and tags. A sender can use a built-in RFID reader to trigger an RFID tag located at the receiver. The impulse transmitted by the sender generates an interruption to wake up the microcontroller of the corresponding receiver. The microcontroller activates the radio voltage regulator and oscillator for receiving data packets. According to the energy consumption model and the RFIDImpluse, the authors presented an algorithm to select the optimal MAC protocol (i.e., BMAC [97], IEEE 802.15.4 [98], and RFIDImpluse) and sleeping mode configuration for a given traffic condition in WSNs. The experimental results showed that the proposed adaptive low-power sleep scheme (RFIDImpluse) consumes up to 20 times less energy than the IEEE 802.15.4 and BMAC in a low traffic scenario [96].

An energy efficient protocol based on RFID, called Reservation Aloha for No Overhearing (RANO), was proposed by Lee, Kim, and Kim [99]. RANO aimed at reducing energy consumption for overhearing during signalling packet exchange. In RANO, sensor nodes broadcast the communication sequence information so that each sensor node can be stay in the active mode only for the period of data transmission and is in sleep mode for the remaining time. RANO was implemented on RFID hardware and the experimental results indicate that RANO saved approximately 60 times the energy compared to the standard protocols (i.e., the active RFID standard).

RFID relies on a low power radio module to wake up the sensor device at proper time. A similar mechanism is used in UWSNs, which will be reported in Section 2.3.1.2 and 2.3.1.3.

2.3.1.2 T-Lohi MAC Protocol

T-Lohi was a tone-based reservation MAC protocol in UWSN [44]. The essential techniques of T-Lohi were the channel contender detection and counting with low power consumption, which were implemented by the SNUSE modem (discussed in Section 2.2.1). With T-Lohi, sensor nodes contended to reserve the underwater acoustic channel for data transfer. Figure 2.1 shows the frame structure used in T-Lohi that consists of a reservation period and a data transfer period. The reservation period contained several contention rounds (CR) until one sensor node successfully reserves the channel.

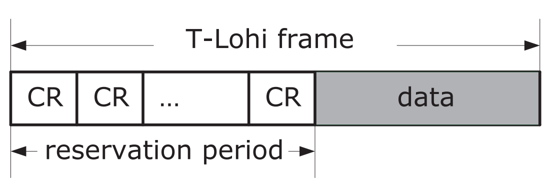

Figure 2.1: Frame structure of T-Lohi

The authors in [44] proposed three variants of T-Lohi based on their time synchronization approach: ST-Lohi (synchronized T-Lohi), cUT-Lohi (conservative unsynchronized T-Lohi), and aUT-Lohi (aggressive unsynchronized T-Lohi). In ST-Lohi, all sensor nodes are synchronized in time. cUT-Lohi and aUT-Lohi use different durations of CRs. Each CR of cUT-Lohi was three times as long as that of aUT-Lohi. Simulation results show that T-Lohi can achieve better channel utilization and consumed less energy than TDMA, CSMA, and ALOHA. Furthermore, ST-Lohi and aUT-Lohi can achieve higher throughput than cUT-Lohi because of the shorter duration of CR. Energy efficiency was further improved by cUT-Lohi due to packet collision avoidance by using longer CRs.

2.3.1.3 Cooperative Underwater Multichannel MAC Protocol (CUMAC)

Zhou *et al.* proposed CUMAC [100] to solve the multi-channel hidden terminal problem for UWSNs. This problem can be solved by using one transceiver to monitor the control channel [100]. Thus, two transceivers were required for each sensor node (the other transceiver was used for data transmission). Considering the high cost of underwater devices, for each sensor node, the authors in [100] used one underwater transceiver (i.e., underwater acoustic mode) for data transfer and one low-cost tone device for sending and receiving tone signal (i.e., the SNUSE underwater acoustic modem [90]). There were two main techniques employed by CUMAC: cooperative collision detection and tone pulse sequence. In the cooperative collision detection, each sensor node cooperated with its neighboring nodes to select a data channel by sharing the channel usage information. The channel usage information of the neighboring nodes can be obtained by signalling packet exchange. A tone pulse was defined as a short tone signal and a sequence of the tone pulse is called tone pulse sequence. In CUMAC, the tone pulse sequence was broadcast by a sensor node at a predetermined time and arrived at different sensor nodes at different times (considering the long propagation delay in UWSNs). Under a careful scheduling design, a sensor node can catch the tone pulse sequence at the right time and make a proper decision about what to do, such as transmitting data or listening to the channel. Compared to IEEE 802.11, CUMAC improves the network throughput with a lower energy consumption in one-hop and multi-hop UWSNs. The acoustic modem used in CUMAC used a transmitting power level of 0.6 W with the transmission range of 500 m. However, the paper does not report the information on the underwater acoustic communication model used or the manufacturer of the acoustic modem.

2.3.2 Synchronous Coordination Schemes

Synchronous coordination schemes use time synchronization among all sensor nodes before data transmission so that each sensor node wakes up at the proper time to send or receive data. It sleeps when there is no data to transmit or receive. Several synchronous coordination schemes have been reported and are presented as follows.

2.3.2.1 Sensor-MAC Protocol (S-MAC)

S-MAC [58] is an energy-efficient MAC protocol proposed for WSNs where the operation of sensor nodes alternates between wake-up mode and sleep mode for each cycle. The duty cycle was defined as the ratio of the length of time in sleep mode to the wake-up period.

S-MAC utilized a coordinated adaptive sleeping scheme with a small duty cycle. Sensor nodes mostly stay in an inactive state (sleep mode), only becoming active (wake-up mode) when detecting data packets. Thus, energy consumption for idle listening is reduced and the lifetime of the WSN is prolonged. By exchanging signalling packets, each sensor node maintains a table to record the schedules of all its neighboring nodes in order to wake up at the proper time to transmit data packets. Simulation results show that S-MAC consumes less energy than IEEE 802.11 and can achieve a prolonged network lifetime. Moreover, through its implementation on the UC Berkeley Mote [101], S-MAC was shown to achieve an effective balance between energy consumption and network throughput [58].

2.3.2.2 Timeout-MAC Protocol (T-MAC)

T-MAC improved the performance of S-MAC using a timer to dynamically terminate the active state (wake-up mode) in one cycle [59]. In T-MAC, the duration of an active state varied in different cycles in order to adapt to scenarios with different data volume, denoted as a dynamic wake-up schedule. Figure 2.2 illustrate a high-level comparison of the lengths of wake-up mode and sleep mode in S-MAC and T-MAC.

In T-MAC, sensor nodes can conserve energy by decreasing the time spent on idle listening and adaptively adjusting duty cycles to accommodate different traffic conditions. According to the simulation results, T-MAC outperforms S-MAC and CSMA in terms of average energy consumption, without compromising the network throughput. T-MAC was implemented on the hardware designed by the authors. The experimental results

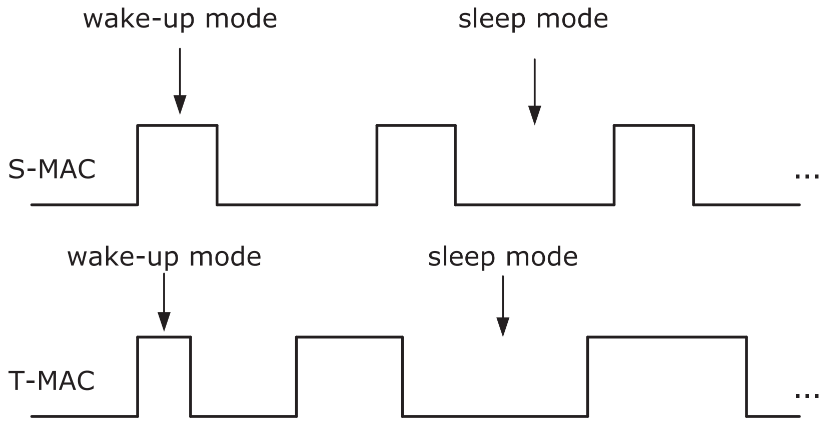

Figure 2.2: Comparison between S-MAC and T-MAC

indicated that T-MAC [59] outperforms S-MAC by a factor of five under different traffic load conditions.

2.3.2.3 Underwater Wireless Acoustic Networks MAC Protocol (UWAN-MAC)

Park and Rodoplu proposed the UWAN-MAC protocol for UWSNs [102] . UWAN-MAC is a distributed scalable energy-efficient MAC protocol using similar network operations of S-MAC. In the UWAN-MAC protocol, before data transmission, each sensor node broadcasts signalling packets (i.e., time stamp) which includes information about the amount of time in sleep mode during one cycle and records information transmitted by its neighboring nodes. In the long propagation delay scenario, the time stamp relaxes the stringent requirement for time synchronization and guaranteed that neighboring nodes would wake up at the correct time in order to receive data packets without the knowledge of the propagation delay. Figure 2.3 presents the basic idea of UWAN-MAC.

As shown in Figure 2.3, node A sends a time stamp to node B. When receiving the time

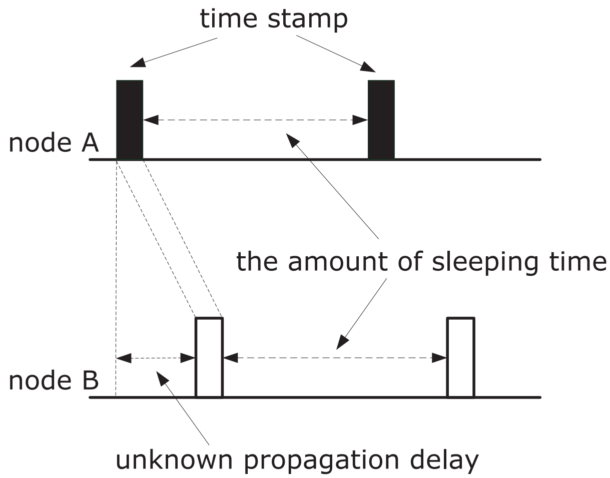

Figure 2.3: Basic idea of UWAN-MAC

stamp, node B wakes up at the correct time without the knowledge of the propagation delay because node B knows the amount of sleeping time of node A. Additionally, in UWAN-MAC, all sensor nodes were required to broadcast their time stamps when new sensor nodes are deployed in the network.

For S-MAC and T-MAC, when the number of nodes increases, energy consumption may increase due to frequent signalling packet exchange to ensure each sensor node has the knowledge of the schedules (i.e., time to wake-up and time to sleep) of all other nodes. In UWAN-MAC, communication overhead caused by broadcasting time stamps may degrade its performance and consequently limit the network lifetime. For UWAN-MAC, the transmitting power level was 10 W. However, the corresponding transmission range was not specified.

2.3.3 Asynchronous Coordination Schemes

In asynchronous coordination schemes, sensor nodes use different predetermined wake-up and sleep patterns for each cycle of network operations in order to achieve high energy efficiency and to guarantee network connectivity based on certain properties in linear algebra and optimization. No time synchronization is required in the network operations.

2.3.3.1 Quorum-based Energy Conserving Protocol (QEC)

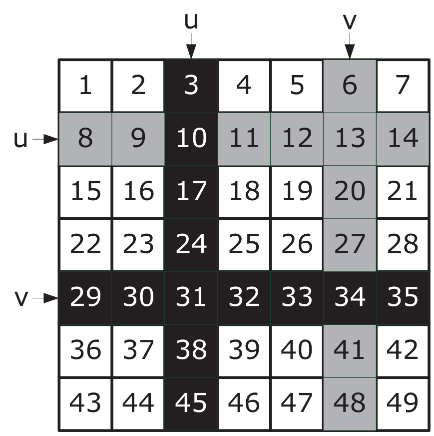

Figure 2.4: Basic idea of QEC

Quorum-based energy conserving protocol (QEC) [63] is an asynchronous wake-up scheme for ad hoc networks. QEC guarantees at least two overlapping active intervals between any two nodes in one cycle [63]. Figure 2.4 presents the basic idea of network operation in QEC. When node u and node v each arbitrarily choose a row and a column from a square of size n, respectively, their active intervals would overlap for at least two active slots, e.g., the 10-th and the 34-st slots shown in this figure (n=7). It is obvious that a large value of n can lead to better energy conservation but it would also increase the latency. Therefore, the authors in [63] proposed an adaptive QEC by varying the value of n to accommodate different traffic loads and thus achieve a balance between energy efficiency and packet delay. The simulation results showed that QEC can consume less energy than IEEE 802.11.

2.3.3.2 Cyclic Difference Set (CDS)-based Protocol

As a further improvement, the CDS-based protocol [64] determines the number and positions of active and inactive intervals (i.e., slots) in one cycle using a difference set of a ($\mathcal{V}$, k, λ)-balanced incomplete block design (BIBD) [103, 104], where $\mathcal{V}$, k, and λ represent the total number of slots, the number of active slots, and the minimum number of overlapping slots in one cycle, respectively. The detail of ($\mathcal{V}$, k, λ)-BIBD will be explained in Chapter 4. The CDS-based protocol guarantees at least one active overlapping interval between any two nodes for any cyclic shift.

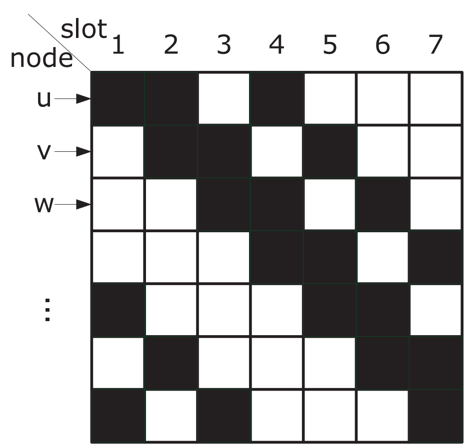

Figure 2.5: Example of the network operations in the CDS-based protocol

Figure 2.5 shows an example of network operations in the CDS-based protocol. In one period, each sensor node has seven slots including three active slots and four inactive slots ($\mathcal{V}$ = 7, k = 3, and λ=1). The positions of active slots and inactive slots were determined by the CDS. In the example shown in this figure, nodes choose their active slots in one cycle period shown as black square positions. There exists one active overlapping slot between any two nodes. That is, the network connectivity can be guaranteed by using the CDS.

2.3.3.3 Exponential Adaptive CDS-based Protocol (EACDS) and Multiplicative Adaptive CDS-based Protocol (MACDS)

In the QEC and the CDS-based protocols, all sensor nodes must operate using the same duty cycle; otherwise, they may fail to communicate with each other. Choi and Shen extended the CDS-based protocol and proposed two new approaches of sleeping pattern scheduling, i.e., the EACDS-based scheme and the MACDS-based scheme [62] . The key idea of these two schemes was the use of hierarchical arrangements of sets with the Kronecker product [105]. The EACDS-based scheme utilized a difference set scaled by another difference set, which is called the exponential set [62]. The scaling was done by the Kronecker product and guaranteed that there was at least one overlapping slot between any two EACDSs with different duty cycles. For example, a difference set ($\mathcal{V}_I$, k_I, λ_I), called an initial set, is scaled by another difference set ($\mathcal{V}_E$, k_E, λ_E), called an exponential set. Then, the higher level hierarchical set can be obtained by the Kronecker product, i.e., ($\mathcal{V}_I$, k_I, λ_I)$\otimes$($\mathcal{V}_E$, k_E, λ_E), where operator $\otimes$ denote the Kronecker product. The MACDS-based scheme used a multiplier set instead of the exponential set. All multiplier sets [62] were selected from the rotational set group (not difference sets). The performance evaluation revealed that the MACDS-based scheme conserves more energy whereas the EACDS is more suitable for scenarios where many different duty cycles co-exist. The EACDS-based scheme and the MACDS-based scheme were designed for ad hoc networks and delay tolerant networks (DTN). They may not be suitable for underwater applications, where the delay spread is large and multi-path propagation is significant. Therefore, the feasibility of these approaches must be carefully reexamined in the context of underwater applications.

2.4 Energy-Efficient Routing Protocols in WSNs and UWSNs

The routing protocols discussed earlier for WSNs put much effort into increasing throughput and decreasing packet delay and packet error rate. However, in power-constrained communication and long-term marine monitoring applications, data transfer with minimum energy consumption becomes more significant than merely improving network throughput. In this section, we summarize energy-efficient routing protocols for WSNs and routing protocols for 2D and 3D UWSNs.

2.4.1 Energy-Efficient Routing Protocols for WSNs

A large number of routing algorithms have been proposed to prolong the network lifetime and to balance the energy consumption among sensor nodes. Some routing algorithms employ linear programming (LP) to assign the amount of data flows in the network.

In wireless ad hoc networks, Chang and Tassiulas [70] formulated the routing problem as an LP problem to prolong the network lifetime in two scenarios: constant and arbitrary data packet generation rates. Additionally, the authors proposed a routing metric that reflected the transmitting power level on each link and the variation of residual energy of sensor nodes. The performance of the proposed routing algorithm was better in approaching the theoretical optimum (i.e., the maximum network lifetime obtained from LP) than that of some routing protocols widely used in WSNs such as minimum hop routing [106] and minimum total energy routing [107]. However, the proposed routing algorithm and the corresponding LP formulation only considered two cases: single-source-single-destination and limited number of source nodes. In these two cases, a large number of sensor nodes only acted as relays without generating their own sensing data packets.

Madan and Lall [71] proposed a set of distributed routing algorithms to maximize network lifetime by the LP and the sub-gradient algorithms. Utilizing the LP and the subgradient algorithms can achieve a low computational complexity and enable the optimal routing approach to converge quickly when the number of sensor nodes is large. However, the scenario of single-source or limited number of source nodes may not be realistic in some applications, where every sensor node has to transmit its own data packets. Gatzianas and Georgiadis [108] extended the research work in [70, 71] to the application of data gathering in WSNs by a mobile sink. They define the network lifetime as the period of time during which the network is able to route a feasible flow to each sink location. The feasible flows of different links were assigned by the LP and the sub-gradient algorithms. The authors concentrated on imposing flow conservation to all possible locations of the sink node and on removing some trivial constraints in the LP problem so that the optimization problem can be solved efficiently. The solution combined the standard sub-gradient algorithm and the minimum cost network flow algorithm. These two algorithms can achieve a low computational complexity even for large-scale and high-density networks.

2.4.2 Routing Protocols for 2D UWSNs

2.4.2.1 Focused Beam Routing Protocol (FBR)

The focused beam routing protocol (FBR) [52, 109] minimizes energy consumption by dynamically selecting an ideal relay located in the cone of a transmitter. Each source node knows its own position information and the position of the destination node. The source node utilizes RTS and CTS packets to search possible relay candidates, which are performed by multicasting with different transmitting power levels and different angles of cones. After sending the RTS packet, a sending node is able to increase the transmitting power level if no sensor node replies with a CTS packet. A receiving node closer to the sending node is given a higher priority to be selected as a relay node than those further away. The performance of FBR may degrade in sparsely-distributed UWSNs when only a few sensor nodes are in the cone of the transmitter. The large overhead caused by the frequent exchange of RTS/CTS packets may shorten the network lifetime. For data transmission, 0.65 W, as the transmitting power level, can achieve 2000 m in FBR. These values are quite different from those in related literature [52, 110]. Such low power levels have not been shown to achieve such long transmission ranges elsewhere in the literature, nor are these numbers consistent with any available acoustic modem.

2.4.2.2 Routing Protocol with Node Replacement Policy

In order to reduce the overhead of signalling packet exchanges, Mohapatra *et al.* [111] fully utilized the position information of sensor nodes when designing routing algorithms. They considered a more concrete application of UWSNs such as seismic monitoring, and proposed a routing algorithm combined with node replacement policies (i.e., fixed interval replacement, fixed residual energy with percentage-based replacement, and fixed residual energy with day-based replacement), formulated as a mixed integer programming problem. In [111], the base routing algorithm was the minimum-hop routing algorithm [106], which means that the relay candidates should reach the sink node via fewer hops compared to the source node. However, the residual energy was not taken into consideration in routing. Therefore, the sensor nodes closer to the sink node tended to quickly exhaust their energy because more data packets are forwarded through them.

2.4.3 Routing Protocols for 3D UWSNs

2.4.3.1 Vector based Forwarding Routing Protocol (VBF)

To address packet losses and sensor node failures (e.g., energy exhaustion) in 3D UWSNs, VBF was proposed by Xie *et al.* [112]. In VBF, a routing vector was defined as a virtual routing pipe between a source and a destination. If a node is close to the routing vector (i.e., less than a predetermined distance threshold), this node adds its own position in the packet and forwards the packet. Otherwise, this node will not participate in forwarding. The low density of the UWSN may lead to forwarding failures because few nodes are located in proximity to the routing vector, which is similar to FBR. In VBF, the authors used a commercial acoustic modem UWM1000 manufactured by LinkQuest [112, 113]. The transmitting power was 2 W with the transmission range of 100 m. The paper does not specify the underwater acoustic channel model used and other environmental parameters such as noise level and modulation scheme.

2.4.3.2 Q-learning-based Adaptive Routing Protocol (QELAR)

As an improvement of VBF, QELAR aimed to prolong the network lifetime by balancing the energy consumption among sensor nodes deployed in 3D UWSNs [114]. A reinforcement learning technique was employed as the theoretical foundation of QELAR. The routing decision in 3D UWSNs was mapped to the general framework of the reinforcement learning technique. The reward function, as an essential component of the reinforcement learning technique, was introduced in QELAR by taking into account the residual energy of sensor nodes. This reward function provides adequate relay candidates to make routing decisions. QELAR outperforms VBF in terms of packet delivery rate and packet delay. However, frequent updates of operation environmental information, such as the residual energy of neighboring nodes and the average energy consumption in a group of sensor nodes, was the bottleneck of QELAR. Another issue of QELAR was that each sensor node must keep constantly awake in order to receive the residual energy information of neighbouring nodes.

2.4.3.3 Distributed Routing Algorithms based on Packet-Train Transmission

The packet-train transmission scheme [51] was proposed to decrease the packet error rate and increase the acoustic channel utilization in underwater acoustic communication. As shown in Figure 2.6, a sending node transmits a juxtaposition of short data packets (called a packet-train) before releasing the current acoustic channel.

The corresponding receiving node can reply with an acknowledgement (ACK) packet for each packet-train and specify the packets missed in the current packet train to be included in the next packet-train. The size of the packet-train, which is the key issue of this problem, was formulated as an offline optimization problem by considering the length of data packet header and ACK, and the propagation delay of the acoustic signal. The routing protocol in [51] can achieve minimum energy consumption during data transmission in 3D UWSN without compromising the packet error rate. It is possible for the cost of retransmission to become fairly high when the underwater acoustic channel deteriorates. A maximum transmitting power of 0.5 W was used in the work, but the transmission range and the

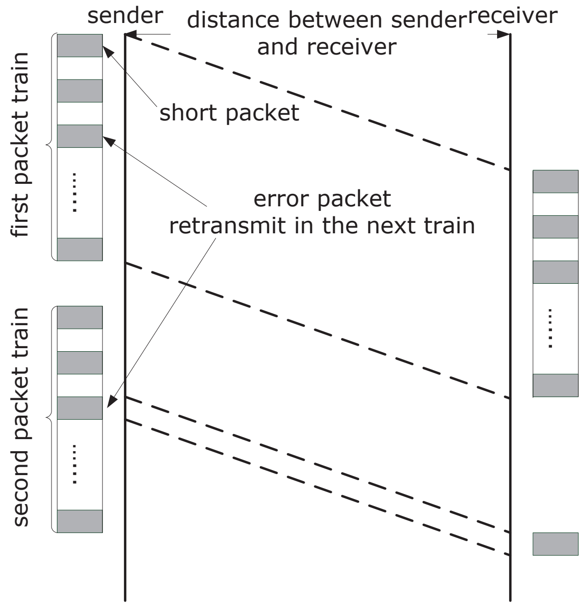

Figure 2.6: Illustration of packet train in UWSNs

underwater acoustic channel model are not specified.

2.4.3.4 Linear Coded Digraph Routing Scheme (LCDR)

LCDR [115] aimed to increase the end-to-end throughput of the TCP and to improve the link reliability for military applications. Before forwarding data packets, network coding was performed by the sensor nodes located on the seafloor and surface. A multipath routing algorithm was a critical component of LCDR, which employed a directed acyclic graph (DAG) to construct a multipath from the source node to the destination. Sensor nodes only transmit high-priority data packets (data packets are given high priority when the buffer is almost full) without network coding. Low priority packets were transmitted as a linear combination of data packets (i.e., coded packet). The end-to-end throughput can be significantly improved by utilizing network coding and novel buffer management. The traffic loads in the simulation were not entirely realistic and may lead to a short network lifetime due to the limited amount of battery energy of underwater acoustic sensor nodes. Moreover, the network coding operation required each sensor node to stay awake to decode the coded packets during data transfer, which may increase its energy consumption.

2.5 Data Collection Using Mobile Sinks

Data collection using mobile sinks has been studied in WSN in recent years aiming at increasing data delivery rates and decreasing packet delay. Underwater acoustic channel characteristics are different from terrestrial wireless channels, in particular, large propagation delay and severe signal attenuation. An AUV, as a controllable mobile sink, can be used to gather data from sensor nodes deployed in UWSNs. AUVs can also sense, collect, and transmit data using sensors and acoustic modems equipped on its cabin. In this section, we present the data collection schemes reported in the literature, where mobile sinks are used, both for WSNs and UWSNs.

2.5.1 Data Collection Using Mobile Sinks in WSNs

Luo and Hubaux [116] proposed an energy-efficient data collection scheme using a mobile sink. They first described the traffic load distribution in WSNs with a static base station. Sensor nodes near the base station exhaust their batteries quickly due to forwarding a large volume of data. To prolong the network lifetime, the authors introduced a mobile sink and proposed a routing metric by jointly considering the sink mobility and the traffic load balance. The trajectory of the mobile sink was analysed to achieve an energy-efficient data collection. The simulation results showed that the proposed data collection scheme achieves a 500% improvement of the network lifetime compared to the scheme using the static base station.

To further reduce energy consumption of sensor nodes, Gao, Zhang, and Das proposed an efficient data collection scheme [117] for WSNs where the mobile sink moves along a predetermined path. All sensor nodes can transmit data packets to the mobile sink directly through one hop or multiple hops. The authors formulated the problem of maximizing the amount of collected data with shortest paths (MASP) as a 0-1 integer linear programming problem, aimed at balancing the energy consumption of sensor nodes and the total amount of collected data [117]. An algorithm with 2D binary chromosomes was proposed to solve the MASP problem with low computational complexity. Additionally, a two-phase protocol based on the communication zone partition without the position information of sensor nodes was proposed to achieve a balance between computational complexity and energy efficiency of sensor nodes.

To reduce the packet latency and increase the network throughput in WSNs with a mobile sink, Xing *et al.* proposed two algorithms to calculate proper paths for the mobile sink [118]. The first algorithm utilized the Steiner Minimum Tree to search paths from source nodes to the mobile sink, which allowed the mobile sink to efficiently collect data with a short tour. In the second algorithm, the mobile sink collected the data from sensor nodes following a fixed track. The authors provided an algorithm to balance the energy consumption of sensor nodes and the data packet delay.

For the sparsely-distributed WSNs, Song and Hatzinakos [119] proposed a transmission scheduling algorithm aiming to maximize the successful data transmission probability and to minimize the energy consumption of sensor nodes. The path of the mobile sink was predetermined. The optimization was formulated by the framework of dynamic programming using a simplified model, i.e., single-node-to-sink transmission. The proposed transmission scheduling algorithm can also be used in applications of highway traffic surveillance.

2.5.2 Data Collection Using AUVs

As controllable mobile sinks, AUVs have been widely used for scientific data sensing and collection, object detection, and military surveillance. In [120], an efficient path-planning algorithm was proposed for searching a feasible trajectory of AUVs from 2D underwater imagery. The authors presented a fast marching-based approach for AUVs path-planning by jointly considering the computational efficiency and the computational accuracy [120]. Additionally, the fast marching-based approach allowed the curvature of the path to be constrained, which enabled consideration of the turning radius of AUVs. An anisotropic fast marching-based algorithm was proposed to deal with underwater currents and can be extended for similar directional constraints. In [120], the ocean was assumed to be static and environmental conditions were assumed to be known *a priori*.

An experimental platform of UWSNs for long-term monitoring of coral reefs and fisheries was presented in [121]. The acoustic communication was only used for navigation and signalling packet exchange. AUVs hovered near sensor nodes (located on the seafloor) and collected and stored the data from sensor nodes via high-speed optical communication. Optical data transmission can increase the network throughput and decrease the packet delay in seawater. However, the underwater optical communication heavily relies on the marine environment and communication distance. The navigation and control technique becomes significant when using the optical link because the optical signal cannot achieve a long communication range as shown in Table 2.2.

Hollinger *et al.* studied the data gathering problem using AUVs [8]. Their objective was to achieve a balance between the amount of collected information and the traveling time of the AUV (the AUV was assumed to be energy limited). The AUV path planning problem was formulated as the traveling salesperson problem (TSP), which was categorized into two kinds: the deterministic prize-collecting TSP and the TSP with neighboring nodes. In the deterministic prize-collecting TSP, for the AUV, all sensor nodes (located on the seafloor) were not required to be visited. A penalty function was assigned to each sensor node based on the corresponding information content. The AUV neglects some sensor nodes and pays the required penalty. An example of the TSP with neighboring nodes is shown in Figure 2.7. The AUV visited the center of a covered set of neighborhoods and the objective of this problem was to search a covered set of probabilistic neighborhoods.

Time Division Multiple Access (TDMA) and random access (similar to ALOHA) were two scheduling protocols used to evaluate the performance of two TSPs when an AUV

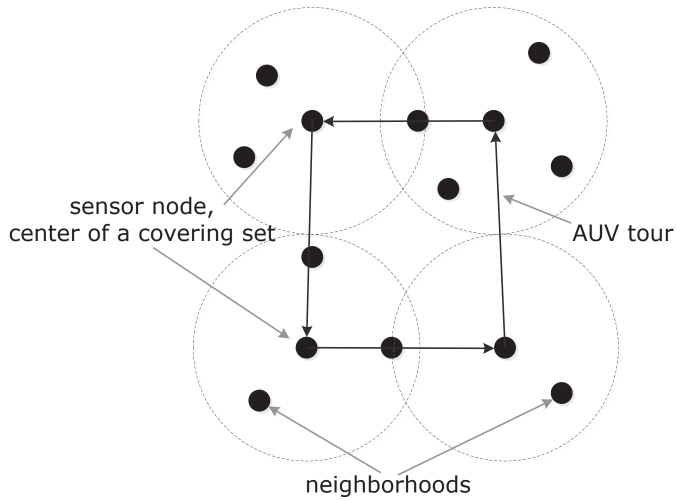

Figure 2.7: Example of the TSP with neighboring nodes

communicates with multiple sensor nodes [8]. The simulation results showed that proper underwater communication models and scheduling protocols were important elements of selecting an appropriate path planning algorithm. Furthermore, the path planning algorithm can be utilized in UWSNs with different densities and different requirements of information quality. Although the underwater acoustic channel model and the acoustic modem (i.e., Micro-modem) were provided [8], the paper does not specify the transmitting and receiving power levels and the corresponding transmission range.

AUVs can be equipped with various sensors for monitoring different marine environment parameters. In [122], the authors proposed a task allocation framework for AUVs participating as a team to execute missions under energy-limited communication conditions. Two kinds of AUVs were utilized in the task allocation framework: propeller-driven vehicles and gliders. The propeller-driven vehicle is battery-operated with high maneuverability while the glider can provide higher resolution data of ocean explorations with a low speed. Figure 2.8 presents the deployment of AUVs in seawater and the communication among AUVs and a surface ship.

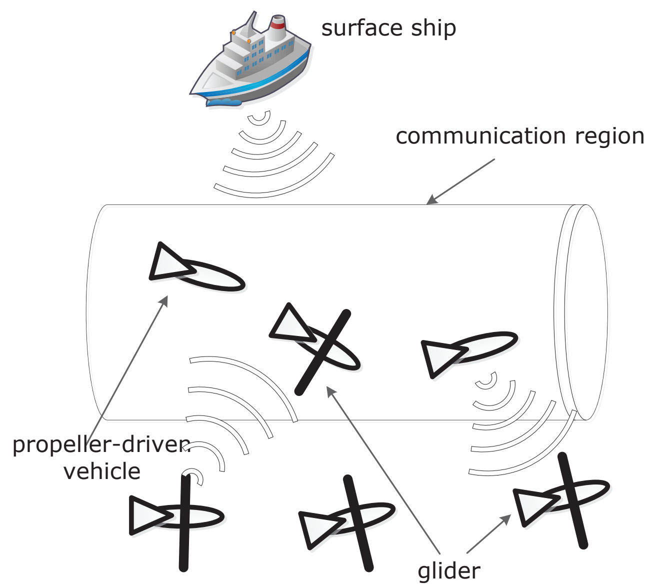

Figure 2.8: Illustration of the communication between propeller-driven vehicles and gliders

As a result of the task allocation framework, the formed team was a subset of AUVs that was better suited to accomplish the mission with energy constraints and application requirements. Four different criteria were considered in the task allocation framework: 1) the communication region size and the underwater acoustic communication overhead (caused by signalling packet exchange); 2) underwater currents in the communication region; 3) the relationship between underwater currents and communication regions; and 4) the energy efficiency between a team of only gliders and a team of only propeller-driven vehicles. The simulation results were related to energy consumption. However, the paper does not present the power consumption parameters of the underwater communication in the propeller-driven vehicle or the gliders.

2.6 Power Consumption Parameters used in the Literature

In this section, we summarize in Table 2.3 the power consumption parameters, which are used in different schemes for UWSNs as discussed in previous sections. In general, in underwater acoustic communications, the transmitting power level is much higher than the receiving power level. The listening power is lower than the receiving power. Note that the majority of the papers in the literature do not provide enough information such as underwater acoustic channel models, transmission range, noise level, transducer efficiency, and operation frequency. For the same acoustic modem, different parameters such as transmitting power level and transmission range are used in different papers. It is extremely difficult to take guidance from these papers to select meaningful parameters due to lack of adequate information. However, from Tables 2.2 and 2.3, we observe that the transmitting and receiving power levels dominate energy consumption during data transmission. We detail the underwater acoustic channel model and the configuration of energy consumption parameters in Chapters 3, 4, 5, 6, and 7 before presenting simulation results.

Table 2.3: Configuration of power consumption parameters in different literatures

Protocol/Scheme	Transmitting power (W)	Receiving power (W)	Transmission range (m)	Acoustic modem
T-Lohi [44]	2	0.02	500	SNUSE
CUMAC [100]	0.6	N/A	500	N/A
UWAN-MAC [102]	10	3	N/A	Micro-modem
FBR [48]	0.65	0.08	2000	N/A
VBF [112]	2	0.75	100	UWM1000
QELAR [114]	10	3	75	N/A
Distributed routing [51]	0.5	N/A	N/A	Micro-modem
Hollinger, etc. [8] (AUV data collection)	N/A	N/A	N/A	Micro-modem
Basagni, etc. [43] (optimized packet size)	0.12[1]	0.1	N/A	N/A

[1] The transmitting power is 0.12 W for a transmission distance of 1 m in [43]. The maximum transmitting power and the corresponding transmission range are not specified.

2.7 Terms Used in the Thesis

The following terms are defined and used for the following chapters.

- **Sink node** – a sensor node that has the additional responsibility to collect information from all other sensor nodes and send this information to the surface node.
- **Source node** – any sensor node except the sink node.
- **Relay node** – a sensor node that receives information from a source node or another relay node, and forwards this information to the sink node or another relay node.
- **Sending node** – a source or relay node that is sending information to a relay node or sink node.
- **Receiving node** – a sink or relay node that is receiving information from a relay or source node.
- **One-hop node** – a sensor node that is within the transmission range of the sink node.
- **Traffic intensity** – number of data packets per day that every sensor node reports to the sink node.

2.8 Summary

In this chapter, we presented different statistical underwater acoustic channel models derived from sea trials. It is difficult to determine which one of these models is the best because of the temporal and spatial variation of the underwater acoustic channel. We summarize several sea trials in different aspects. We compared different underwater acoustic modems and an underwater optical modem used for academic and commercial purposes. Power consumption parameters of the Micro-modem and the EvoLogics modem were used for energy consumption calculations in the dissertation. Different coordination schemes for WSNs and UWSNs were investigated. Routing protocols aiming at energy-efficient data transmission and network lifetime extension are also reviewed for both WSNs and UWSNs. Additionally, different data collection schemes with mobile sinks were presented. The objectives of data collection schemes are reviewed, which may vary based on different application requirements, such as decreasing packet latency, increasing network throughput, and achieving energy-efficient data transmission.

Chapter 3

Acoustic Propagation Properties of Underwater Communication Channels

The propagation properties of acoustic signals in seawater have been researched in the past 50 years in order to gain a basic understanding of underwater communication. A number of underwater acoustic models have been developed to investigate the underwater acoustic channel in terms of transmission range, communication frequency, and transmission loss of acoustic signals. Because of the time varying and space varying nature of the underwater acoustic channel, these models exhibit different strengths and limitations. This chapter[1] is meant to investigate the intrinsic propagation characteristics of acoustic signals and their transmission loss in seawater, which are required to explore and develop new network protocols for UWSNs. We first outline the properties of acoustic signal propagation in

[1]The material in this chapter has been presented at IEEE ICC'12 [123]

seawater, including the sound speed profile, the absorption loss of acoustic signals, and the principle of transmission loss. Then, we compare the normal mode model to the ray-theoretical model. As well, we present a semi-empirical formula for transmission loss estimation, and three different approaches to transmission loss calculation based on the ray-theoretical model. We use the Bellhop program [124] to evaluate the effects of different environmental parameters such as the ocean bathymetry data on the transmission loss of acoustic signals.

3.1 Acoustic Signal Propagation Properties in Seawater

In this section, we present the sound speed profile, the absorption loss of the acoustic signal in seawater and the principle of transmission loss, which are the basic propagation characteristics of the acoustic wave in seawater.

3.1.1 Sound Speed Profile

The sound speed profile is a fundamental set of oceanographic parameters that determine the behavior of sound propagation in the ocean. Many empirical formulas have been developed to calculate the sound speed in seawater with respect to water temperature, salinity, and pressure (or depth). A simple and commonly used sound speed formula is given by [21]:

$$\begin{aligned} v_s = {} & 1449.2 + 4.6\mathrm{T} - 0.055\mathrm{T}^2 + 0.00029\mathrm{T}^3 \\ & + (1.34 - 0.01\mathrm{T})(s - 35) + 0.016 d_e, \end{aligned} \tag{3.1}$$

where v_s is the sound speed in seawater in meters per second, T is the water temperature in degrees Celsius, s is the salinity in parts per thousand and d_e is the depth of seawater in meters.

The sound speed profile can be generally divided into several layers associated with different temperature distributions in Figure 3.1.

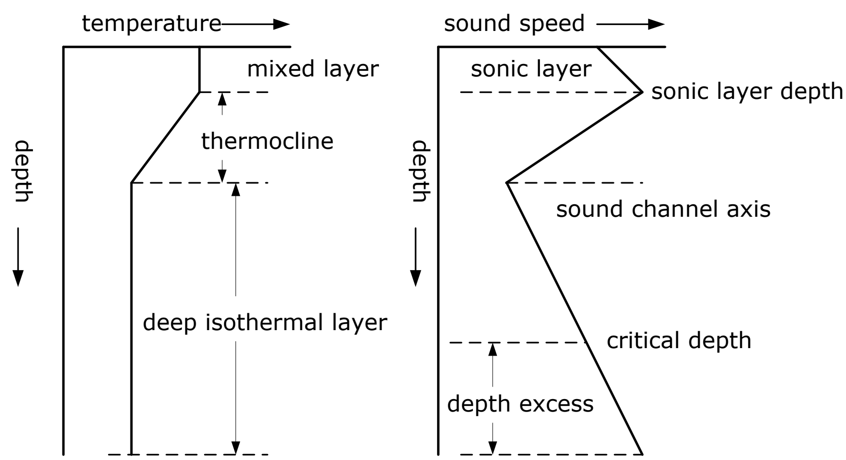

Figure 3.1: The relationship between sound speed and temperature [19]

The sonic layer is below the sea surface that is usually associated with a well-mixed layer of near-isothermal water, called the mixed layer [19]. In this layer, the sound speed is affected by the changes in heating, cooling, and wind action. The sound speed also increases with the depth because of the pressure impact. Moreover, the upward refraction of the sound wave keeps the acoustic energy concentrated near the surface. Thus, the sound wave can propagate over a long range [21].

The thermocline is below the mixed layer [20], where the sound speed decreases with the depth due to the decrease of water temperature. The deep isothermal layer is below the thermocline and extends to the sea floor, where the water temperature changes little. In this layer, the sound speed increases with the depth because of the water pressure and the sound-speed profile become nearly linear with a positive gradient.

The minimum sound speed can be obtained between the negative sound speed gradient in the thermocline layer and the positive sound speed gradient in the deep isothermal layer [20, 21]. The corresponding depth is defined as the sound channel axis. The intensity of acoustic signals over the sound channel axis maintains well because acoustic signals experience little transmission loss from the reflections at the surface and bottom. Therefore, very long range propagation can be achieved [125].

3.1.2 Absorption Loss in Seawater

Signal attenuation in seawater typically consists of absorption loss, diffraction, and scattering. It is sufficient to consider the absorption loss as the main source for signal attenuation [21]. Different empirical formulas to describe absorption have been proposed by researchers in the past 50 years [20, 21]. A simple and efficient formula that describes the frequency dependent absorption was proposed by Thorp in 1967 [21, 125]:

$$10 \log a(f) = \frac{0.11 f^2}{1 + f^2} + \frac{44 f^2}{4100 + f^2} + 2.75 \times 10^{-4} f^2 + 0.003, \tag{3.2}$$

where f is the center frequency of the sound source and $a(f)$ is the absorption coefficient of the acoustic signal. This formula is under a temperature of 4 ℃, a Ph of 8.0, and a depth of about 1,000 m. This formula is suitable for low frequency region (100 Hz ~ 3 kHz), and it holds well to approximate the measurement results for frequency above 3 kHz. This formula is sufficiently accurate for most problems in ocean acoustics [19]. Figure 3.2 shows the absorption coefficient graph from this equation.

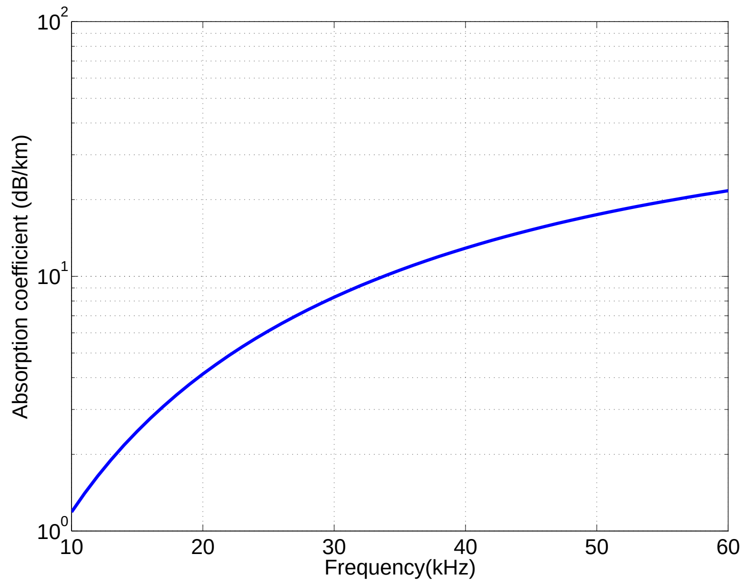

Figure 3.2: Absorption coefficient of the acoustic signal in seawater [21]

3.1.3 Transmission Loss

Transmission loss is defined as ten times the logarithm (the base is 10 in the subsequent equations) of the ratio of the reference intensity, denoted by I_{ref} in W/m^2, measured at a point 1 m from the source to the intensity I in W/m^2, measured at a distant point in decibels [21]:

$$TL = 10 \log \frac{I_{\text{ref}}}{I}. \tag{3.3}$$

In seawater, the transmission loss of the acoustic signal, expressed in decibels, can be considered to be the sum of geometrical spreading loss and absorption loss [20]. The geometrical spreading loss measures how the acoustic signal weakens when it propagates outward from the sound source. In general, two important types of the geometrical spreading include spherical spreading and cylindrical spreading, as shown in Figure 3.3 [21]. In Figure

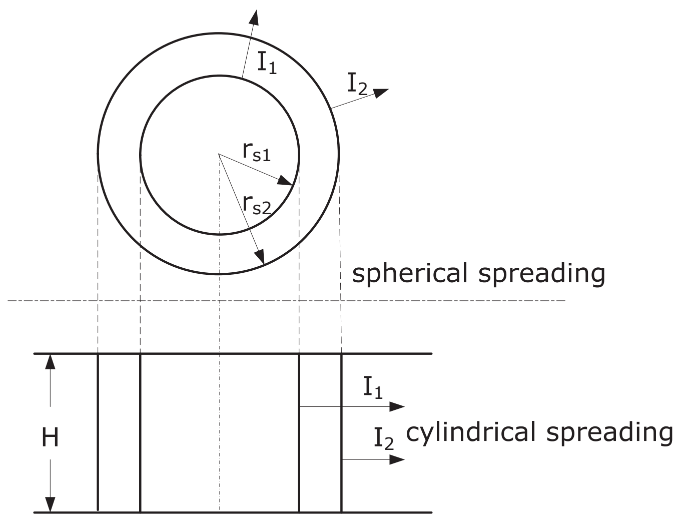

Figure 3.3: Illustration of spherical and cylindrical spreading

3.3, a point sound source is assumed in an unbounded homogenous medium. The power of sound intensity is identical in each direction in this medium. Therefore, the sound energy is homogenously distributed at the spherical surface. The power at the spherical surface, denoted by p_{sp} in W, can be expressed by:

$$p_{sp} = 4\pi {r_{s1}}^2 I_1 = 4\pi {r_{s2}}^2 I_2, \tag{3.4}$$

where I is sound intensity. r_{s1} or r_{s2} is the radius of sphere. If $r_{s1} = 1$ m, the spreading loss, i.e., the transmission loss, denoted by TL, at r_{s2} is

$$TL = 10 \log \frac{I_1}{I_2} = 10 \log {r_{s2}}^2 = 20 \log r_{s2}. \tag{3.5}$$

When the medium has plane upper and lower boundaries as shown in the bottom part of Figure 3.3, the geometrical spreading is not spherical because the sound cannot pass the boundaries. In this case, the power of sound source is distributed in the cylindrical surface. $\mathcal{H}$ is the distance between the upper and lower boundaries. The power at the cylindrical surface, denoted by p_{cy} in W, can be expressed by:

$$p_{cy} = 2\pi r_{s1} \mathcal{H} I_1 = 2\pi r_{s2} \mathcal{H} I_2. \tag{3.6}$$

If $r_{s1} = 1$ m, the spreading loss at r_{s2} is

$$TL = 10 \log \frac{I_1}{I_2} = 10 \log r_{s2} \tag{3.7}$$

In general, the spherical spreading loss exists in the near range and the cylindrical spreading loss exists in the moderate and long ranges. To obtain a relatively accurate transmission loss of acoustic signal propagation in the ocean, a popularly used semi-empirical formula, by jointly considering the geometrical spreading loss and the absorption loss, is discussed discussed in Section 3.2.2.4.

3.2 Underwater Acoustic Channel Models and Transmission Loss

According to the different approaches to solve the wave equation, underwater acoustic channel models fall into two categories: the normal mode model and the ray-theoretical model [126, 127]. In this section, we review and compare these two models. Three different approaches to transmission loss calculation based on the ray-theoretical model and the semi-empirical formula are studied.

3.2.1 Comparison between Normal Mode Model and Ray-Theoretical Model

In the normal mode model, the eigenfunctions of normal mode are used to describe the sound propagation in seawater. Each eigenfunction is a solution of the wave equation. Adding all normal modes can satisfy the boundary and source conditions when the seafloor is assumed to be a perfect reflection plane [20, 126]. In contrast, based on the assumption on existence of wavefronts and rays, the ray-theoretical model considers the acoustic waves as a beam of rays that establish the different paths from the sound source to the corresponding receiver. The acoustic energy can be easily described and calculated using the ray-theoretical model [19]. Furthermore, the ray-theoretical model can provide a clear description on the transmission loss estimation by assuming the ocean as a horizontally stratified medium. The surface and bottom of the ocean are also assumed to be horizontal planes [127]. Table 3.1 compares the normal mode model and the ray-theoretical model.

Table 3.1: Ray-theoretical model versus Normal mode model

	Ray-theoretical model	Normal mode model
Principle	sound-ray diagram	eigenfunction of normal mode
Application scope	high frequency & near field	low frequency & far field
Limitation	1. difficult to model diffraction 2. curvature radius of rays cannot have a big change in a wavelength	1. solution explanation 2. practical boundary condition 3. higher computational complexity

As discussed in Table 3.1, the ray-theoretical model is more suitable for applications where the center operating frequency is higher. Moreover, the ray diagram clearly describes the propagation of the acoustic signal in seawater, which can be used to calculate the transmission loss with low computational complexity. In the next section, we study three different approaches to transmission loss calculation based on the ray-theoretical model and a semi-empirical formula that is widely used in practice.

3.2.2 Three approaches of Transmission Loss Calculation and Semi-Empirical Formula

Based on the ray-theoretical model, three different ways of transmission loss calculation can be derived from the acoustic pressure field, which are the coherent transmission loss, the incoherent transmission loss, and the semi-coherent transmission loss [20]. Compared to the semi-empirical formula [19, 21] (we discuss lately), these three ways of transmission loss calculation tend to better describe the sound propagation and estimate the transmission loss by considering the ocean as a horizontally stratified medium and assuming the surface and bottom of the ocean as horizontal planes. Therefore, these three ways are considered to be relatively accurate and the semi-empirical formula provides a convenient approach to estimate the transmission loss in the complicated marine environment. In general, one of these methods can be selected based on the environmental information availability and the accuracy desired.

3.2.2.1 Coherent Transmission Loss

For the coherent transmission loss, the pressure field at all measurement points involves all eigenrays, which means that the pressure of each eigenray j, denoted by P_j, contributes to the complex pressure based on its intensity and phase. The pressure field is obtained by summing up the contributions of all eigenrays. The distance between the sound source and the receiver is d_{sr} and the depth of the sound source in the ocean is z. The sound pressure, denoted by $P_{so}(d_{sr}, z)$, can be expressed by:

$$P_{so}(d_{sr}, z) = \sum_{j=1}^{N(d_{sr},z)} P_j, \tag{3.8}$$

where $N(d_{sr}, z)$ is the total number of eignrays [127].

3.2.2.2 Incoherent Transmission Loss

The coherent transmission loss can provide accurate estimation. However, the details of the interference patterns and the accurate environmental information will likely be unavailable [20]. On the other hand, the evaluation of sonar performance or network performance may only need an approximate transmission loss. The incoherent transmission loss is introduced by ignoring the phase of the pressure associated with each eigenray. The pressure field now becomes

$$P(d_{sr}, z) = \left[\sum_{j=1}^{N(d_{sr},z)} \left| P_j \right|^2 \right]^{\frac{1}{2}}, \tag{3.9}$$

where $|\cdot|$ returns the absolute value of sound pressure [19].

3.2.2.3 Semi-coherent Transmission Loss

For many practical applications, a solution which can keep its characteristics insensitive to the detailed environmental information and can smooth out other characteristics that cannot be predicted would be highly desirable [20]. Many different techniques in this category tend to be informal and often partially empirical solution based. One example of the solution for semi-coherent transmission loss calculation is given by

$$P(d_{sr}, z) = \left[\sum_{j=1}^{N(d_{sr},z)} W(\theta) \left| P_j \right|^2 \right]^{\frac{1}{2}}, \tag{3.10}$$

where $W(\theta)$ is the shading function used to weight the amplitude of a ray as a function of its launching angle [128].

3.2.2.4 Semi-empirical Formula

Marsh and Schlkin [21, 52] proposed a semi-empirical formula for transmission loss calculation without considering particular propagation conditions:

$$10 \log_{10} TL = \mathcal{K} \cdot 10 \log_{10} d_{sr} + (d_{sr}/10^3) \cdot 10 \log_{10} a(f), \tag{3.11}$$

where $\mathcal{K} = 1$ is for cylindrical spreading, $\mathcal{K} = 2$ is for spherical spreading, and $\mathcal{K} = 1.5$ is for the transition region. $a(f)$ is the absorption loss, calculated by Equation 3.2.

In Acoustic Toolbox, finite element analysis is utilized to estimate transmission loss of acoustic signals [128, 129]. However, finite element analysis is computationally intensive and time consuming. The semi-empirical formula given by Equation 3.11 can be considered as a good alternative to achieve the balance between accuracy and computational complexity for the estimation of transmission loss of acoustic signals in seawater. In the next section, we compare these methods under a set of the real environmental parameters.

3.3 Simulation Results

In this section, we compare three approaches to transmission loss calculation based on the ray-theoretical model against the semi-empirical formula by different depths of seawater and the bathymetry data.

3.3.1 Simulation Settings

The environmental parameters in our studies are from the coast of Newfoundland at 46°29.5'N ~ 48°29.4'W. Two different depth levels, which correspond to shallow water (i.e., 100 m) and deep water (i.e., 3,000 m) conditions, are considered. The corresponding sound speed profiles are shown in Figure 3.4(a) and Figure 3.4(b), respectively, which are from National Oceanic and Atmospheric Administration (NOAA) [130]. The sound source and the receiver are assumed to be located at the same depth. The sound source is omnidirectional with a center frequency of 30 kHz.

3.3.2 Transmission Loss in Shallow Water

In order to assess the impact of depth on transmission loss, we consider four locations where the sound source and the receiver are placed at 10 m, 25 m, 50 m, and 95 m from the ocean surface, respectively. The horizontal distance between the sound source and the receiver is 3000 m for long-haul transmissions. Seafloor is assumed to be flat and rigid.

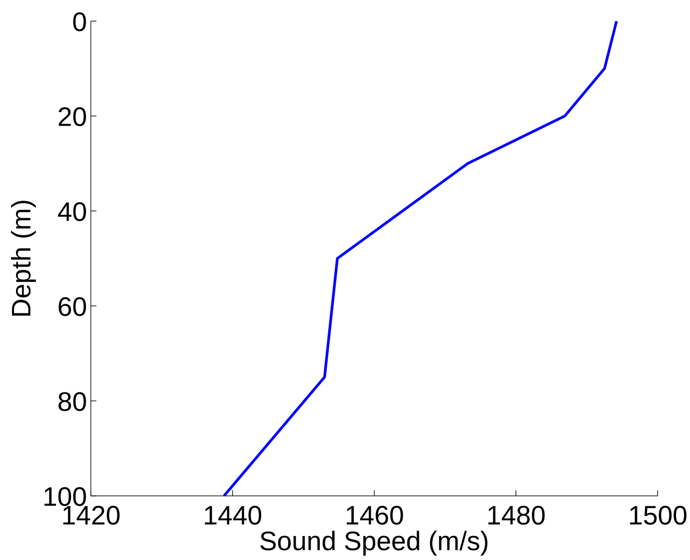

(a) Shallow Water

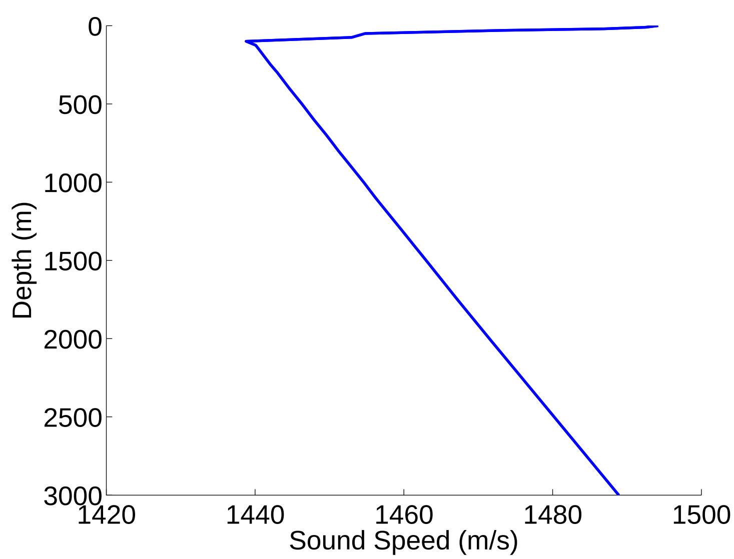

(b) Deep Water

Figure 3.4: Sound speed profile

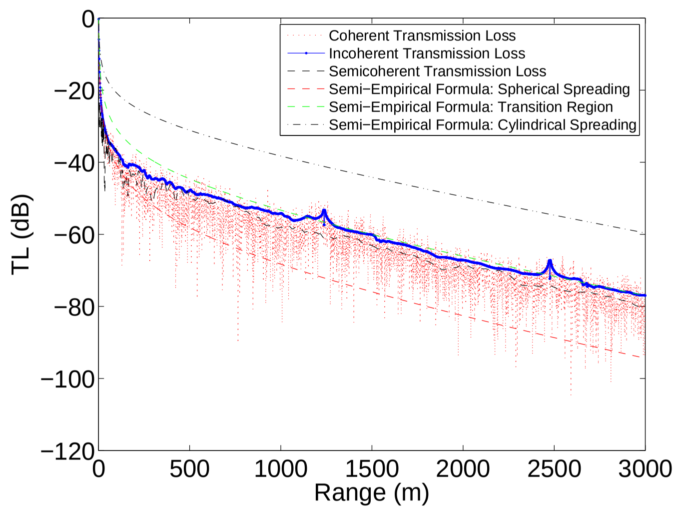

Figure 3.5: Shallow water: sound source depth = 10m

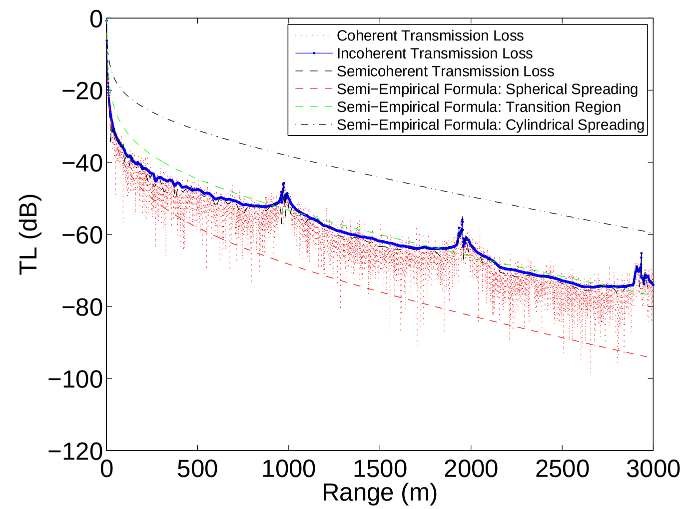

Figure 3.6: Shallow water: sound source depth = 25m

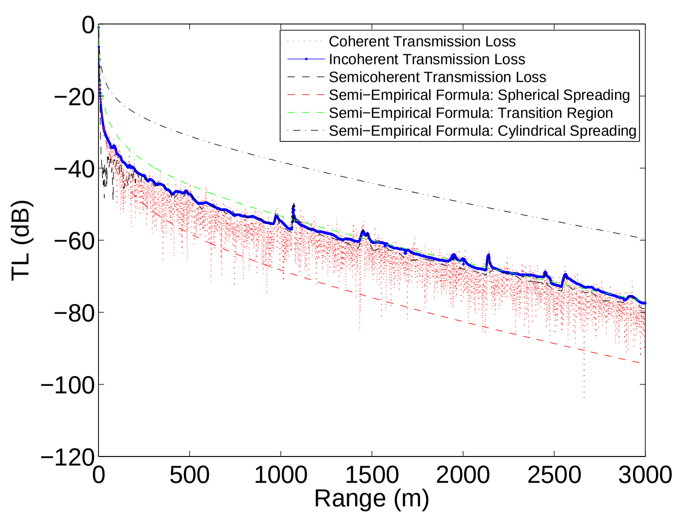

Figure 3.7: Shallow water: sound source depth = 50m

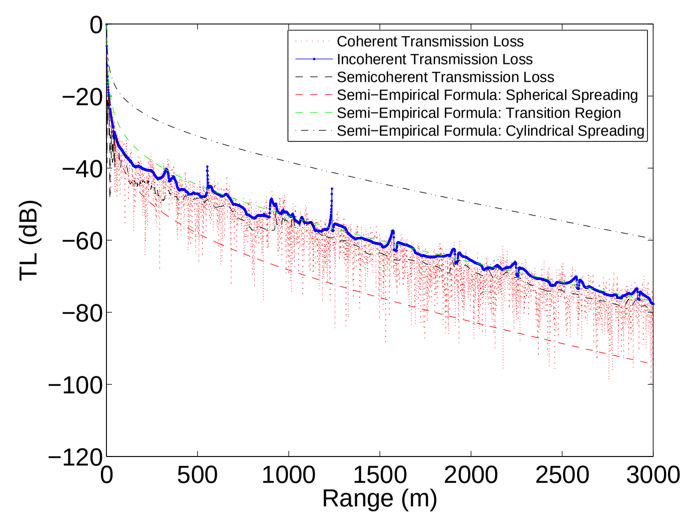

Figure 3.8: Shallow water: sound source depth = 95m

Figures 3.5, 3.6, 3.7, and 3.8 compare the transmission loss calculated based on ray-theoretical approach and the semi-empirical formula in shallow water condition. In these figures, we can observe the same trends for both approaches for the near field: the coherent transmission loss (red point), the incoherent transmission loss (blue line), and the semi-coherent transmission loss (black dash line) are larger than the results from the semi-empirical formula with $\mathcal{K}$ = 1.5 (green dash line). However, for the far field, transmission loss results from the ray-theoretical model fluctuates around the results from the semi-empirical formula ($\mathcal{K}$ = 1.5). On the other hand, among the three approaches of transmission loss calculation from the ray theory, the coherent transmission loss has more fluctuation than the other two approaches. As expected, compared with the coherence transmission loss, the incoherent transmission loss (blue line) has less fluctuation as the phase information of rays is not considered. Semi-coherent transmission loss has the least fluctuation because it smooths out environmental characteristics.

It can be also noticed from Figures 3.8 that more fluctuation exists than in the other three figures because the acoustic signals get quickly reflected by the seafloor as the source is placed close to the bottom. From all four figures, we can conclude that the semi-empirical formula provides reasonable results for the estimation of acoustic signal attenuation with low computational complexity.

3.3.3 Transmission Loss in Deep Water

In this study, the sound source and the receiver are located at 10 m, 750 m, 1,500 m, and 2,995 m, respectively. The horizontal distance between the sound source and the receiver is 3,000 m for long-haul transmissions. Seafloor is assumed to be flat and rigid.

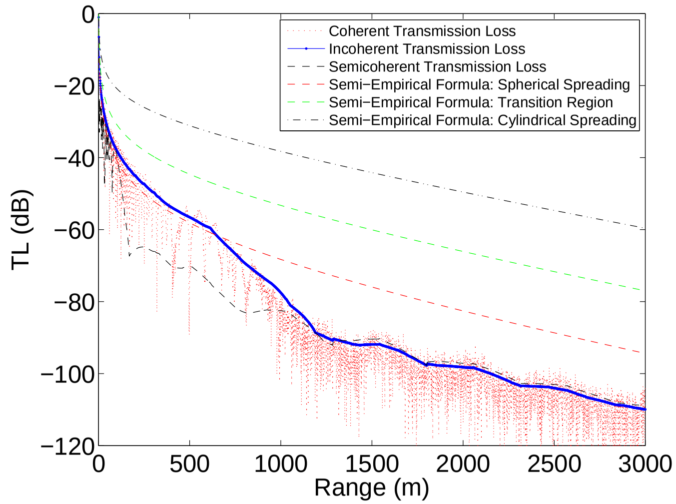

Figure 3.9: Deep water: sound source depth = 10m

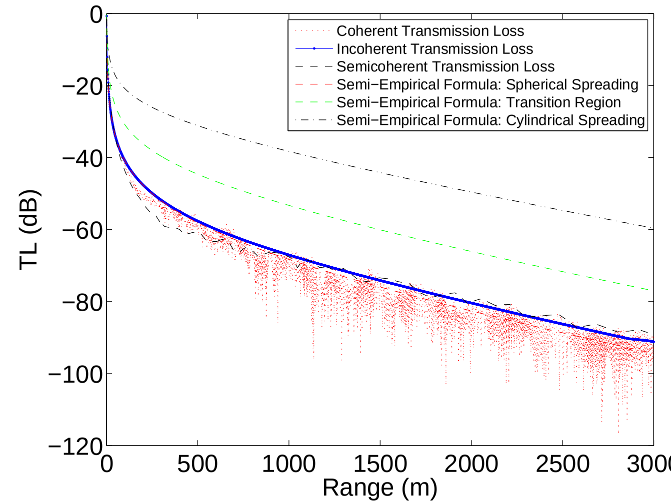

Figure 3.10: Deep water: sound source depth = 750m

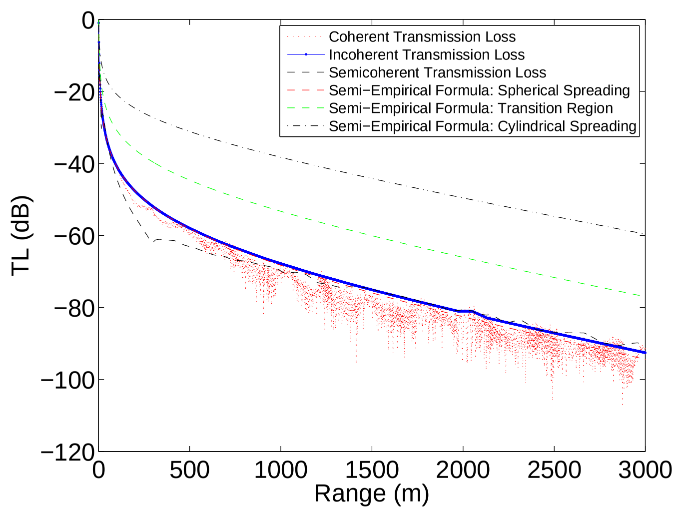

Figure 3.11: Deep water: sound source depth = 1,500m

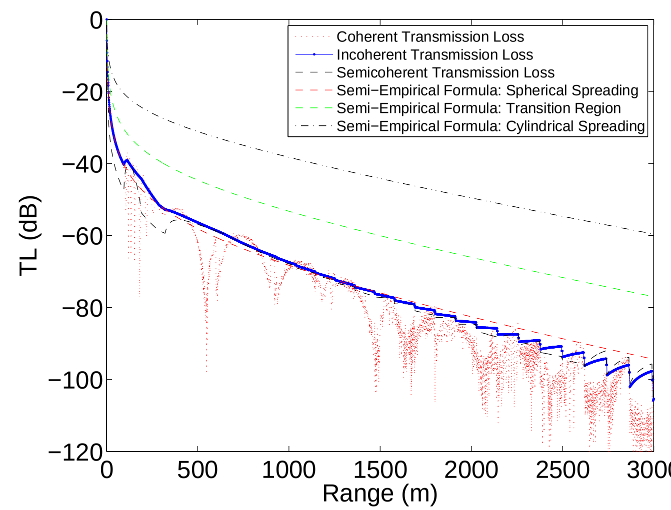

Figure 3.12: Deep water: sound source depth = 2,995m

The transmission loss comparisons for deep water are plotted in Figures 3.9, 3.10, 3.11, and 3.12, respectively. Compared to the results from the shallow water scenarios, the transmission loss curves become smoother in deep water for both near field and far field. This is because the energy of acoustic signals is more concentrated in deep sea. The same trends are observed in all four figures that the transmission loss obtained from the ray-theoretical model is very close to those from the semi-empirical formula using spherical spreading ($\mathcal{K}$ = 2). The trend and distribution of the curves for the transmission loss calculated by three approaches based on the ray theory are similar to those in the shallow water studies.

For the far field, however, the transmission loss calculated by the three approaches based on the ray-theoretical model are larger than that of the semi-empirical formula when the spherical spreading is used, as shown in Figures 3.9 and 3.12. From Figure 3.9, it is obvious that the transmission loss results using the ray-theoretical model becomes greater than that from the semi-empirical formula with spherical spreading loss ($\mathcal{K}$ = 2) for a distance of over 500 m. This is because less acoustic signal energy will be captured by the receiver placed at 10 m near the sea floor due to the reflections, and refractions. The sound ray travel a long distance from the 10 m to the seafloor and the acoustic signal experience severely attenuation and absorption during transmission. When the sound source is close to the seafloor, the attenuation become less and the transmission loss resulting from both schemes become comparable, as shown in Figure 3.12. The results from the ray-theoretical model tend to have more fluctuation than those from the semi-empirical formula in the far field because the sound source is close to the seafloor and the acoustic signal reflected by the seafloor will attenuate when the horizontal distance increases.

3.3.4 Transmission Loss with Bathymetry Data

To demonstrate how the practical environmental parameters affect the transmission loss results using different methods, we study the performance using real bathymetry data for the region of our interest. The bathymetry data is obtained from the National Oceanic and Atmospheric Administration (NOAA), which is given in Table 3.2 [130]. In our work, the receiver is deployed at 90 m from the surface and the horizontal distance between the sound source and the receiver is 4000 m.

Table 3.2: Bathymetry data

South		North	
Range(km)	Depth(m)	Range(m)	Depth(m)
0	95.0	0	95.0
1.583	93.0	1.583	97.0
3.706	93.0	3.706	95.0
East		West	
Range(km)	Depth(m)	Range(m)	Depth(m)
0	95.0	0	95.0
1.276	95.0	1.276	95.0
2.551	96.0	2.551	94.0

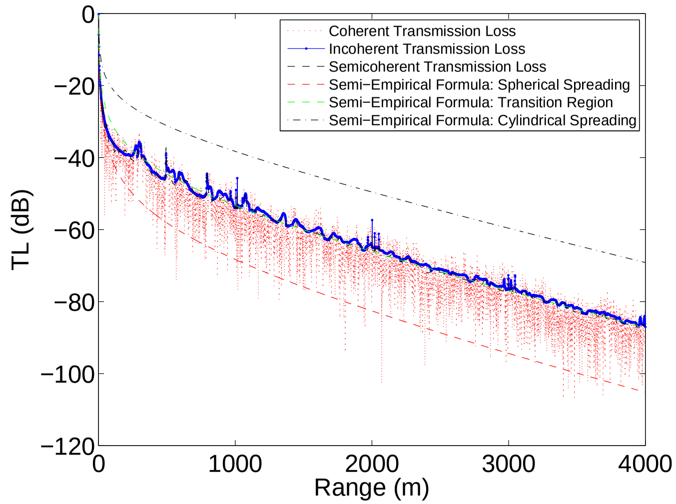

Figure 3.13: Source Depth: 90m south

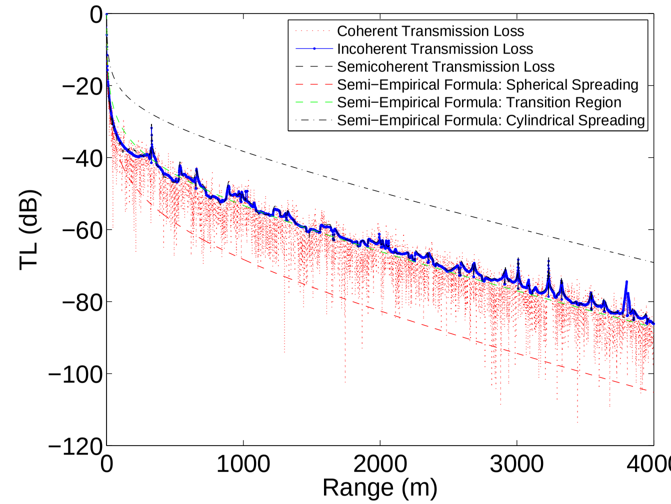

Figure 3.14: Source Depth: 90m north

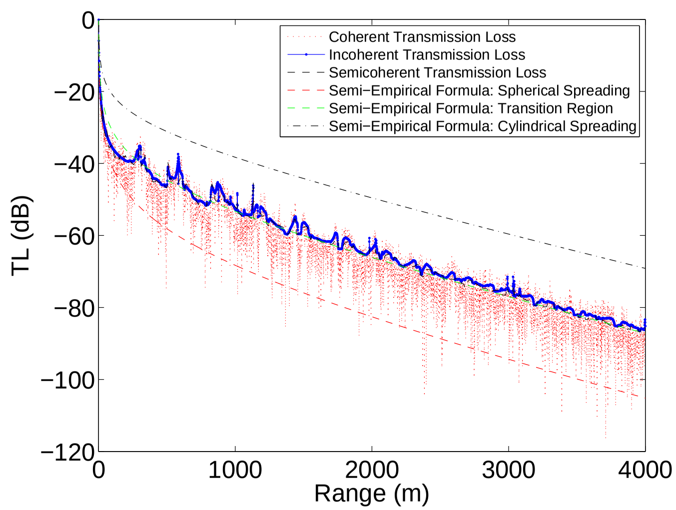

Figure 3.15: Source Depth: 90m west

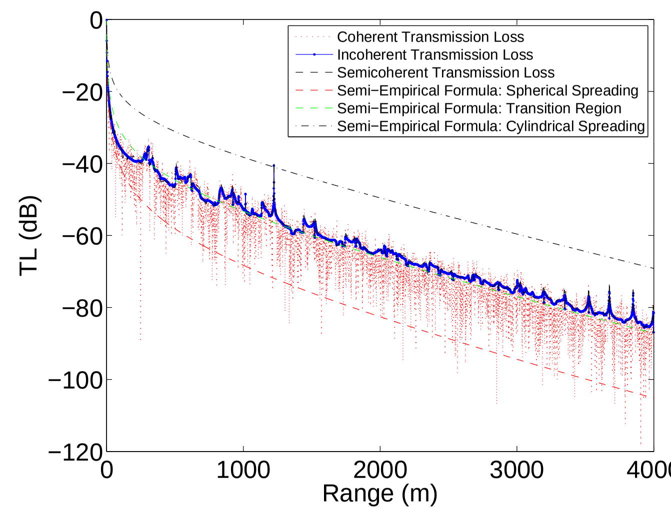

Figure 3.16: Source Depth: 90m east

Figures 3.13, 3.14, 3.15, and 3.16 show the transmission loss results where the receivers are located in all four directions from the sound source. Compared with Figure 3.8, the transmission loss in Figure 3.13 does not have a large variation because the seafloor does not have large undulation, and the semi-empirical formula with $\mathcal{K}$ = 1.5 gives a good approximation. However, for locations which are 1500 m and 3700 m away from the sound source, the results from the ray-theoretical model show more fluctuation because of the reduction of the ocean depth. As a result, more energy will be captured due to the reflection of the seafloor. On the other hand, after passing about 3700 m, the incoherent transmission loss becomes smoother to the south than to the north because the depth after 3706 m in bathymetry has little variation to the south.

3.4 Summary

In this chapter, we have reviewed the properties of acoustic signal propagation in the ocean in terms of sound speed profile, spreading loss, and absorption loss. We have studied different models, such as the ray-theoretical model and the semi-empirical formula, which are used for the transmission loss evaluation. Using different marine conditions, we compared the results from the three approaches of transmission loss calculation (derived from the ray-theoretical model) with results from the semi-empirical formula. Our results indicated that, in shallow water scenarios, the transmission loss of acoustic signals is close to the results from the semi-empirical formula with $\mathcal{K}$ = 1.5. For deep sea conditions, the transmission loss is close to the results from the semi-empirical formula with $\mathcal{K}$ = 2 (corresponding to the spherical spreading loss). In general, we consider the semi-empirical formula with the spherical spreading loss as a conservative estimation of the transmission loss for the link budget in underwater acoustic communications. Our work in analyzing the transmission loss of acoustic signals provides a clear foundation for developing new UWSN protocols. We build the following chapters upon this foundation.

Chapter 4

An Energy-Efficient Asynchronous Wake-Up Scheme for UWSNs

Compared to terrestrial wireless sensor networks (WSNs), energy efficiency in UWSNs is even more critical because acoustic sensor nodes rely on non-rechargeable and unchangeable batteries to provide essential power for long-term sensing, data collection and communication[1]. Moreover, due to the high cost of acoustic underwater sensor nodes and their non-trivial deployment cost, the number of nodes in UWSNs is often much smaller than in terrestrial WSNs, and the topologies of UWSNs are often predetermined and regular (e.g., linear, ring, star and grid topologies). Communication intensity among sensor nodes is often much lower than the intensity of their data sensing and processing operations, which means that the transceivers of sensor nodes spend most of their time in idle listening. Therefore, in order to

[1]The material in this chapter has been accepted by Wiley Journal of Wireless Communication and Mobile Computing [131].

achieve energy conservation and prolong network lifetime, it is important to develop effective power saving mechanisms for UWSNs.

In this chapter, we propose an asynchronous wake-up scheme for UWSNs with a grid topology utilizing combinatorial designs. Using this design, energy consumption can be reduced without sacrificing network connectivity. We investigate how the traffic intensity affects the utilization ratio of a sink node. Additionally, we study network scalability when multiple sink nodes are employed. This chapter is organized as follows. The proposed asynchronous wake-up scheme in Section is presented in Section 4.1. The utilization ratio of sink node and the network scalability are analyzed in Section 4.2. The performance evaluation of the proposed scheme is presented in Section 4.3. This chapter is concluded in Section 4.4.

4.1 Proposed Asynchronous Wake-up Scheme

In this section, we present the proposed asynchronous wake-up scheme. We first present the underwater channel model and the topology of UWSNs. Preliminaries of combinatorial designs[62, 103] are then discussed. The proposed asynchronous wake-up scheme aims at reducing energy consumption for idle listening and guarantees connectivity among sensor nodes in UWSNs.

4.1.1 Underwater Acoustic Channel Model

As discussed in Chapter 3, we use the semi-empirical formula (Equation 3.11) [21, 52] to study the underwater acoustic channel and calculate the transmission loss of the acoustic signal in seawater.

We utilize the sonar equation [21] to calculate the proper transmission power corresponding to a certain transmission range:

$$SL - NL - TL + DI = DT, \tag{4.1}$$

where SL is the transmit sound source level (dB re 1 μPa^2); DI is the directivity index ($DI = 0$ if the sound source is omnidirectional); DT is the detection threshold of the acoustic modem, which represents the required signal-to-noise ratio (SNR) to decode received packets; and NL is the noise level that includes thermal noise and surface wave. NL can be estimated by [21, 132]

$$10\log_{10} NL = \eta_0 - 18\log_{10} f, \tag{4.2}$$

where η_0 is the constant level in dB re 1 μPa^2/Hz, f is the center frequency of the acoustic modem.

The transmit power in watts needs to be converted to dB re 1 μPa^2, which can be obtained by [21, 125]

$$10\log_{10} p_t = 10\log_{10} SL - 170.8 - 10\log_{10}\xi, \tag{4.3}$$

where 170.8 dB is the conversion factor between the acoustic pressure in dB re μPa^2 and acoustic power in watts. ξ is the transducer efficiency.

In this chapter, we use the binary phase shift keying (BPSK) signal [30]. The bit error rate (BER) of BPSK signal can be calculated as [133]

$$BER = Q\left(\sqrt{2 \cdot 10^{(SNR/10)}}\right), \tag{4.4}$$

where $Q(x) = \frac{1}{\sqrt{2\pi}} \int_x^\infty exp(-t^2/2)dt$. L_d stands for the size of a data packet. The packet error rate (PER) can be expressed by

$$PER = 1 - (1 - BER)^{L_d}, \tag{4.5}$$

4.1.2 Topology of UWSNs

We consider a multi-hop UWSN with a square grid topology for the long-term marine environmental monitoring application. A total of $N \times N$ sensor nodes are located on the seafloor, which is assumed to be 2-dimensional (assuming N is odd, without loss of generality, as explained in the summary). Their geometric positions form a square lattice. The distance between two closest adjacent nodes is d_c. The sink node is located at the center of the grid. In Section 4.2, we will further discuss the scenario where multiple sink nodes are deployed in the grid network. We assume that there is only one surface node and it communicates only with sink node (s).

Similar to what has been assumed in other work in the literature [1], we assume that the each sensor node is equipped with an omnidirectional transceiver and the transmission range of sensor nodes is a circle, as shown in Figure 4.1 [1, 134]. The transmission range of the sink node is the same as regular sensor nodes. Two nodes can communicate with each other as long as they are within transmission range. Relay nodes are needed when the receiving node is out of transmission range of the sending node. Again, this assumption is consistent with other reported work in this area [45, 111]. The position information of all nodes is known *a priori*. Consequently, every sensor node (for example: node u) can easily determine how to reach the sink node with fewest hops by maintaining two sets: (1) H_u: a set of next hop candidates within range of node u; (2) R_u: a set of nodes for which node u serves as a relay candidate. Both of these two sets are determined offline.

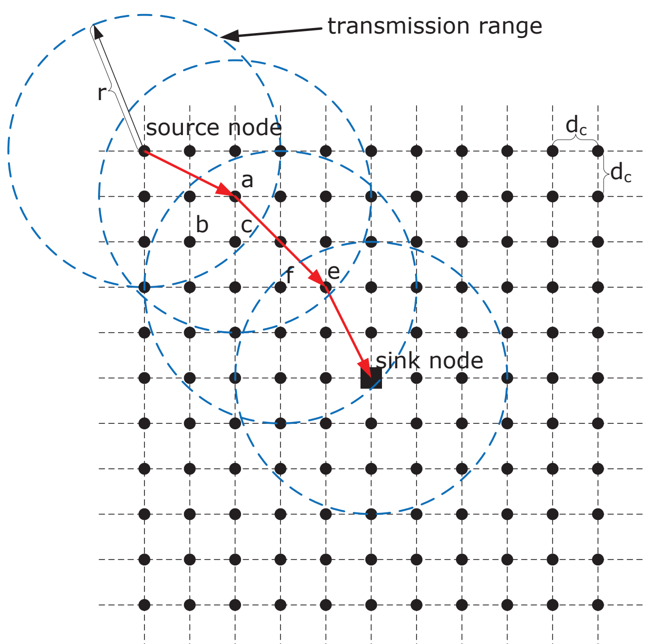

Figure 4.1: Example of UWSN with a square grid topology

In Figure 4.1, a 3-hop UWSN using 11×11 square grid topology is given as an example to illustrate how the source node transfers data packets to the sink node in 3 hops. Circles with dashed line represent the transmission range of sensor nodes. The example shows the case where the source node is located at the corner of the grid. H_s and H_a represent the H set of the source node and node a, respectively. From H_s, the source node knows that node a is the relay node, which can reach the sink node in 2 hops. Then, from its next hop node set, H_a, node a chooses node e as its relay node because node e can directly communicate with the sink node. Note that node b or node c could have been chosen in the first hop as the relay node, and node f could have been chosen in the second hop. Here, we consider a simple strategy for relay node selection, i.e., a node that first acknowledges the data request becomes the relay node.

4.1.3 Objective, Assumptions and Modes of Operations

We assume that the sink node is equipped with sufficient battery energy to outlast all other sensor nodes. Packet collision need not be considered in long-term monitoring applications of UWSNs because low traffic load conditions often prevail. Our objective is to design an asynchronous wake-up scheme that ensures network connectivity with the minimum possible energy consumption. This is achieved by taking the shortest path to the data sink, i.e., using the smallest required number of relay nodes, and keeping the sensor nodes in sleep mode as much as possible. In our design, every sensor node has two modes of operations: wake-up mode and sleep mode. In the wake-up mode, the transceiver is turned on for data transmission, receiving and channel listening, whereas it is turned off in the sleep mode so that energy consumption can be minimized. The operation of each sensor node alternates between the wake-up mode and sleep mode. Both the wake-up mode and the sleep mode may contain different numbers of time slots. We call a time slot an "active slot" when the sensor node operates in the wake-up mode and an "inactive slot" when it stays in the sleep mode. The operation status of a sensor node alternates between a predetermined number of active slots and inactive slots. Given the same duration for each active and inactive slot, denoted as T_{slot}, the period of one working operating cycle of a sensor node (T_n) can be expressed by:

$$T_n = m \cdot T_{\text{slot}}, \tag{4.6}$$

where $m \in \mathbb{Z}^+$. Considering the propagation delay of acoustic signals in seawater, we have:

$$T_{\text{slot}} = \frac{2r}{v_s} + T_R + T_a, \tag{4.7}$$

where v_s is the velocity of sound in seawater and r is the transmission range of a sensor node. T_R and T_a denote the transmission time of a data request packet and an ACK packet, respectively.

In each active slot, a sending node which has data to send will attempt to establish a connection with a receiving node by broadcasting a data request packet, whereas a receiving node will simply listen to the channel. Upon receiving the data request packet, the receiving node will reply with an ACK packet then data transmission starts. Both nodes will resume their original operating cycle after the data transfer is completed [62, 64].

4.1.4 An Introduction to Cyclic Difference Set

4.1.4.1 Balanced Incomplete Block Design (BIBD) [103, 104]

Definition 4.1 (($X, \mathcal{A}$) **Design**). *A design is a pair* $(X, \mathcal{A})$ *with two properties: (1)* X *is a set of elements called points; (2)* $\mathcal{A}$ *is a collection of nonempty subsets of* X *called blocks.*

Definition 4.2 (($\mathcal{V}, k, \lambda$)–**BIBD**). $\mathcal{V}, k, \lambda \in \mathbb{Z}^{+}, v > k \geq 2$. *A* $(\mathcal{V}, k, \lambda)$*–BIBD is a design* $(X, \mathcal{A})$ *with three properties: 1)* $|X| = \mathcal{V}$*; 2) Each block contains exactly* k *points; 3) Every pair of distinct points is contained in exactly* λ *blocks.*

For example, for a $(7,3,1)$-BIBD: $X = \{1,2,3,4,5,6,7\}$ and $\mathcal{A} = \{\{1,2,4\},\{2,3,5\},\{3,4,6\},\{4,5,7\},\{5,6,1\},\{6,7,2\},\{7,1,3\}\}$. It is obvious that: $\mathcal{V} = |X| = 7$ and each block has 3 elements ($k = 3$). Any two blocks in $\mathcal{A}$ have one common element ($\lambda = 1$) [103, 104].

In this chapter, we only consider the cyclic difference set, a subset of BIBD design, which can avoid exploring all possible BIBD designs.

4.1.4.2 Cyclic Difference Set [103, 104]

Definition 4.3 (**Cyclic Difference Set**). *Given a set* D *with* $\mathcal{V}$ *elements and* k *subset elements,* D*:* $a_1, a_2, \cdots, a_k \pmod{\mathcal{V}}$ *is called a* $(\mathcal{V}, k, \lambda)$*–cyclic difference set if for every* $d \neq 0 \pmod{\mathcal{V}}$ *there are exactly* λ *ordered pairs* (a_i, a_j)*, such that* $a_i - a_j = d \pmod{\mathcal{V}}$*.*

When CDS is used to denote the active or inactive slot of a sensor node, under any cyclic shift, the property of cyclic difference set guarantees that there is at least one slot for each pair of nodes when both nodes are in the wake-up mode [64, 103]. In the context of asynchronous wake-up scheme design, $\mathcal{V}$ and k are used to represent the total number of slots and the number of active slots in one cycle of a sensor node, respectively. λ represents the number of overlapping slots. According to Singer's theorem [103], a cyclic difference set can be expressed by:

$$(\mathcal{V}, k, \lambda) = (q^2 + q + 1, q + 1, 1), \tag{4.8}$$

where q is a prime power. According to Definitions 4.1, 4.2 and 4.3 and Singer's theorem, the asynchronous wake-up scheme design in UWSNs can be formulated as: every cycle of a sensor node consists of $q^2 + q + 1$ slots, where $q + 1$ slots are active slots and q^2 slots are inactive slots. Using such design, one overlapping active slot can be guaranteed under any cyclic shift even if the slot boundaries are not synchronized [64, 103].

4.1.5 The Design of Asynchronous Wake-up Scheme

We divide each operating cycle of a sensor node into a number of sub-cycles. Each sub-cycle has the same number of total slots and active slots. Different active slot positions are used in different sub-cycles and they are chosen according to the selected cyclic different set. We use the black rectangle and white rectangle to represent the active slot and inactive slot, respectively.

4.1.5.1 Sub-cycle Design

Based on the cyclic difference set properties, we devise a sub-cycle consisting of q^2+q+1 $(q \geq 2)$ slots, of which only q slots are active slots. The positions of these active slots are determined as in the cyclic difference sets. There exist $q+1$ (C^q_{q+1}) possible position combinations for q active slots in one sub-cycle. For example, when $q = 2$, we get a $(7,3,1)$−cyclic different set: $D = \{1,2,4\}$. There are 3 possible position combinations which has two active slots in one sub-cycle, and they are $\{1,2\}$, $\{1,4\}$ and $\{2,4\}$, as shown in Figure 4.2.

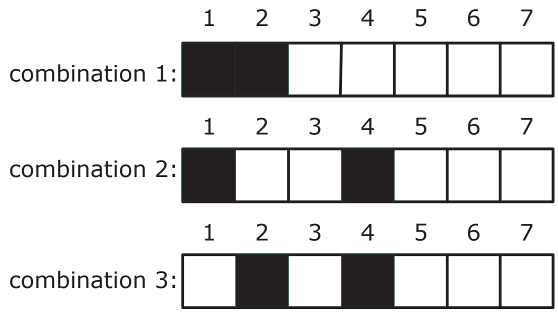

Figure 4.2: Active slots position allocation for sensor nodes using a (7,3,1)-cyclic difference set ($q = 2$)

4.1.5.2 Construction of One Complete Working Cycle

One full operating cycle of a sensor node contains concatenation of all possible sub-cycles, each corresponding to a distinct position combination of any q active slots. Therefore, an operating cycle is comprised of $(q+1)$ sub-cycles, which corresponds to $(q+1)\cdot(q^2+q+1)$ slots, $(q+1)\cdot q$ of which are active slots. Any ordering of sub-cycles can be used for concatenation. According to Equation (4.6), $T_n = (q+1)\cdot(q^2+q+1)T_{\text{slot}}$. The duty cycle is $q/(q^2+q+1)$. Figure 4.3 shows an example when $q = 2$.

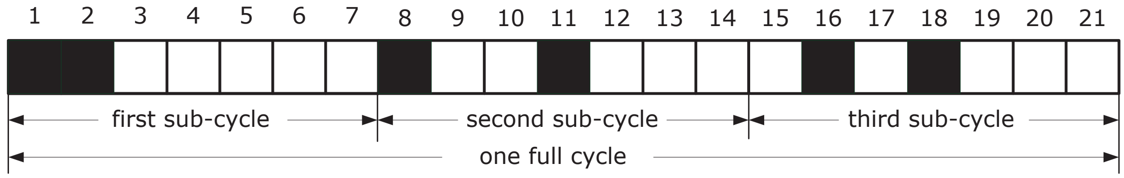

Figure 4.3: Example of one full cycle of 3 sub-cycles and 6 active slots ($q = 2$)

4.1.6 Connectivity Analysis for the Proposed Wake-up Scheme

Theorem 4.1. *By utilizing the proposed asynchronous wake-up scheme, it is guaranteed that any two sensor nodes can hear the data requests from each other as long as they are within communication range.*

The following proof is similar to that in [62, 64], but modified to correspond to the proposed scheme.

Proof. In the proposed asynchronous wake-up scheme, each cycle contains $(q+1)\cdot(q^2+q+1)$ slots. Hence, there are $(q+1)\cdot(q^2+q+1)-1$ possible cyclic shifts (we deem 0 cyclic shift not to be a cyclic shift), which are shown in Figure 4.4, where "sc" denotes sub-cycle. The top frame within the dash rectangular box in Figure 4.4 presents one full cycle of the proposed scheme.

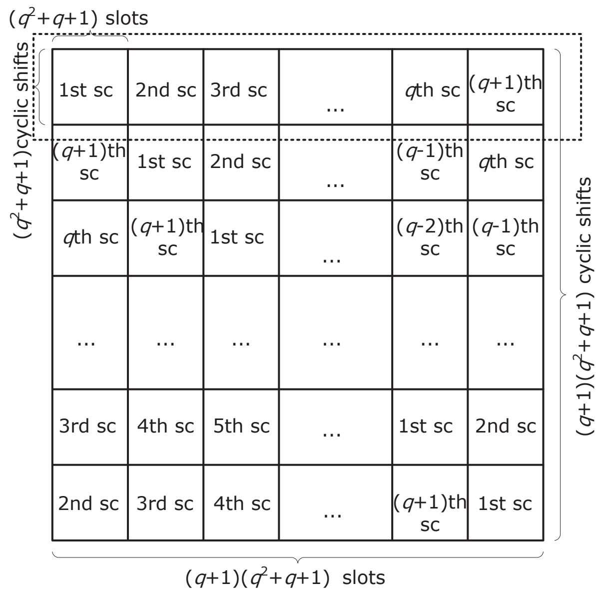

Figure 4.4: Possible cyclic shifts when $N_c \mod (q^2+q+1) = 0$

N_c is the number of cyclic shifts between any two possible cyclic shifts. We consider the following cases.

- Case 1: Aligned slot boundaries when $N_c \mod (q^2+q+1) = 0$

  Each sub-cycle has q positions for active slots, which are chosen from $(q+1)$ positions of active slots determined by the corresponding difference sets. There are at least $(q-1)$ overlapping positions between any two sub-cycles. In Figure 4.4, there are at least $(q-1)$ overlapping active slots between any two rows in each column. We use an example to illustrate this case in Figure 4.5. Consequently, it is guaranteed that there is at least one overlapping active slot between any two cyclic shifts.

- Case 2: Aligned slot boundaries when $N_c \mod (q^2+q+1) \neq 0$

According to Definition 3 and Singer's Theorem, any two sensor nodes will be guaranteed to have at least one overlap active slot if there exists $(q+1)$ active slots out of every (q^2+q+1) slots utilizing the cyclic difference set. In the proposed scheme, we choose q active slots from $(q+1)$ possible active slots determined by the cyclic difference sets for each sub-cycle as shown in Figure 4.2. The position of active slots in each sub-cycle do not change afterwards. Therefore, in the first sub-cycle, there are q overlapping active slots. In the second sub-cycle, there are other q active slots overlapping with each other. This property can be extended up to until the $(q+1)$th sub-cycle. The total number of overlapping slots is $q(q+1)$, which equals to the number of possible cyclic shifts (q^2+q). Therefore, the connectivity can be guaranteed when $N_c \mod (q^2+q+1) \neq 0$.

- Case 3: Unaligned slot boundaries

We assume that the data request transmission time is at least one order of magnitude smaller than the duration of one slot. In general, the cyclic shifts between nodes a and b can be expressed by: $N_c \cdot T + \varphi$, where $N_c \in \mathbb{Z}^+, \varphi < T$. When $\varphi = 0$, the slot boundary of node a and node b differ by $N_c \cdot T$, which corresponds to what have been studied in Case 1 and Case 2.

When $\varphi \neq 0$, the clock of node a and node b differ by $N_c \cdot T + \varphi$. node a can hear the data request transmitted by node b in slot i and node b can hear the data request transmitted by node a in slot j $(i \neq j)$. Since node a and node b follow the proposed asynchronous wake-up scheme, the overlapping sections between node a and node b have durations of $T - \varphi$ and φ. The total duration of these sections are T, i.e., the duration of one slot.

Consequently, our design can guarantee the connectivity among all possible cyclic shifts. ■

To better illustrate the proposed active slot allocation scheme, we present three examples, which correspond to Case 1, Case 2, and Case 3, respectively in the following paragraphs.

- Case 1: Aligned slot boundaries, where $N_c \mod (q^2 + q + 1) = 0$

  We can choose $\{1, 2\}$, $\{1, 4\}$, and $\{2, 4\}$ as the positions for active slots for three sub-cycles, which are derived from the $(7, 3, 1)-$cyclic different set. The positions of active slots are shown in the top row in Figure 4.5. The two highlighted rows in Figure 4.5 illustrate Case 1 when $N_c = 7, 14$, respectively. From Figure 4.5, in one sub-cycle, there is at least one overlapping active slot between the top row and any two rows highlighted by two rectangular boxes.

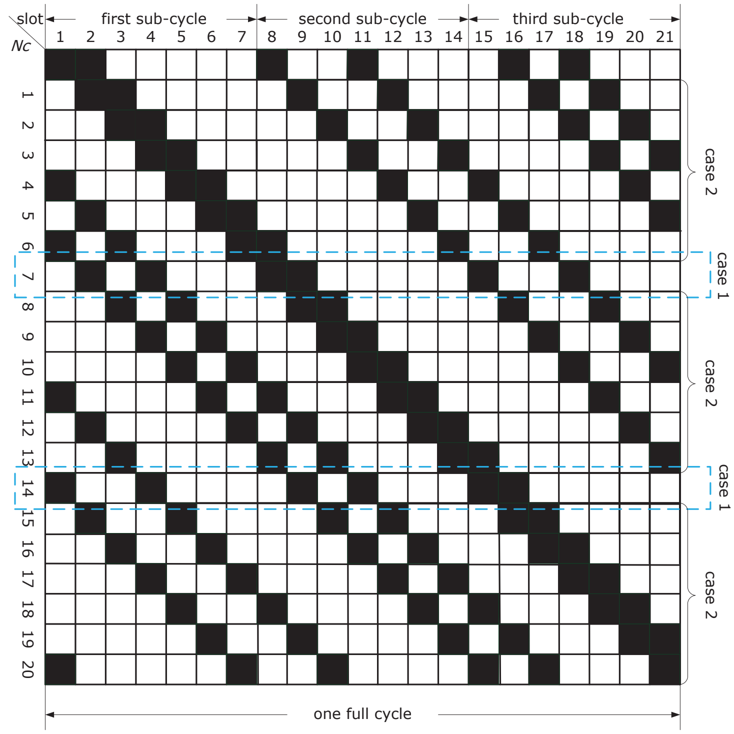

Figure 4.5: Cyclic shifts in Case 1 and Case 2

- Case 2: Aligned slot boundaries, where $N_c \mod (q^2+q+1) \neq 0$

  We use the previous example as shown in Figure 4.5. From Figure 4.5, it can be observed that any two rows (represent two kinds of cyclic shift, respectively) can overlap with each other at least one active slot when $N_c \mod (q^2+q+1) \neq 0$.

- Case 3: Unaligned slot boundaries

  As shown in Figure 4.6, the data request transmitted by node a can be received by node b at time slot 18, whereas the data request transmitted by node b can be received by node a at time slot 2. It can be seen that there will be at least one overlapping slot for any value of N_c as well.

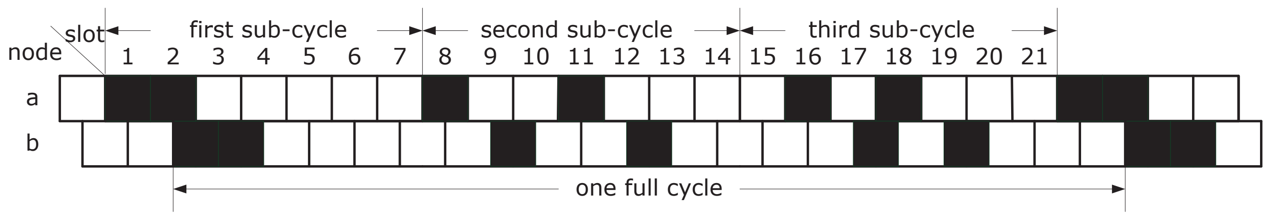

Figure 4.6: Example of no alignment of slot boundaries ($N_c = 0$)

4.1.7 Analysis of the Proposed Wake-up Scheme

We summarize duty cycles used in the proposed scheme and the CDS-based protocol [64] in Table 4.1. For a given value of q, the proposed scheme can generate a smaller duty cycle than the CDS-based protocol. It is obvious that a larger value of q can achieve a smaller duty cycle and thus reduce more energy consumption for idle listening. However, normally, for a given smaller duty cycle, a sensor node requires more active slots to connect to a next-hop sensor node. In Section 4.3, we present the simulation results using $q = 2, 3, 4, 5, 7, 8, 9,$ and 11.

Table 4.1: Duty cycles of the proposed scheme and the CDS-based protocol

q	Proposed scheme $q/(q^2+q+1)$	CDS-based protocol $(q+1)/(q^2+q+1)$
2	28.57%	42.85%
3	23.08%	30.77%
4	19.05%	23.81%
5	16.13%	19.35%
7	12.28%	14.04%
8	10.96%	12.33%
9	9.89%	10.99%
11	8.27%	9.02%

As discussed in Section 2.3.3.3, EACDS and MACDS use hierarchical arrangements of sets with the Kronecker Product (denoted by $\otimes$). In EACDS, a difference set $(\mathcal{V}_I,\ k_I,\ \lambda_I)$, called an initial set, is scaled by another set $(\mathcal{V}_E,\ k_E,\ \lambda_E)$, called an exponential set. Then, the higher level hierarchical set can be obtained by the Kronecker product, i.e., $(\mathcal{V}_I,\ k_I,\ \lambda_I)^n \otimes (\mathcal{V}_E,\ k_E,\ \lambda_E)$, $n \in \mathbb{Z}^+$. MACDS uses a multiplier set instead of the exponential set, which can be expressed by $(\mathcal{V}_I,\ k_I,\ \lambda_I) \otimes (\mathcal{V}_M,\ k_M,\ \lambda_M)$. All multiplier sets are selected from the rotational set group (not difference sets)[62].

According to Section 4.1.6, the proposed scheme can guarantee a network connectivity among sensor nodes with the smaller duty cycle compared to the CDS-based protocol [64]. Therefore, the sleeping pattern formed by the proposed scheme can be used in EACDS and MACDS instead of the difference set, i.e., ($\mathcal{V}_I$, k_I, λ_I) in the operation of Kronecker product. $\big((q+1)\cdot(q^2+q+1),(q+1)\cdot q,1)\big)$ is the sleeping pattern scheduling formed by the proposed scheme as discussed in the previous sections. Then, EACDS can be expressed by: $\big((q+1)\cdot(q^2+q+1),(q+1)\cdot q,1)\big)\otimes(\mathcal{V}_E,k_E,\lambda_E)$. MACDS is: $\big((q+1)\cdot(q^2+q+1),(q+1)\cdot q,1)\big)\otimes(\mathcal{V}_M,k_M,\lambda_M)$.

We compare the proposed scheme that is extended using Kronecker product to the EACDS and MACDS in Table 4.2 and Table 4.3, respectively. For EACDS, we choose ($\mathcal{V}_E$, k_E, λ_E) = (3, 2, 1). For MACDS, ($\mathcal{V}_M$, k_M, λ_M) is selected from the rotational set group as used in [62]. For the proposed scheme and the CDS used in EACDS and MACDS, we take $q = 2$ as an example. From Table 4.2 and Table 4.3, we can observe that, for a given value of q, n, and ($\mathcal{V}_M$, k_M, λ_M), the smaller duty cycle can be generated by the proposed scheme using the Kronecker product than EACDS and MACDS.

Table 4.2: Duty cycles of the proposed scheme with Kronecker product and EACDS

n	Proposed scheme with Kronecker product	EACDS
1	19.04%	28.57%
2	12.70%	19.04%
3	8.47%	12.70%
4	5.64%	8.47%
5	3.76%	5.64%
6	2.51%	3.76%

Table 4.3: Duty cycles of the proposed scheme with Kronecker product and MACDS

$(\mathcal{V}_M,\, k_M,\, \lambda_M)$	Proposed scheme with Kronecker product	MACDS
(4, 3, 1)	21.43%	32.14%
(5, 3, 1)	17.14%	25.71%
(6, 3, 1)	14.29%	21.42%
(12, 4, 1)	9.52%	14.29%
(24, 6, 1)	7.14%	10.71%
(48, 8, 1)	4.76%	7.14%

4.2 Analysis of Sink Node Usage and Network Scalability

Unlike regular sensor nodes in UWSNs, the sink node, typically located at the center of the network, never sleeps in order to collect data from sensor nodes and report data to the surface node. In this section, we first analyze the utilization ratio of a single sink node. Then, we study how multiple sink nodes can be utilized to address the scalability issue of UWSNs.

4.2.1 Utilization Ratio of a Single Sink Node

We assume that the probability of every sensor node generating a data request is the same. N_s represents the number of sink nodes in the network. $i^{(u)}$ gives the number of data packets that node u sends to the sink node every day, which is defined as the traffic intensity. T_{day} is the duration of one day in seconds. R_d is the the number of bits per second that an acoustic modem is able to send or receive. In an $N \times N$ UWSN (sink nodes are located at the center region of the network), the utilization ratio of a sink node ($\mathcal{U}$) can be expressed as:

$$\mathcal{U} = \frac{2 \cdot (N^2 - N_s) \cdot L_d \cdot i^{(u)}}{T_{\text{day}} \cdot R_d}, \tag{4.9}$$

where $(N^2 - N_s)$ represents the number of regular sensor nodes in the network. A constant of 2 is used in Equation (4.9) by taking into account the process of receiving data packets (from sensor nodes) and sending data packets to the surface node.

Generally speaking, a high utilization ratio of sink node means that more data can be collected. However, high sink node utilization ratio also means that the sink node will be busy in receiving data from different sensor nodes and transmitting data to the surface node. The probability of network congestion increases when one-hop nodes and sink nodes carry a large amount of data traffic. Therefore, in long-term monitoring applications of UWSNs, low traffic intensity and low utilization ratio of the sink node often become a necessity.

4.2.2 Network Scalability

In this section, we study how to support a large size network for such UWSN applications. Constrained by the utilization ratio of the sink node, traffic intensity normally needs to be kept low. To support network expansion, an approach is to incorporate multiple sink nodes on the seafloor. The question then becomes how many sensor nodes or how large a UWSN using the square grid topology can be as the number of sink nodes increases. This question can be formulated as:

$$\max \quad N^2 - N_s \tag{4.10}$$

$$\text{s.t.} \quad r_{sink} = r \tag{4.11}$$

$$\mathcal{U} \leq 0.5 \tag{4.12}$$

$$d_{sink-surface} < r, \tag{4.13}$$

where $d_{sink-surface}$ represents the distance between a sink node and the surface node. r_{sink} denotes the transmission range of a sink node, which is the same as the transmission range of a regular sensor node here. According to the analysis in Section 4.2.1, we configure the utilization ratio of a sink node to be below 0.5 in order not to affect the working of the network. The sink utilization ratio of 0.5 represents that the sink node spends half of its total time on collecting data from the sensor nodes and transmitting all the data to the surface node. In this work, the sink nodes are deployed at the center region of the network (on the grid point), which is essentially constrained by the transmission range of the sink node to reach the surface node. Figure 4.7 shows an example of multiple sink nodes deployment, where the number of sink nodes is 1, 4 or 8.

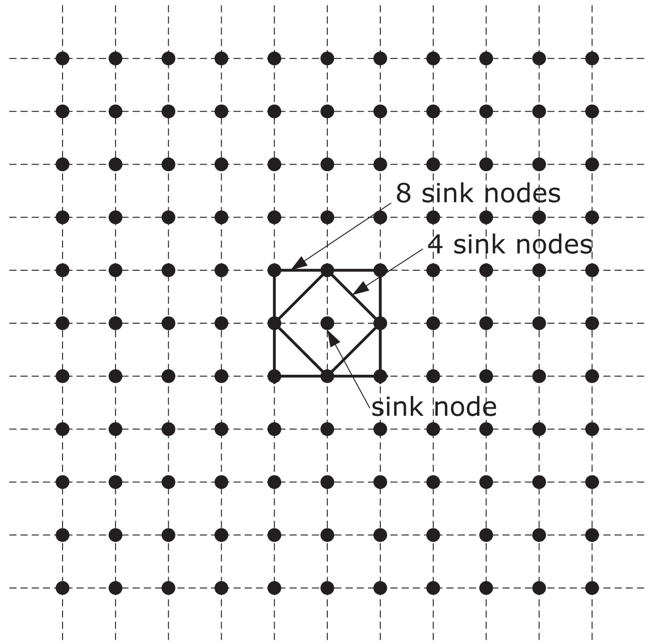

Figure 4.7: Multiple sink nodes deployment

The distance between a sink node and the surface node ($d_{sink-surface}$) should be within their communication range in order to stay connected. In our work, we assume one surface node. The surface node is more powerful in terms of their communication capabilities, which means that the surface node can have a limited number of multiple transceivers to communicate with underwater sink nodes. It is also capable of receiving data packets from multiple sink nodes simultaneously. It is obvious that deploying more sink nodes can help to support larger networks. In Figure 7, we only present some examples of multiple sink nodes deployed in the center of the UWSN, i.e., 4 and 8 sink nodes. Different numbers of sink nodes can be used in UWSNs, however, we have to consider two factors of sink nodes deployment: 1) It is not realistic that too many sink nodes are deployed in UWSNs because the high cost of sensor nodes and high energy consumption of a sink node (frequently replacing the sink nodes is not realistic); 2) The surface node can support only a limited number of transceivers to communicate with underwater sink node simultaneously, which does not allow too many sink nodes deployed in UWSNs.

4.3 Performance Evaluation

In this section, we study the performance of the proposed asynchronous wake-up scheme. The utilization ratio of sink node and the scalability of network are also evaluated.

4.3.1 Simulation Parameters

In our work, the parameters we used correspond to the Micro-modem, which is a widely used low-power acoustic modem with a small foot-print, designed by the Woods Hole Oceanographic Institution (WHOI). It uses a Texas Instruments TMS320C5416 digital signal processor (DSP) [30, 66]. In choosing the simulation conditions and parameters, we emphasize the importance of the applicability of our simulation results to practical UWSNs applications. The receiving power (p_r) and idle listening power (p_l) are 3 W and 0.08 W, respectively. The sleeping power is 0 W because the transceiver of the acoustic modem is completely turned off. For a given range r =1,000 m and with f = 30 kHz, η_0 = 50 μPa^2/Hz, $\mathcal{K}$ = 2, and ξ = 0.8, according to Equations (4.1) and (4.5), we can achieve (nearly) zero PER with a transmission power (p_t) of 20 W. It is also reported in the technical specification of several commercial acoustic modems that, in the general states of ocean, a transmit power of 20 W can reliably achieve the transmission range of 1,000 m [30, 52]. Although some researchers have employed different transmission powers corresponding to achieve different transmission ranges and data rates [52, 57, 66, 83, 102], our goal is to conservatively ensure a highly reliable data transfer so, transmit power of 20 W is used, which corresponds to a transmit sound source level of 182 dB re 1 μPa^2 (calculated by Equation (4.3) in Section 4.1.1), where we use the energy consumption model is taken from [132]:

$$\mathcal{E}_t = p_t(L_d/R_d), \tag{4.14}$$

where $\mathcal{E}_t$ is the energy consumption for transmitting a data packet. We also use Equation (4.14) to calculate the energy consumption for receiving and idle listening. The simulation parameters are summarized in Table 4.4.

Table 4.4: Simulation parameters in Chapter 4

Parameters	Value
center frequency of the acoustic modem f	30 kHz
transducer efficiency ξ	0.8
constant level η_0	50 μPa^2/Hz
transmission range r	1,000 m
sound speed v_s	1,500 m/s
data rate of acoustic modem R_d	5,000 bit/s
distance between two closet adjacent nodes d_c	550 m
utilization ratio of a sink node $\mathcal{U}$	10%~80%
traffic intensity $i^{(u)}$	10~50
transmitting power p_t	20 W
receiving power p_r	3 W
idle listening power p_l	0.08 W
sleeping power p_s	0 W
size of a data packet L_d	1200 B
size of an ACK or a data request	32 B

4.3.2 Energy Consumption

We first evaluate the average energy consumption per sensor node with different duty cycles. The duty cycle can be calculated as $\frac{q}{(q^2+q+1)}$, where q is a prime power. The size of the network is 15×15. Each node transmits 50 data packets per day to the sink node, which corresponds to $\mathcal{U} \approx 50\%$. As shown in Figure 4.8, the percentage marked on the bar chart represents the proportion of energy consumption during the idle listening using different duty cycles. From the figure, we observe that when the duty cycle decreases, the average energy consumption per node decreases. The reason is that the energy consumption during idle listening is reduced using smaller duty cycles. In the proposed asynchronous wake-up scheme, fewer active slots are used by sensor nodes in one cycle to deliver data packets, but without loss of connectivity in the network. The proportion of energy consumption for idle listening gradually decreases from 31% to 12%, which implies that more energy can be used for data transmission. It is worth noting that, for different duty cycles, the energy consumption for transmitting or receiving is almost the same because we fixed the total number of data packets to be transferred. It is clear that the energy consumed by transmitting and receiving data packets dominates the energy consumption for sensor nodes.

On the other hand, we realize that the energy consumption for transmitting slightly goes up as the duty cycle decreases. The reason is that, in the proposed asynchronous wake-up scheme, the smaller duty cycle leads to more active slots in one cycle. For example, there are 6 active slots out of 21 total slots in one cycle when the duty cycle is 28.57%. However, a smaller duty cycle, e.g., 8.27%, can be achieved when a sensor node has 132 active slots out a total of 1596 slots in one cycle. In an average sense, a sensor node needs more active slots (sending data requests) to connect to a next-hop node using a duty cycle of 8.27% than with a 28.57% duty cycle.

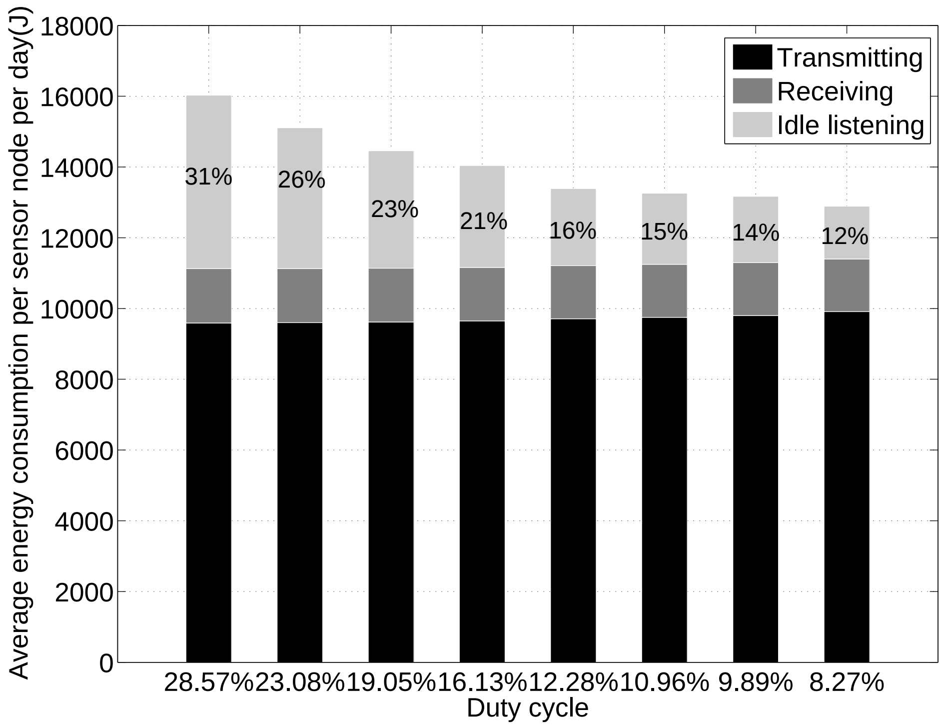

Figure 4.8: Average energy consumption per node versus duty cycle, 15×15 square grid. The percentage on each bar shows the proportion of energy consumption for idle listening.

It is worth noting that the packet delay performance is not the main concern here as this work focuses on long-term marine monitoring applications, where delay is not a major impacting factor. Nevertheless, the proposed scheme lengthens the packet delay slightly. For example, when there are 6 active slots out of 21 total slots in one cycle, which corresponds to a duty cycle of 28.57% ($q = 2$), two sensor nodes will have 6 active slots in one cycle to establish their connections. However, for a lower duty cycle of 8.27% ($q = 11$), there will be 132 active slots out a total of 1596 slots in each cycle for two sensor nodes to communicate with each other. Because the duration of each time slot (both active slots and inactive slots) is the same, operating in a low duty cycle, e.g., 8.27%, prolongs the duration of the connection establishment, thus leading to a longer delay. In general, a lower duty cycle will help to reduce the energy consumption, but will inevitably cause the increase of packet delay.

We also study the average energy consumption per sensor node by varying the network sizes. Two duty cycles, i.e., 28.57% and 8.27%, which correspond to scenarios of short and long packet delay, are considered to demonstrate the average energy consumption per node for different network sizes in one data transmission round, where each sensor node will transmit 50 data packets to the sink node. As shown in Figure 4.9, the energy consumption for idle listening can be reduced by utilizing smaller duty cycle for different network sizes. The reasons are similar to what we have explained for Figure 4.8. Because the volume of data is different with varying network sizes, the energy consumed by transmitting and receiving data packets gradually increases when the network size increases. Sensor nodes in a smaller network, e.g., 9×9, consume less energy than those in a larger network, e.g., 17×17, in each data transmission round for the following two reasons: 1) a sensor node can communicate with the sink node in fewer hops. In our simulation, the maximum number of hops is 4 in the 9×9 UWSN; however, this number becomes 8 when the network size increases to 17×17; 2) with fewer sensor nodes in the network, energy consumption for forwarding traffic becomes less.

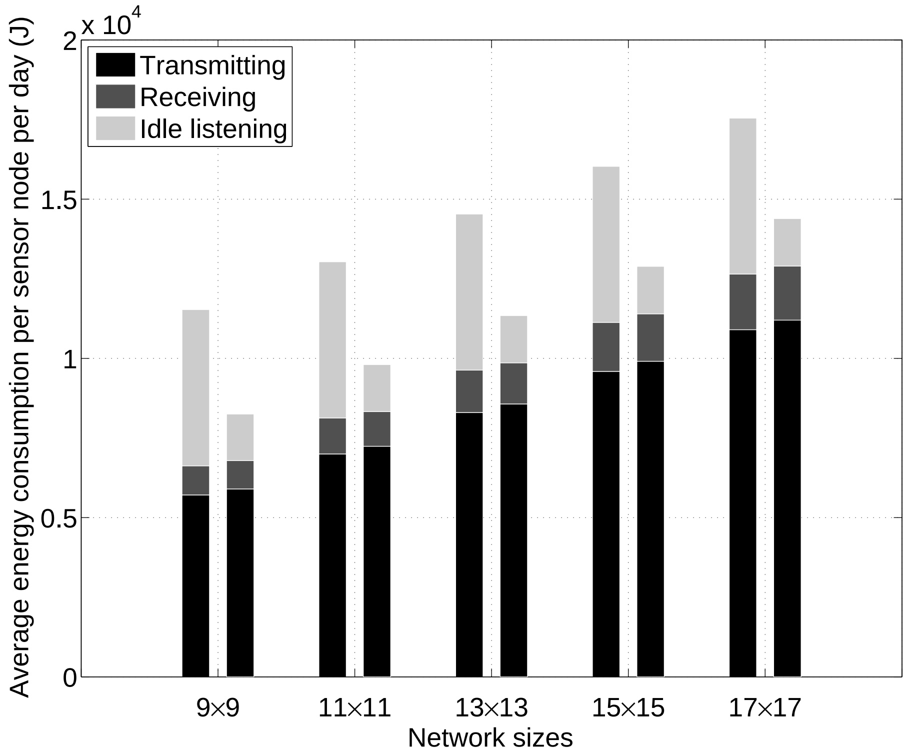

Figure 4.9: Average energy consumption per node versus network size. The left bar shows the average energy consumption using a duty cycle of 28.57%. The right bar shows the average energy consumption using a duty cycle of 8.27%.

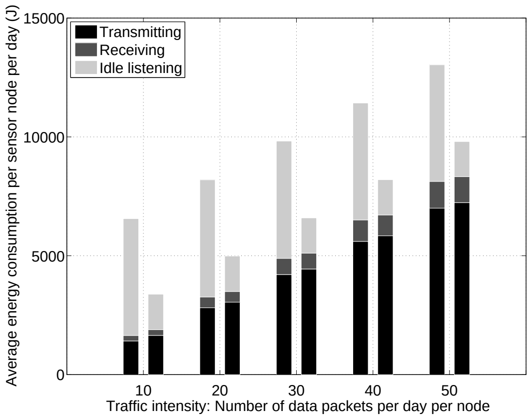

(a) Network size: 11×11

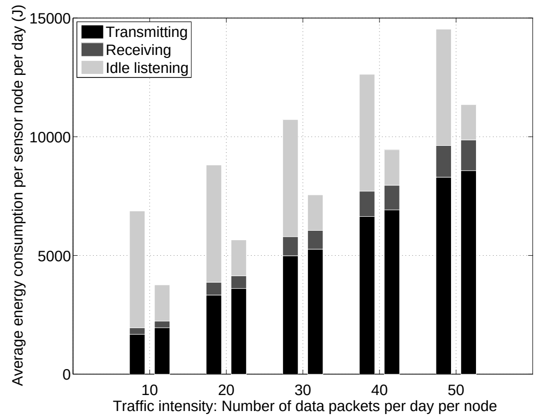

(b) Network size: 13×13

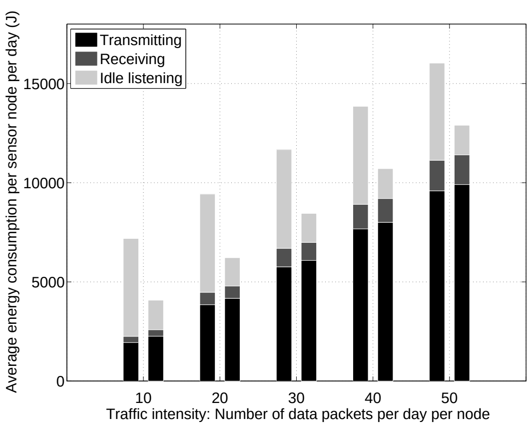

(c) Network size: 15×15

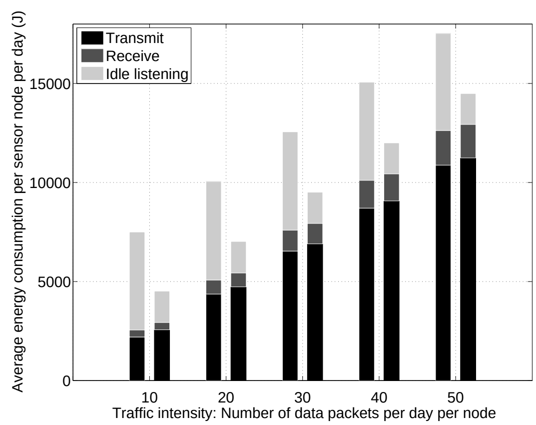

(d) Network size: 17×17

Figure 4.10: Average energy consumption per node versus traffic intensity. The left and the right bar show the average energy consumption using duty cycles of 28.57% and 8.27%, respectively.

Figure 4.10 shows the average energy consumption per sensor node with varying traffic intensity for two duty cycle scenarios of 28.57% and 8.27%, respectively, which correspond to high and low duty cycle conditions in 11×11, 13×13, 15×15, and 17×17 networks. From the figure, we observe that the energy consumed for idle listening can be conserved when using smaller duty cycles and they are little changed for all traffic load scenarios as the traffic intensity increases. However, we do note that the proportion of energy consumed for idle listening decreases because more energy is consumed for transmitting and receiving data. From that, we conclude that for network applications with low traffic intensity, sensor nodes consume a large proportion of energy for idle listening. Our proposed scheme provides an effective approach to reduce energy consumption for such applications. When traffic intensity increases, more energy is consumed for transmitting and receiving data packets hence the energy consumption for idle listening becomes less significant.

We compare the performance of proposed asynchronous wake-up scheme with that of the CDS-based protocol in [64] under different traffic intensities. The network sizes are 11×11, 13×13, 15×15, and 17×17. The duty cycle of the CDS-based protocol can be calculated by $\frac{q+1}{(q^2+q+1)}$. We choose $q = 2$ and $q = 4$ for both the proposed scheme and the CDS-based protocol. As shown in Figure 4.11 and Figure 4.12, we observe that, for different traffic intensity, the proposed scheme consumes less energy for idle listening than the CDS-based protocol. This is because the low duty cycle design introduced by the proposed scheme, where idle listening has been minimized as well as fewer active slots are utilized by sensor nodes in one cycle to deliver data packets. It is worth noting that all these are achieved without sacrificing the network connectivity.

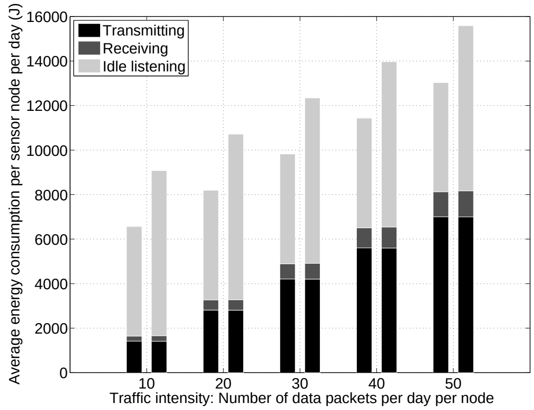

(a) Network size: 11×11

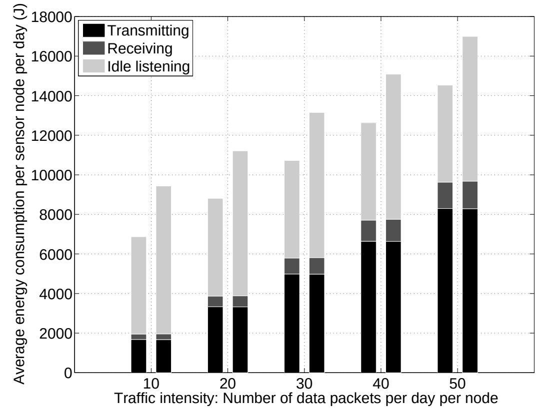

(b) Network size: 13×13

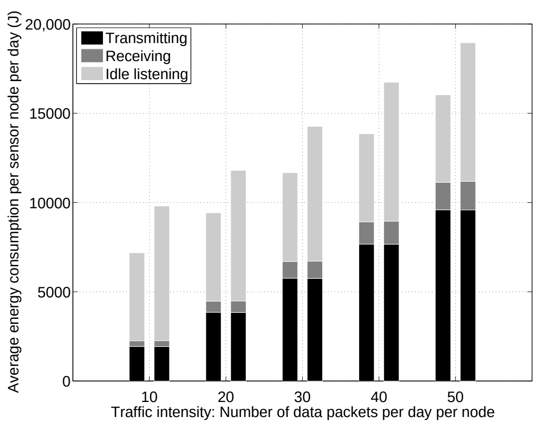

(c) Network size: 15×15

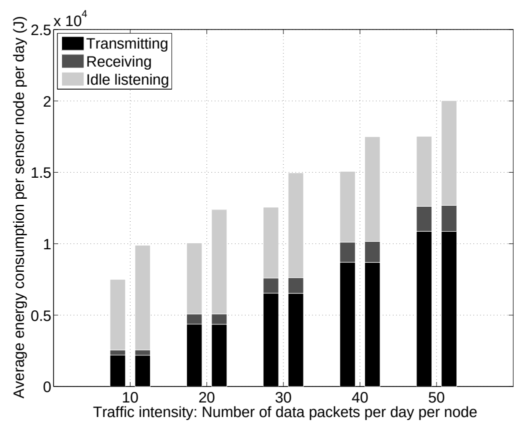

(d) Network size: 17×17

Figure 4.11: Average energy consumption versus traffic intensity comparison (q=2). The left bar presents the case using the proposed scheme. The right bar shows the case using the CDS-based protocol [64].

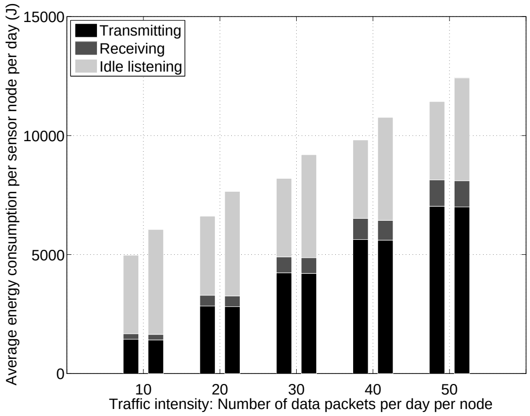

(a) Network size: 11×11

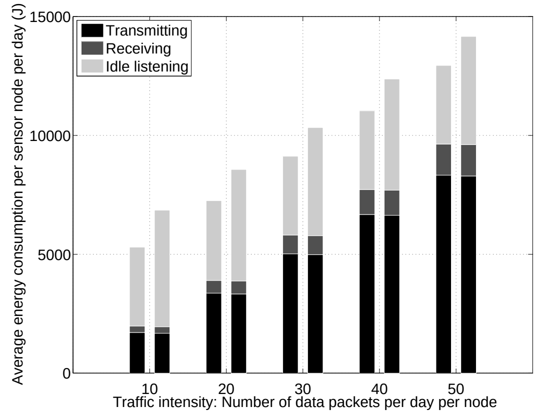

(b) Network size: 13×13

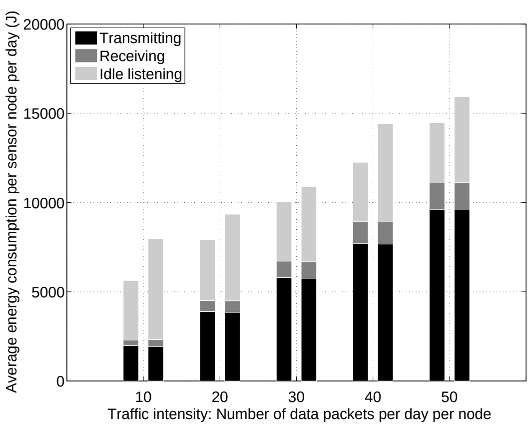

(c) Network size: 15×15

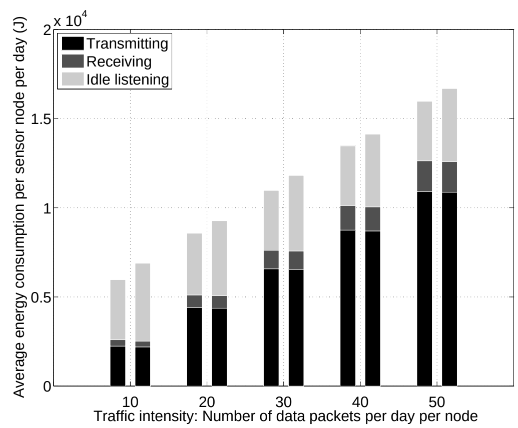

(d) Network size: 17×17

Figure 4.12: Average energy consumption versus traffic intensity comparison (q=4). The left bar presents the case using the proposed scheme. The right bar shows the case using the CDS-based protocol [64].

4.3.3 Sink Node Utilization Ratio and Network Scalability

In this subsection, we investigate the utilization ratio of a sink node with varying traffic intensity and network size. We then study the scalability of a network with the help of multiple sink nodes.

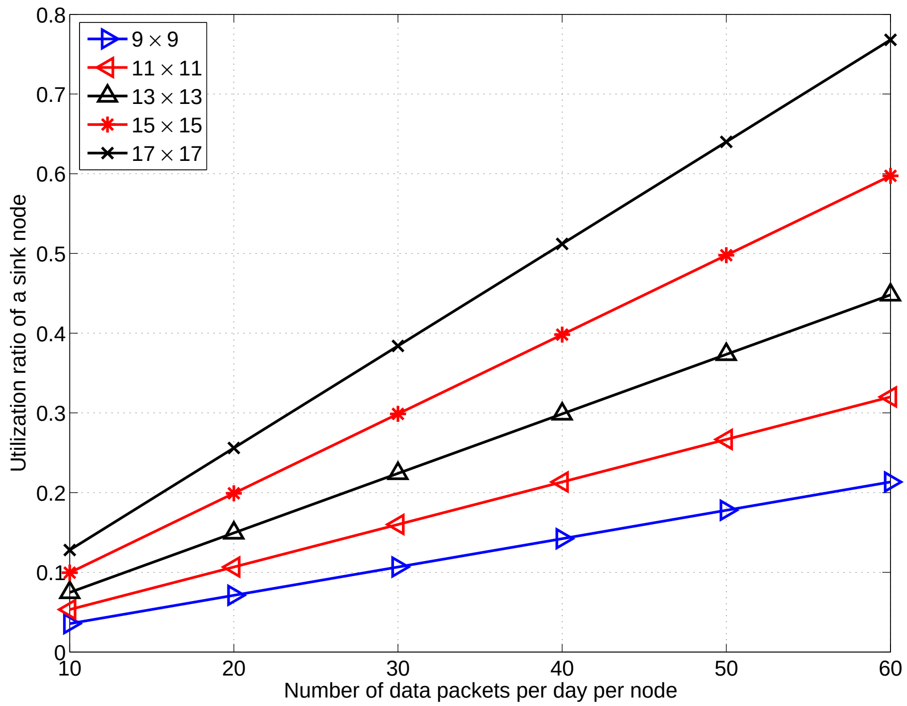

Figure 4.13: Utilization ratio of a sink node versus traffic intensity

Figure 4.13 shows the utilization ratio of the sink node under different network sizes in the case of single sink node deployed at the center of the network. The topology is the same as what has been shown in Figure 4.1. We vary the traffic intensity from 10 to 60 data packets per day per sensor node. From the figure, we can observe that the utilization ratio of the sink node increases with the traffic intensity.

Moreover, for a given utilization ratio, smaller networks can accommodate higher traffic intensity because the total amount of traffic generated by the sensor nodes is small. For a given traffic intensity, a larger network leads to a higher utilization ratio of the sink node because it spends more time on receiving and transmitting data packets. From Figure 4.13, we find that the sink node actually spends more than half of its time relaying the traffic for a network of 17×17 when the traffic intensity reaches 40 data packets per day per sensor node. The same situation is observed for a smaller network size, e.g., 15×15, however, with increased traffic intensity, e.g., more than 50 data packets per day per sensor node. As explained earlier, we assume that half of the sink node's time will be spent on collecting data from source nodes and relaying them to the surface node, therefore, the utilization ratio of sink node should be always kept below 50%.

When multiple sink nodes are incorporated to enhance the network scalability, we assume that the surface node is located at the center of UWSN. The distance between a sink node and the surface node $d_{sink-surface}$, is determined by $d_{sink-surface} = \sqrt{d_e^2 + {d_{sink-center}}^2}$, where $d_{sink-center}$ represents the distance between a sink node and the center of UWSN and d_e is the depth of the water. $d_{sink-center}$ is related to the depth of seawater and should not exceed the transmission range of the sink nodes. Here, we assume that the depth is 500 m and the distance between two adjacent sensor nodes is 500 m.

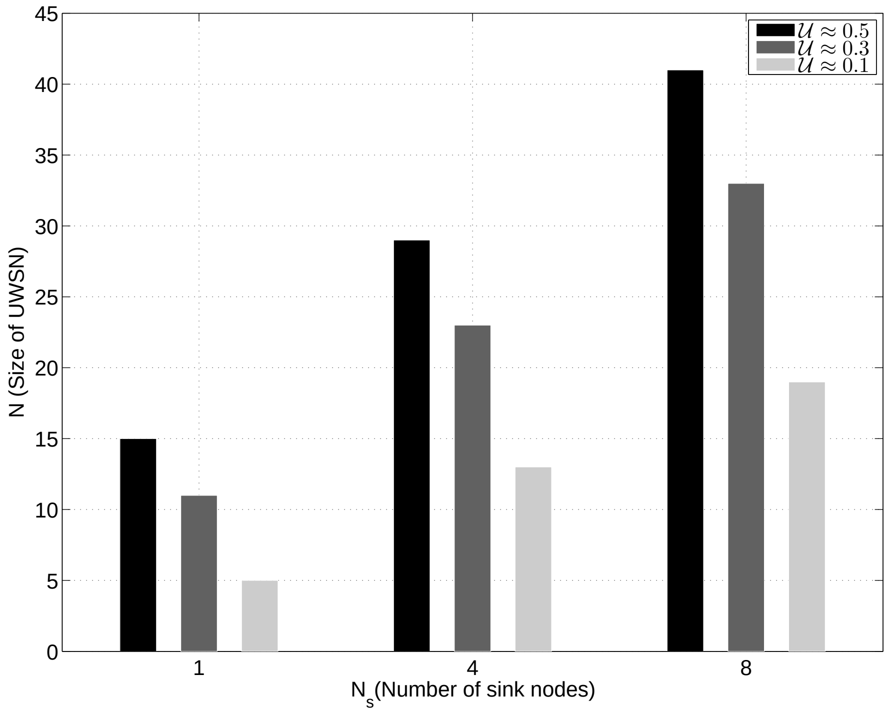

Figure 4.14: Network scalability versus number of sink nodes

In Figure 4.14, we plot the maximum achievable network size versus the number of sink nodes for different utilization ratios of each sink node (in average sense). The same traffic intensity is considered, that is, 50 data packets per day per sensor node. It is clear that networks of larger sizes can be supported when multiple sink nodes are introduced. This is because the utilization ratio of the sink node is the bottleneck which restricts the amount of traffic to be relayed to the surface node. For example, with 8 sink nodes deployed in the region, as shown in Figure 4.7, we can easily handle a network size of 41×41 under a utilization ratio of 0.5, whereas only a size of 15×15 can be supported in the case of a single sink node. Although the choice of multiple sink nodes helps to carry more traffic and can be used to support larger networks, it is inevitable that the design of the surface node will become more complicated, and the cost will be higher if it is to incorporate multiple transceivers to support simultaneous communication with the sink nodes. Besides that, as the network size increases, the sink nodes deployed away from the center of network will need to increase the transmit power to communicate with the surface node, which leads to larger energy consumption and a shortened lifetime.

4.4 Summary

In this chapter, we focused on the energy efficiency issue in UWSNs for long-term environment -al monitoring applications, and proposed an asynchronous wake-up scheme to reduce energy consumption for idle listening. The proposed wake-up scheme, based on combinatorial designs, improve energy efficiency without compromising network connectivity. We also studied the sink node utilization ratio and the network scalability for large sized networks. Our simulation results showed that the proposed wake-up scheme achieves its goal by effectively reducing the energy consumption for idle listening, and this results is consistent for different sized networks. Compared with a CDS-based coordination scheme, the proposed wake-up scheme can reduce energy consumption for idle listening. Furthermore, incorporating multiple sink nodes, our proposed scheme can effectively handle higher traffic intensity and support larger networks. As well, the proposed asynchronous wake-up scheme can be extended using Kronecker product, which can generate smaller duty cycles than EACDS and MACDS. Additionally, selecting grids with an even number of total sensor nodes would lead to similar results. When N is even, I could select one of the four sensor nodes in the middle as the sink node. As the sink node would be slightly off-centre in this case, the results also would be somewhat different. Another option would be to include an additional node in the middle of the network. If I do so, the resulting network will be symmetric, but the performance would be slightly higher.

Moreover, the proposed scheme is not limited to UWSNs with a square grid topology, and can be modified and used in UWSNs with other regular or irregular topologies. It is well-known that the transmitting power and receiving power dominate the energy consumption for different commercial acoustic modems. When other type of acoustic modems are considered, the trend of energy consumption will be very similar to what has been discussed in this chapter, even though the absolute value might be different because the power consumption parameters of different acoustic modems may vary. Therefore, the proposed scheme can be easily extended for more sophisticated acoustic modems and provide similar results as those discussed in this chapter.

Chapter 5

Balancing between Robustness and Energy Consumption for UWSNs

In Chapter 4, we proposed an asynchronous wake-up scheme in UWSNs with a square grid topology. In this topology, all sensor nodes are assumed to be deployed on the seafloor and their geometric positions form a square lattice. However, it is difficult to guarantee that all sensor nodes are deployed exactly in their desired locations because harsh marine conditions, such as currents and underwater terrain, lead to the inevitable deployment error[1]. As discussed in previous chapters, energy efficiency is an even more critical issue for UWSNs compared to WSNs because the acoustic sensor nodes rely on limited amount of non-rechargeable and unchangeable batteries. Transmitting and receiving power levels are quite larger than the idle listening power level (discussed in Section 2.2.1). When a

[1]The material in this chapter has been presented at IEEE WCNC'15 [135]

sending node and its intended receiving node are out of the communication range caused by the deployment error, transmission failure will occur. Finding a new receiving node (updating the list of next-hop nodes) and retransmission data packets consume extra energy and decrease network lifetime.

In this Chapter, we address the problem of transmission failure caused by deployment error of sensor nodes in long-term marine environmental monitoring applications. In this analysis, we consider a 2D UWSN with a square grid topology and we assume the position information of acoustic sensor nodes to be known *a priori*. After first presenting the underwater acoustic channel model for UWSNs, we analyse the problem of deployment error in UWSNs using a mathematical model. A range parameter threshold, α, is introduced to balance the robustness of the network and the energy consumption of sensor nodes, where $\alpha = r/d_c$, r is the transmission range of a sensor node, and d_c is the distance between the two closest adjacent sensor nodes. We assume a fixed transmitting power for each sensor node in our work, which corresponds to a fixed transmission range. The balance between network robustness and energy consumption in different network sizes is studied.

Chapter 5 is organized into six parts. The underwater acoustic channel model and the network topology for our work is presented in Section 5.1. A mathematical model of deployment error in UWSNs is presented in Section 5.2. The network robustness is investigated in Section 5.3. A new scoring function is proposed in Section 5.4 to balance the network robustness and the energy consumption during data transfer. We report the numerical results in Section 5.5 and conclude the chapter in Section 5.6.

5.1 Preliminaries

For consistency, we use the same underwater channel model discussed in Chapter 3. We use BPSK for signal modulation to calculate BER and PER as presented in Section 4.1.1.

Similar to the topology used in Chapter 4, we assume a total of N^2 sensor nodes deployed in 2D space, where their geometric positions are on the square lattice. The sink node is located at the center of the grid topology. The shortest distance between two adjacent nodes is d_c. There is only one surface node. The sink node will transmit the data collected from the sensor nodes to the surface node via the vertical link, which is out of the scope of this work. The position information of all nodes is known *a priori*. Each sensor node can determine how to reach the sink node with the fewest hops using two sets: (1) H_u: a set of next hop candidates within the range of node u; (2) R_u: a set of nodes for which node u serves as a relay candidate. Both of these two sets are calculated offline.

5.2 Deployment Error Model

5.2.1 Probability Distribution of Distance between Two Sensor Nodes

It is difficult to guarantee that all sensor nodes would be accurately positioned on the grid points due to the location error and the environmental factors such as ocean currents and underwater terrain. As shown in Figure 5.1, we place two sensor nodes a, b on the seafloor and their coordinates are (X_a, Y_a) and (X_b, Y_b). We assume that X_a, Y_a, X_b and Y_b are

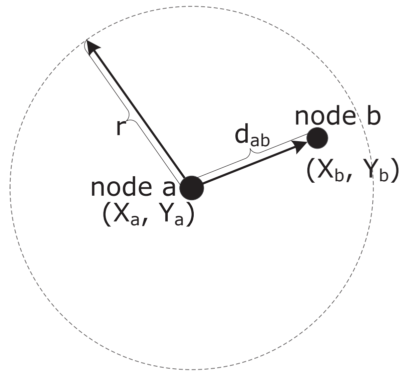

Figure 5.1: Illustration of the distance between two sensor nodes

independent Gaussian variables: i.e., $X_a \sim \mathcal{N}(\mu_{ax}, \sigma^2)$, $Y_a \sim \mathcal{N}(\mu_{ay}, \sigma^2)$, $X_b \sim \mathcal{N}(\mu_{bx}, \sigma^2)$, $Y_b \sim \mathcal{N}(\mu_{by}, \sigma^2)$. The distance between node a and node b ($d_{a,b}$) can be expressed by: $d_{a,b} = \sqrt{(X_a - X_b)^2 + (Y_a - Y_b)^2}$ in the Cartesian coordinates. The distance between two sensor nodes follow a Rician distribution if their coordinates follow the Gaussian distribution [133]. Consequently, the probability of a receiver (assume node b in Figure 5.1) in the communication range of a sender (assume node a in Figure 5.1) can be expressed by:

$$P_{a,b} = P(d_{a,b} \leq r) = 1 - \mathcal{Q}\left(\frac{s}{\sqrt{2}\sigma}, \frac{r}{\sqrt{2}\sigma}\right), \tag{5.1}$$

where $\mathcal{Q}$ is Marcum Q-function and

$$s = \sqrt{(\mu_{ax} - \mu_{bx})^2 + (\mu_{ay} - \mu_{by})^2}. \tag{5.2}$$

5.2.2 Standard Deviation of the Deployment Error

Let the coordinate of a sensor node be (X, Y). We assume that the probabilities of deployment errors on x-axis and y-axis smaller than k are larger than η, respectively, which can be expressed as

$$P(\mu_X - k < X < \mu_X + k) > \eta, \tag{5.3}$$

$$P(\mu_Y - k < Y < \mu_Y + k) > \eta, \tag{5.4}$$

where μ_X and μ_Y represent the expected coordinate values of $x-$axis and $y-$axis, respectively. η is the confidence interval. In UWSNs of a square grid topology, μ_X and μ_Y should be equal to the coordinate value of corresponding grid point.

Suppose the preferred coordinate of a sensor node is (1000, 0), η = 95%, k = 10 m. We obtain: $\sigma < 5$, which means the probability of deployment error smaller than 10 m is larger than 95% when the standard deviation (σ) of X or Y is less than 5. Another example, k =100 m and the other parameters are same as mentioned in the first example. We obtain: $\sigma < 51$, which means the probability of deployment error smaller than 100 m is larger than 95% when the standard deviation (σ) of X or Y is less than 51. The standard deviation (σ) of X or Y increases when the error of deployment becomes larger. The probability distribution of the distance between two sensor nodes and the corresponding standard deviation (σ) are used in the following sections.

5.3 Robustness of UWSNs

In this section, we explore the robustness of UWSNs with a square grid topology. The robustness of UWSNs can be improved by redundant relay nodes or novel deployment strategies if links are prone to fail due to the deployment error [136] [137]. The larger the number of relay node candidates, the higher will be the robustness. Here, channel effects and packet collision are not ignored. As we discussed in Section 5.1, all possible relay nodes on the different paths from a source node to the sink node can be determined by H and R sets. Given source node j located in the first quadrant of a UWSN with a square grid topology and its coordinate is (X_0, Y_0), we know that it is m hops (fewest hops) from the sink node. We assume that the sink node is located at the origin of the UWSN with a square grid topology and its coordinates are (X_m, Y_m). We define the set of paths from source node j to the sink node as

$$\begin{aligned} \mathfrak{P}_m^{(X_0,Y_0)} &= \{\mathcal{P}_j = \langle (X_0,Y_0),(X_1,Y_1),...,(X_m,Y_m)\rangle \\ &\quad \mid \text{for } i = 0,1,2,...,m-1, X_i > X_{i+1} \text{ or } \; Y_i > Y_{i+1}\}, \end{aligned} \tag{5.5}$$

where $\mathcal{P}_j$ is one disjointedly independent error free path from source node j to the sink node. $\mathfrak{P}_m^{(X_0,Y_0)}$ in the second, third, or fourth quadrant of the UWSN is the similar expression as we described above.

The network robustness, denoted by $\mathcal{R}$, can be expressed by:

$$\mathcal{R} = \sum_{j=1}^{N^2-1} \sum_{\mathcal{P}_j \in \mathfrak{P}_m^{(X_0,Y_0)}} \text{Prob}(\mathcal{P}_j), \tag{5.6}$$

where $\text{Prob}(\mathcal{P}_j) = \prod_{i=0}^{m-1} P_{i,i+1}$. $\text{Prob}(\mathcal{P}_j)$ is the probability of being able to send data from source node j to the sink node. $\mathcal{R}$ is a figure of merit without the meaning of probability.

We introduce the ratio of r to d, denoted by α, to investigate the robustness of UWSNs. Thus, according to Equation 5.1, Equation 5.6 can be rewritten as

$$\mathcal{R}(\alpha) = \sum_{j=1}^{N^2-1} \sum_{\mathcal{P}_j \in \mathfrak{P}_m^{(X_0,Y_0)}} \prod_{i=0}^{m-1} P_{i,i+1}(d_{i,i+1} < \alpha d). \tag{5.7}$$

It is clear that α and $\mathfrak{P}_m^{(X_0,Y_0)}$ are related. A big value of $|\mathfrak{P}_m^{(X_0,Y_0)}|$ represents that sensor nodes have more paths and relay candidates. The network robustness can be enhanced since a source node has more (redundant) choices even when some paths (or links) have failed.

5.4 Balancing between Network Robustness and Energy Consumption

In this section, our desire is to identify the optimal value of α that maximizes the network robustness, meanwhile, minimizes the energy consumption of sensor nodes. However, these two objectives are difficult to be achieved simultaneously. A certain value of α is able to maximize the network robustness using more relay candidates. Meanwhile, the energy consumption increases during data transfer because the sensor nodes need more hops to transmit data packets to the sink node under this value of α. On the contrary, the larger value of α represents higher density of networks (recall we fix the value of r and vary the value of d). Therefore, more sensor nodes are able to reach the sink node directly but with a poor network robustness. We search the optimal value of α by maximizing a scoring function ($\mathcal{F}$) in order to balance the network robustness and the energy consumption in UWSNs with a square grid topology:

$$\mathcal{F}(\alpha) = w_{\mathcal{R}} \frac{\mathcal{R}(\alpha)}{\max\big(\mathcal{R}(\alpha)\big)} + w_E \frac{\min\big(N_{hop}(\alpha)\big)}{N_{hop}(\alpha)}, \tag{5.8}$$

where $w_{\mathcal{R}}$ and w_E are the weights for the network robustness and the energy consumption of sensor nodes, respectively. $N_{hop}(\alpha)$ denotes, for a given value of α, for all sensor nodes, the total number of hops (from sensor nodes to the sink node). $\min\big(N_{hop}(\alpha)\big)$ indicates the minimum hops among all possible routes. $\max\big(\mathcal{R}(\alpha)\big)$ represents the maximum value of $\mathcal{R}$. Without any doubt, the first term in Equation 5.8 indicates the consideration of robustness when making a routing decision. It is obvious that more hops indicates more forwarding. Moreover, transmitting and receiving power levels dominate the energy consumption during data transmission in UWSNs. For example: typical power consumptions for transmitting, receiving, idle listening and sleeping functions are 20 W, 3 W, 0.08 W and 0 W, respectively [66]. Therefore, the second term in Equation 5.8 reflects the consideration of energy consumption when deciding routes. The design of the scoring function (Equation 5.8) is not only intuitive, but also indicate the cost of energy consumption when considering the network robustness. We can conceive other possible formulas, such as $\mathcal{F}(\alpha) = w_{\mathcal{R}} \frac{\mathcal{R}(\alpha)}{\max\left(\mathcal{R}(\alpha)\right)} / w_E \frac{\min\left(N_{hop}(\alpha)\right)}{N_{hop}(\alpha)}$, but it is difficult to explain such scoring function.

5.5 Numerical Results

In this section, we report the different values of α to balance network robustness and energy consumption of sensor nodes in different network sizes. The maximum distance between two closest adjacent nodes, i.e., d, is 550 m that guarantees at least one relay candidate on the diagonal link. In this chapter, we fix the transmission range of a sensor node and vary the value of d for networks of different sizes. We choose the power consumption parameters of the Micro-modem, which is a widely used in academic and commercial areas [30, 66]. We emphasize the importance of the applicability of our results to practical long-term marine monitoring applications. For a given range r =1,000 m and with f = 30 kHz, $\eta_0 = 50\ \mu\text{Pa}^2/\text{Hz}$, $\mathcal{K}$ = 2, and $\xi = 0.8$, according to Equations 4.1, 4.4, and 4.5, zero BER with a transmitting power of 20 W can be achieved. Several technical specifications report that, in the general ocean state, a transmitting power of 20 W can reliably achieve the transmission range of 1,000 m [19, 30]. Some researchers utilize different transmitting power levels corresponding to different transmission ranges [83, 102]. Our goal is to conservatively ensure a highly reliable data transfer. Thus, the transmit power of 20 W corresponding to the transmission range of 1,000 m is used.

We consider two values of the standard derivation (σ) of the expected coordinate values of a sensor node, i.e., 5 and 51, which correspond to the deployment errors 10 m and 100 m, respectively. According to the Section 5.2.2, the confidence interval can reach 95%. We report the simulation results of grids with odd numbers of nodes in each network size. It is obvious that the sink node would be exactly at the center of the grid. Even number of total sensor nodes would lead to approximately the same conclusion as presented in this chapter, despite the fact that the sink node would be slightly off-center.

We study the scoring function (i.e., Equation 5.8) under different values of α and evaluate them with different combinations of weights, i.e., $w_{\mathcal{R}}$ and w_E ($w_{\mathcal{R}} + w_E$=1). We choose five combinations of the weight for network robustness and the weight for energy consumption to represent the diverse requirements of deployment of UWSNs in practice. $w_{\mathcal{R}} = 1$, $w_E = 0$ and $w_{\mathcal{R}} = 0$, $w_E = 1$ represent that the network robustness and the energy consumption is the only requirement when deploying UWSNs, respectively. $w_{\mathcal{R}} > w_E$ indicates that the network robustness is more important than the energy consumption during data transfer and vice versa. From Figure 5.2 ~ Figure 5.8, we observe that the optimal value of α is smaller when the network robustness is crucial and becomes larger when the energy expenditure is a big concern of deploying sensor nodes on the seafloor. This trend is consistent across different network sizes. A smaller value of α indicates that a sensor node has more relay candidates and more paths to the sink node, thus, the network robustness is enhanced (in this chapter, we fixed the transmission range and vary the distance between two closest adjacent sensor nodes). In contrast, a larger value of α enables more sensor nodes to communicate with the sink node directly, which can be considered as a more energy-efficient approach of data transmission because few sensor nodes join the data forwarding (we can show the bigger value of α than that in Figure 5.2 ~ Figure 5.8. However, the physical meaning is less because the distance between two closest adjacent nodes should not be too short for long-term marine monitoring applications).

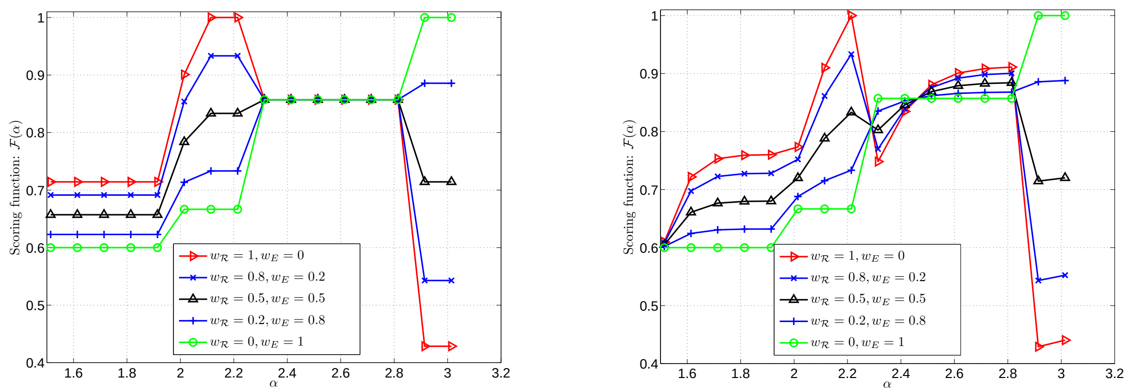

(a) deployment error ≤ 10 m ($\sigma = 5$)

(b) deployment error ≤ 100 m ($\sigma = 51$)

Figure 5.2: Value of scoring function versus value of α, network size: 5×5

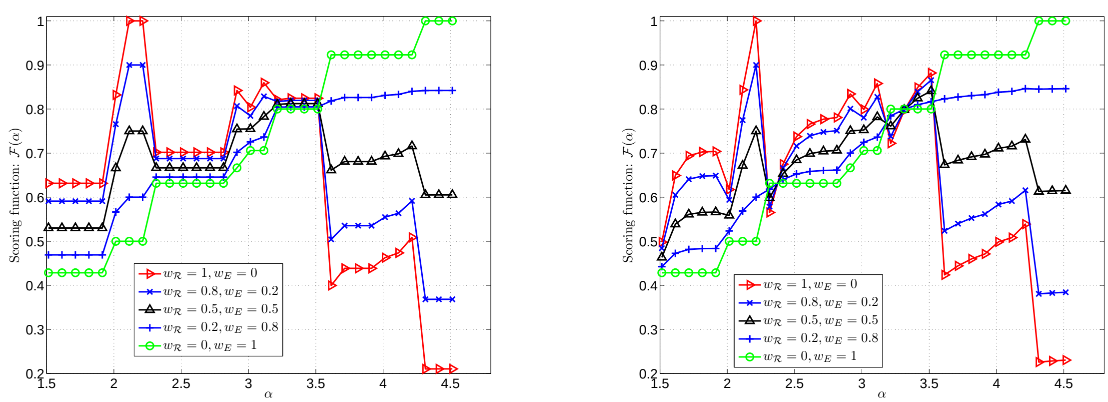

(a) deployment error ≤ 10 m ($\sigma = 5$)

(b) deployment error ≤ 100 m ($\sigma = 51$)

Figure 5.3: Value of scoring function versus value of α, network size: 7×7

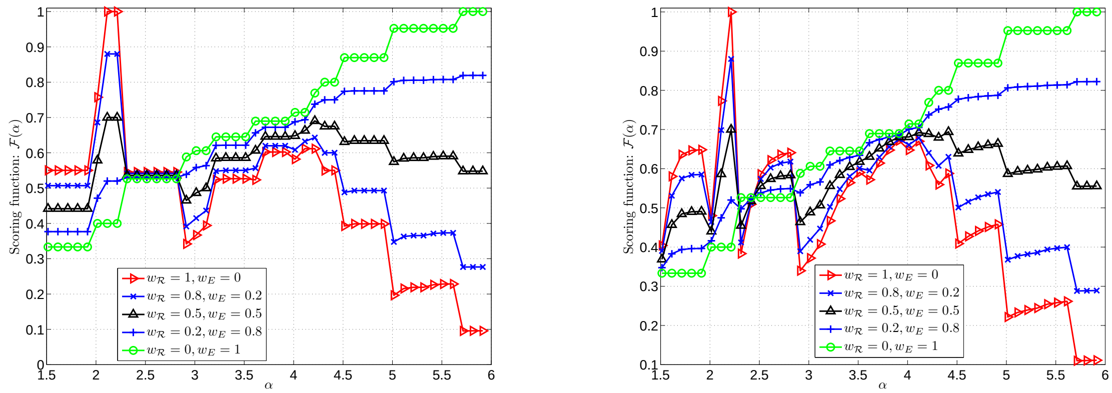

(a) deployment error $\leq$ 10 m ($\sigma = 5$)

(b) deployment error $\leq$ 100 m ($\sigma = 51$)

Figure 5.4: Value of scoring function versus value of α, network size: 9×9

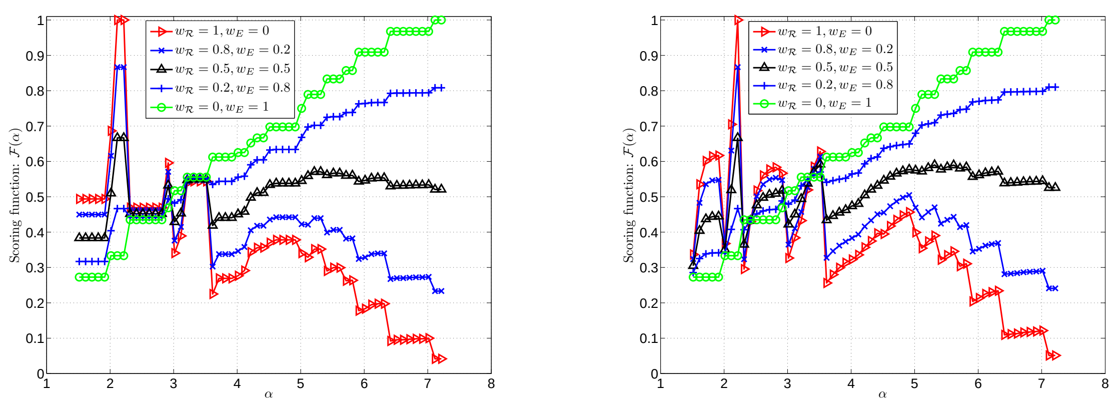

(a) deployment error $\leq$ 10 m($\sigma = 5$)

(b) deployment error $\leq$ 100 m ($\sigma = 51$)

Figure 5.5: Value of scoring function versus value of α, network size: 11×11

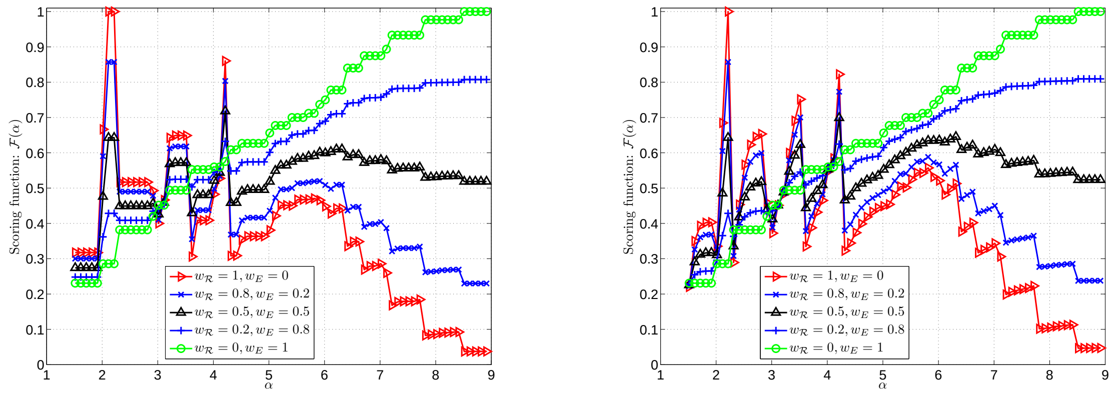

(a) deployment error ≤ 10 m ($\sigma = 5$) (b) deployment error ≤ 100 m ($\sigma = 51$)

Figure 5.6: Value of scoring function versus value of α, network size: 13×13

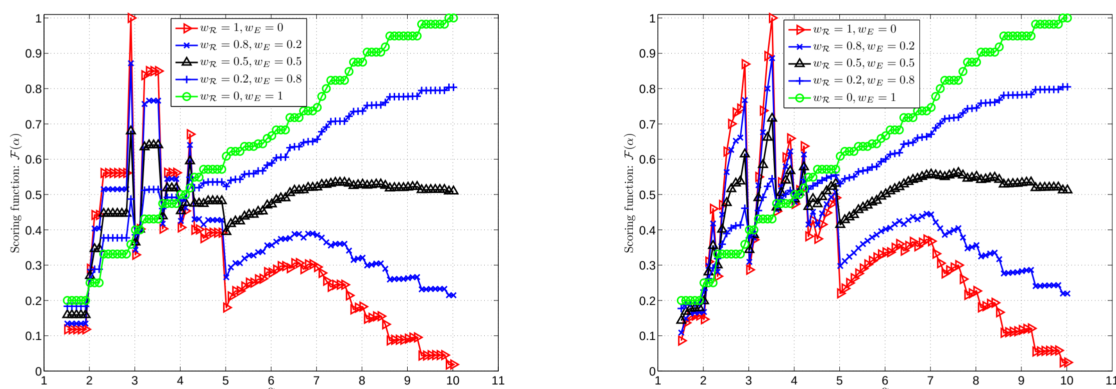

(a) deployment error ≤ 10 m ($\sigma = 5$) (b) deployment error ≤ 100 m ($\sigma = 51$)

Figure 5.7: Value of scoring function versus value of α, network size: 15×15

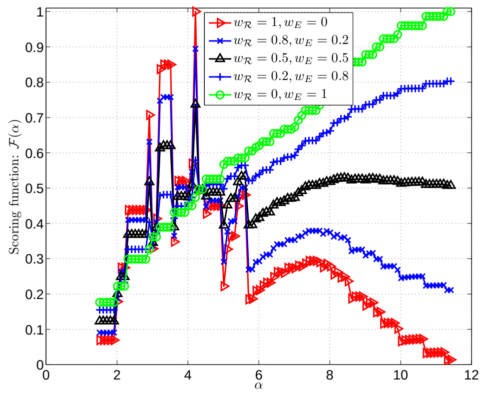

(a) deployment error ≤ 10 m ($\sigma = 5$)

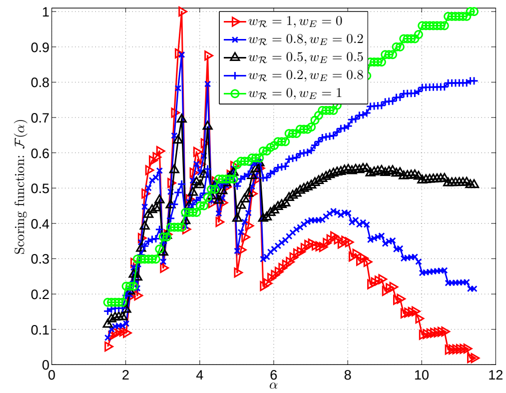

(b) deployment error ≤ 100 m ($\sigma = 51$)

Figure 5.8: Value of scoring function versus value of α, network size: 17×17

Besides the cases of $w_{\mathcal{R}} = 1$, $w_E = 0$ and $w_{\mathcal{R}} = 0$, $w_E = 1$, we present the results of the scoring function with the other three combinations, i.e., $w_{\mathcal{R}} = 0.8$, $w_E = 0.2$; $w_{\mathcal{R}} = 0.5$, $w_E = 0.5$, and $w_{\mathcal{R}} = 0.2$, $w_E = 0.8$. For a given size network and a given deployment error (σ), we observe that the optimal value of α increases when the weight for energy consumption increases and the weight for robustness decreases. The reasons are similar to what we explained in the previous paragraph. When the robustness of network is less important than the energy consumption of sensor nodes, we suggest that more sensor nodes uses fewer hops to communicate with the sink node in order to reduce energy consumption on forwarding. On the contrary, more relay candidates between a source node and the sink node are significant when the network robustness is in the first place of UWSNs deployment.

We also realize that, in networks of certain sizes, the optimal values of α are same under different cases of $w_{\mathcal{R}}$ and w_E. The reason is that increasing the value of α may not reduce the number of hops continuously, which is related to the discrete nature of the square grid topology. The network robustness still dominate the value of the scoring function in spite of more consideration of energy consumption.

In some sized networks of certain sizes with a smaller deployment error, we always obtain several different values of α leading to the same maximum value of the scoring function. The reasons are related to the deployment error and the property of Rician distribution. First, in some sizes of UWSNs with a square grid topology, increasing the value of α does not significantly contribute to the growth of number of relay candidates in each hop since the nature of the square grid topology. Second, $P_{i,i+1}$ is changed little (not sensitive to the distance between two closest adjacent nodes) when the deployment error is smaller (e.g., $\sigma = 5$) due to the properties of Rician distribution.

5.6 Summary

In this chapter, we studied the deployment error of 2D UWSNs with a square grid topology and then gave a probability distribution of the distance between two sensor nodes. Based on this probability distribution, we discussed the robustness of UWSNs and utilize a parameter, namely, the ratio of the transmission range of a sensor node to the distance between two closet adjacent nodes, to achieve a balance between network robustness and energy consumption in underwater acoustic communication. The optimal ratio can be varied to satisfy different requirements of network robustness and energy consumption of UWSNs. Furthermore, selecting grids with a even number of total sensor nodes would lead to approximately the same conclusions as presented in this chapter, despite the fact that the sink node would be slightly off-center. Not limited to UWSNs with a square grid topology, the proposed balance can also be utilized in UWSNs with other regular and irregular topologies when the position of sensor nodes is predetermined. Additionally, similar conclusions as presented in this chapter can be obtained using power consumption parameters from different acoustic modems.

Chapter 6

An Energy-efficient Relay Node Selection Scheme for UWSNs

Communication over a long distance in seawater requires a fairly high transmitting power, so multi-hop communication is a common alternative in UWSNs. Energy efficiency becomes an even more challenging issue when designing routing protocols to support multi-hop communication in UWSNs. Routing protocols for terrestrial WSNs may not be directly useful as most of their efforts were placed on increasing network throughput, decreasing packet delay and reducing packet error rate. Therefore, they must be carefully re-examined in the context of underwater applications. Under energy-constrained conditions and long-term marine monitoring applications, data transfer with minimum energy consumption becomes more significant than merely improving network throughput[1].

[1]The material in this chapter has been submitted to Wiley Journal of Wireless Communication and Mobile Computing [138]

In this chapter, we formulate the relay node selection problem as a linear programming problem and obtain the theoretical maximum lifetime of UWSNs with a square grid topology. We then propose a new routing metric that jointly considers the transmitting power level and the residual energy of the two-end nodes of each acoustic link[2]. We evaluate the performance of the proposed relay node selection scheme with different network sizes and using different initial energy assignments. The results are compared to networks where routing schemes only focus on minimizing the number of hops.

The rest of this chapter is organized as follows. Section 6.1 presents the maximum network lifetime formulation. The proposed energy-efficient scheme of relay node selection is presented in Section 6.2. In Section 6.3, we evaluate the performance of the proposed scheme. The chapter is concluded in Section 6.4.

6.1 Maximum Network Lifetime Formulation

In this section, we present the underwater acoustic channel, the topology of UWSNs, and the network lifetime formulation.

6.1.1 Underwater Acoustic Channel Model

We used the semi-empirical formula [21, 52] to study the underwater acoustic channel and calculate the transmission loss of acoustic signals in seawater. The semi-empirical formula

[2]In this chapter, an acoustic link includes only two nodes, a sending node and a receiving node. They are the neighbouring nodes

and the underwater acoustic channel are also discussed in Chapter 3, which are also utilized in Chapters 4 and 5.

In this chapter, we use the EvoLogics S2CR18/34 [68] modems that provide the sweep -spread carrier (S2C) technique to modulate the acoustic signal. S2C can clearly separate multipath arrivals of acoustic signals by converting their time delays into frequency reallocations. The acoustic signal energy is spread over a wide range of frequencies. The receiver collects the energy and converts the received signals into narrow band signals. Significant depression of multipath disturbances and substantial system gain can be achieved. The communication performance improvement is verified in both simulations and experiments [88, 139, 140]. According to the literature [133, 139, 140], the processing gain of S2C can be expressed by:

$$\mathbb{G} = 10\log_{10}(\mathbb{W}/\mathfrak{R}), \tag{6.1}$$

where $\mathbb{W}$ is the available bandwidth in Hz and $\mathfrak{R}$ is the bit rate at the input to the encoder in bits/s.

We use quadrature phase shift keying (QPSK) [133, 139]. The bit error rate (BER) of QPSK signal can be calculated as [133]

$$BER = 2Q\left(\sqrt{2\cdot 10^{((SNR+\mathbb{G})/10)}}\right)\cdot\left(1-0.5Q(\sqrt{2\cdot 10^{((SNR+\mathbb{G})/10)}})\right), \tag{6.2}$$

where $Q(x) = \frac{1}{\sqrt{2\pi}}\int_x^\infty exp(-t^2/2)dt$. L_d stands for the size of a data packet. The packet error rate (PER) can be calculated by Equation 4.5.

6.1.2 Topology of UWSNs

We consider a multi-hop UWSN with a square grid topology for the long-term marine environmental monitoring applications, which is same as that in Chapters 4 and 5. $N \times N$ sensor nodes are located on the seafloor, which is assumed to be 2-dimensional. Their geometric positions form a square lattice. The distance between two closest adjacent nodes is d_c. The sink node (denoted by u_0) is located at the center of the grid. It collects data (from other sensor nodes) and reports data to the surface node directly. We assume that there is only one surface node and it communicates only with the sink node.

Similar to what has been assumed in other work in the literature [1], we assume that the each sensor node is equipped an omnidirectional transceiver and the transmission range of sensor nodes is a circle. The transmission range of the sink node is the same as that of the other sensor nodes. Two nodes can communicate with each other as long as they are within the transmission range. Relay nodes are needed when the receiving node is out of transmission range of the sending node. Again, this assumption is consistent with other reported work in this area [50, 111]. The position information of all nodes is known *a priori*. Consequently, every sensor node can easily determine the path to reach the sink node with fewest hops by maintaining two sets: (1) H_u: a set of next hop candidates within range of node u; (2) R_u: a set of nodes for which node u serves as a relay candidate. Both these sets are calculated offline.

6.1.3 Network Lifetime Formulation

UWSNs can be modeled as a graph $G = (V, E)$, where V is the set of nodes (or vertices) and E is the set of acoustic links (u, v) (or edges). Nodes u and node v are connected by a link $(u, v) \in E$ if they can communicate with each other directly. $p_t^{(u,v)}$ denotes the minimum transmitting power level to maintain a link between nodes u and v. A sensor node can utilize different transmitting power levels (determined by the acoustic modem) to connect different relays. p_r and p_l stand for the receive and idle listening power level, respectively. $\mathcal{E}_0^{(u)}$ and τ denote the initial energy of a sensor node and the transmission time of a data packet, respectively. Let $i^{(u)}$ be the injection rate of node u in packets per day, i.e., traffic generated by node u. $r^{(u,v)}$ denotes the transit rate from node u to node v.

In this chapter, we employ an energy-efficient asynchronous wake-up scheme with a duty cycle of 8.27%, which has been discussed in Chapter 4. Each sensor node has two operation modes: wake-up mode and sleep mode. In the wake-up mode, a sensor node can listen to the channel, transmit data packets, and receive/forward data packets from other sensor nodes. In the sleeping mode, a sensor node turns off the transmitter in order to reduce energy consumption. The sink node is always in the wake-up mode in order to collect data from other sensor nodes continuously. Consequently, the lifetime of node u, denoted by T_u, can be expressed as

$$T_u = \frac{\mathcal{E}_0^{(u)}}{p_t^{(u,v)}\tau \times \left(i^{(u)} + \sum_{v \in H_u} r^{(u,v)}\right) + p_r\tau \times \sum_{w \in R_u} r^{(w,u)}}, \tag{6.3}$$

where the first and second components of the denominator in Equation (6.3) are the energy consumption for sending and receiving data packets, respectively. The network lifetime, denoted by $\mathcal{T}$, is defined as the amount of time that the first sensor node exhausts its energy reserve. The network lifetime maximization could be expressed as

$$\mathcal{T} = \max\left(\min_{u\in V}(T_u)\right). \tag{6.4}$$

However, in UWSNs with a square grid topology, where the sensing range is considerably greater than the communication range. After the first sensor node exhausts energy, the sink node is able to receive packets via other nodes since we can route data through other areas of the network to get to the sink node. Therefore, in this chapter, the network lifetime (denoted by T to differentiate from $\mathcal{T}$) is defined as the amount of time when so many nodes exhaust their energy reserves that the sink can no longer be reached by sensor nodes. This definition is similar to that in [108]. Our objective is to produce a novel flow assignment to maximize the network lifetime. This problem can be formulated in a linear programming problem as follows:

$$\max \quad T \tag{6.5}$$

$$\text{s.t.} \quad \tau \times T\left(p_t^{(u,v)} \times \sum_{v\in H_u} r^{(u,v)} + p_r \times \sum_{w\in R_u} r^{(w,u)}\right) \le \mathcal{E}_0^{(u)}, \forall u \in V\backslash\{u_0\} \tag{6.6}$$

$$\sum_{w\in R_u} r^{(w,u)} + i^{(u)} = \sum_{v\in H_u} r^{(u,v)}, \forall u, w, v \in V\backslash\{u_0\} \tag{6.7}$$

$$r^{(u,v)} \ge 0, r^{(w,u)} \ge 0. \tag{6.8}$$

Inequality (6.6) is a linear programming formulation for the energy constraint. That is, for node u, the total amount of energy consumed for transmitting and receiving data packets should not exceed $\mathcal{E}_0^{(u)}$. Equation (6.7) is the flow conservation constraint. That is, for each node, the output flow should be equal to the input flow. The input flow has two parts: $r^{(w,u)}$, i.e., the data from previous-hop nodes, and $i^{(u)}$, i.e., the data generated by node u itself.

6.2 Relay Node Selection Scheme

In this section, we propose a scheme of relay node selection for UWSNs. Our objective is to prolong the network lifetime and to collect more information from the sensor nodes located on the seabed.

A sensor node can reach the sink node through different paths by employing different transmitting power levels. For example, the acoustic modem supports three transmitting power levels [68]. In Figure 6.1, node a, as a source node, can transmit data to the sink node via two hops (node 5 as a relay) using the maximum transmitting power level (the first path) or through nodes 3, 5, and 7 with the minimum transmitting power level (the third path). Using the medium transmitting power level, node 4 and node 7 are the two relays on the second path.

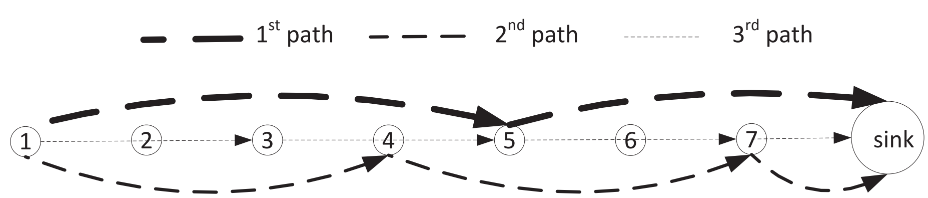

Figure 6.1: Example of different paths from a source to the sink node

Recall that the transmit and receive power levels dominate the energy consumption for data transmission in UWSNs. We utilize the energy consumption of transmitting and receiving a data packet as a link cost. The link cost between node u and node v, denoted by $c^{(u,v)}$, could be expressed by:

$$c^{(u,v)} = \tau \times \left(p_t^{(u,v)} + p_r\right). \tag{6.9}$$

A source node can calculate the costs of different paths based on Equation (6.9) and selects a path with the minimum link cost to transmit data packets. However, in long-term applications, except the sensor nodes located at the edge of the network, most of the sensor nodes act both as source nodes and relays, i.e., the battery energy of a sensor node must be consumed for transmitting and forwarding data packets. Keeping using the minimum cost paths would lead to quick batteries depletion and link failures. In general, an ideal path from a source node to the sink node should include lower transmitting power levels on each hop and avoid using of sensor nodes with lower residual energy as relays. Consider nodes u and v that are with communication range, we use $\mathcal{E}_r^{(u)}$ and $\mathcal{E}_r^{(v)}$ to denote their residual energy. In addition, let $\widehat{p_t}$ be the maximum transmitting power level of the acoustic modem. The link cost between u and v can be further refined to incorporate node residual energy as:

$$c^{(u,v)} = w_p \frac{\tau \times (p_t^{(u,v)} + p_r)}{\tau \times (\widehat{p_t} + p_r)} + w_e \left(\frac{\mathcal{E}_0^{(u)} - \mathcal{E}_r^{(u)}}{\mathcal{E}_0^{(u)}} + \frac{\mathcal{E}_0^{(v)} - \mathcal{E}_r^{(v)}}{\mathcal{E}_0^{(v)}} \right), \tag{6.10}$$

where w_p and w_e $(w_p + w_e = 1, w_p, w_e \geq 0)$ are the weights for power level and energy consumption factors, respectively. Specially, the second term in Equation (6.10) reflects the energy consumption at nodes u and v. $\tau \times (\widehat{p_t} + p_r)$ and $\mathcal{E}_0^{(u)}$ are used to normalize the cost of power and the cost of energy, respectively. The value of the first term in Equation

(6.10) can be calculated offline and the value of second term in Equation (6.10) should be updated as the network operates. We investigate the effect of the update frequency on the performance of the proposed relay node selection scheme in Section 6.3.

6.3 Performance Evaluation

In this section, we evaluate the performance of the proposed relay node selection scheme with different combinations of the weights for power level and residual energy and with different numbers of transmitting power levels. We also compare the performance of the proposed scheme against the minimum hop routing algorithm [106] and the value obtained by the linear programming. Furthermore, we investigate the effect of the update period and battery energy reassignment.

6.3.1 Simulation Settings

Grids with odd number of nodes in each dimension are selected in these simulation trials so that the sink node would be exactly at the center of the grid. We investigate four different sizes of UWSNs with a square grid topology: 11×11, 13×13, 15×15 and 17×17. Selecting grids with even values of N would lead to approximately the same conclusions as presented in this chapter despite the fact that the sink node would be slightly off-center. The distance between two closest adjacent sensor nodes is assumed as 550 m, which leads to at least one relay node existing on the diagonal link. The total initial energy of sensor nodes is $(N^2 - 1) \times 10^6$ J (10^6 J is equal to 0.27 kWh or 238 kcal). Two energy distributions such as equally distributed over all batteries and distributed according to work loads, are explored. The traffic intensity is 108 packets per day per node. In this chapter, the sink node receives data from different sensor nodes and transmits data to the surface node. The probability of network congestion increases when sink nodes carry a large amount of data traffic. Therefore, this traffic intensity enables that the sink node spends less than a half of a day on receiving data and relaying traffic to the surface node.

In our work, the power consumption parameters are taken from the technical specification of the EvoLogics S2CR18/34 modem [68] providing three transmitting power levels corresponding to different transmission ranges, i.e., 2.8 W, 8 W, and 35 W for 1,000 m, 2,000 m, and 3,500 m. The receiving power, the idle listening power and the sleeping power are 1.1 W, 0.08 W, and 0 W. For a given range r =1,000 m and with f = 30 kHz, $\eta_0 = 50$ μPa^2/Hz, $\mathcal{K}$ = 2, $\xi = 0.8$, $\mathbb{W}$ = 40 kHz, and $\mathfrak{R}$ = 2 kb/s [139], according to Equations 6.1, 6.2, and 4.5, we can achieve (nearly) zero PER with a transmitting power ($p_t^{(u,v)}$) of 2.8 W. Similar calculations can be used for the other transmission ranges. Unlike some researchers who have employed different transmitting powers corresponding to achieve different transmission ranges and data rates [52, 66, 81, 102], we employ constant values corresponding to a commercial modem. Our goal is to ensure a highly reliable data transfer. Therefore, the power consumption parameters of the EvoLogics S2CR18/34 acoustic modem are adopted in this chapter. We use the energy consumption model (similar to Equation 4.14) taken from [132]:

$$\mathcal{E}_t = p_t^{(u,v)} \times \tau, \tag{6.11}$$

where $\mathcal{E}_t$ is the energy consumption for node u transmitting a data packet to node v. We also use Equation (6.11) to calculate the energy consumption for receiving and idle listening. Each data packet contains 1200 bytes, which is same with that in the reported literatures [30, 109]. If data packets with varying sizes are used in the proposed scheme, we are confident that the conclusions would remain the same as presented in this chapter. The data rate is 13900 bit/s. Figure 6.2 shows one quadrant of a 15 × 15 UWSN with different transmission ranges.

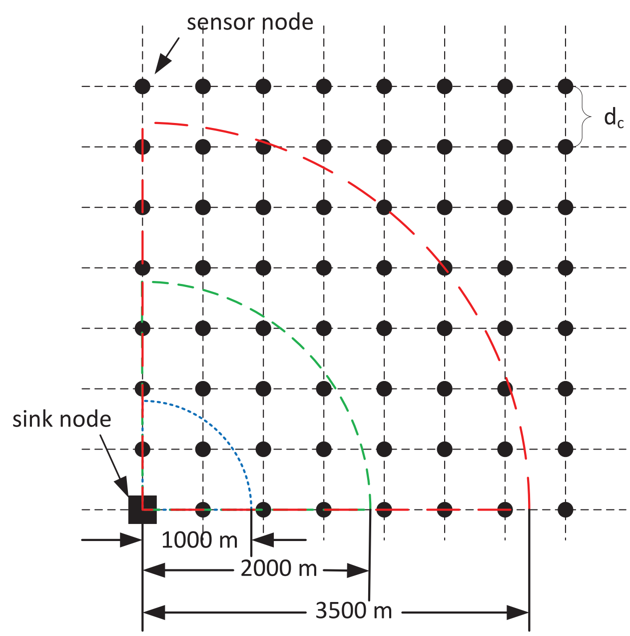

Figure 6.2: Example of a quadrant of UWSNs and different transmission ranges

Parameter settings are summarized in Table 6.1.

Table 6.1: Simulation parameters in Chapter 6

Parameters	Value
network size	11×11, 13×13, 15×15, and 17×17
initial energy of node u $\mathcal{E}_0^{(u)}$	10^6 J
data rate of acoustic modem	13900 bit/s
distance between two closest adjacent nodes d_c	550 m
injection rate in packets per day $i^{(u)}$	108 packets/day
transmitting power $p_t^{(u,v)}$	2.8 W, 8 W, and 35 W
transmission range	1,000 m, 2,000 m, and 3,500 m
receiving power p_r	1.1 W
idle listening power p_l	0.08 W
sleeping power p_s	0 W
size of a data packet	1200 bytes

6.3.2 Performance for Different w_p and w_e weights

In two sets of experiments, we use two transmitting power levels and three transmitting power levels, respectively. The two transmitting power levels are 2.8 W and 8 W, and the three transmitting power levels are 2.8 W, 8 W, and 35 W. As shown in Figures 6.3(a), 6.4(a), 6.5(a), 6.6(a), 6.7(a), 6.8(a), 6.9(a), and 6.10(a) for both these two sets, we can obtain the best ratio of w_p to w_e, which leads to the maximum number of data packets received by the sink node. As the weight for power levels decreases and the weight for energy consumption increases, the number of received data packets by the sink node peaks at 0.6:0.4 for two transmit levels and 0.7:0.3 for three transmit levels.

From another perspective, the numbers of times of using different transmitting power levels and the total number of times that data packets transmitted are plotted in 6.3(b), 6.4(b), 6.5(b), 6.6(b), 6.7(b), 6.8(b), 6.9(b), and 6.10(b) for two and three transmitting power levels. For two or three transmitting power levels, the number of times that data packets transmitted is equal to the summation of the numbers of times of using different transmitting power levels. According to Equation (6.10), the transmitting power level (and receiving power level) and the residual energy dominate the performance of the proposed algorithm. When w_p:w_e is 1:0, the number of times using the lowest transmitting power level is at its maximum value, which means that the nodes choose paths with minimum transmitting power level very frequently. Note that when nodes always use the lowest transmitting power, those near the sink node can be overloaded by forwarding data from other nodes, thus, exhausting their battery energy quickly. As such, when such nodes are about to run out of energy, our proposed scheme would choose high transmitting power levels. On the other hand, when w_p:w_e is 0:1, many nodes would use high transmitting power levels to explicitly avoid low-energy nodes. As a result, data packets are forwarded fewer times with higher energy consumption.

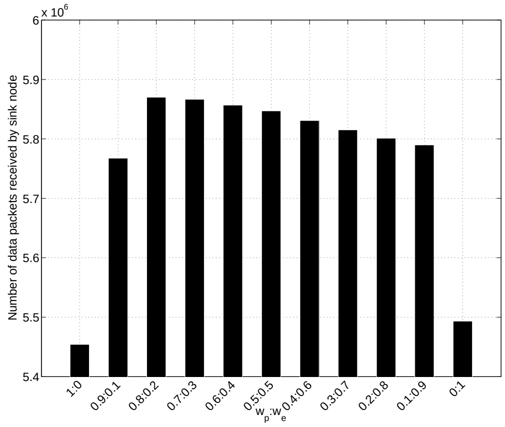

(a) Number of received data packets

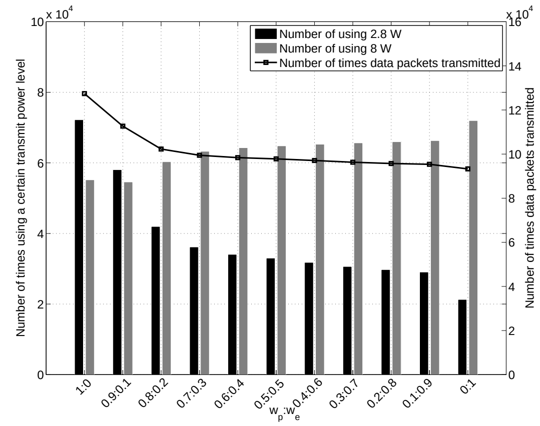

(b) Usage frequency of transmitting power levels

Figure 6.3: Performance versus $w_p : w_e$, two transmitting power levels, network size: 11×11

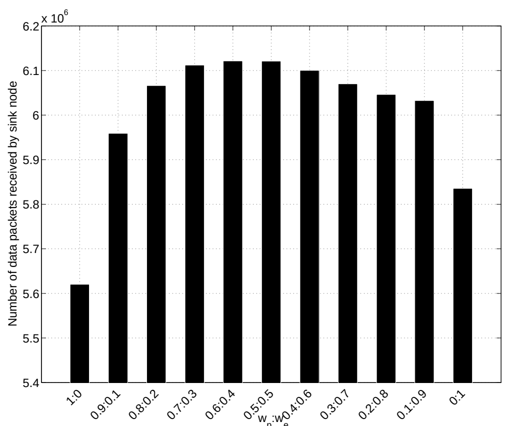

(a) Number of received data packets

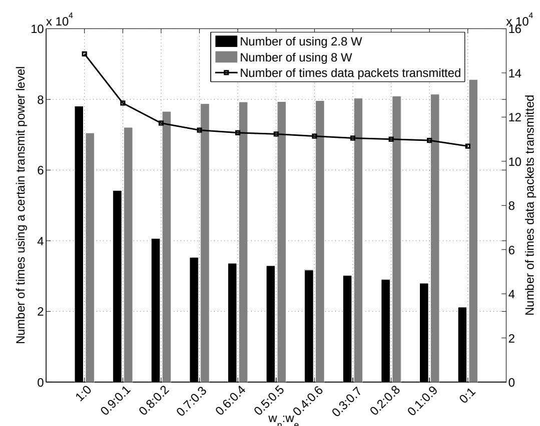

(b) Usage frequency of transmitting power levels

Figure 6.4: Performance versus $w_p : w_e$, two transmitting power levels, network size: 13×13

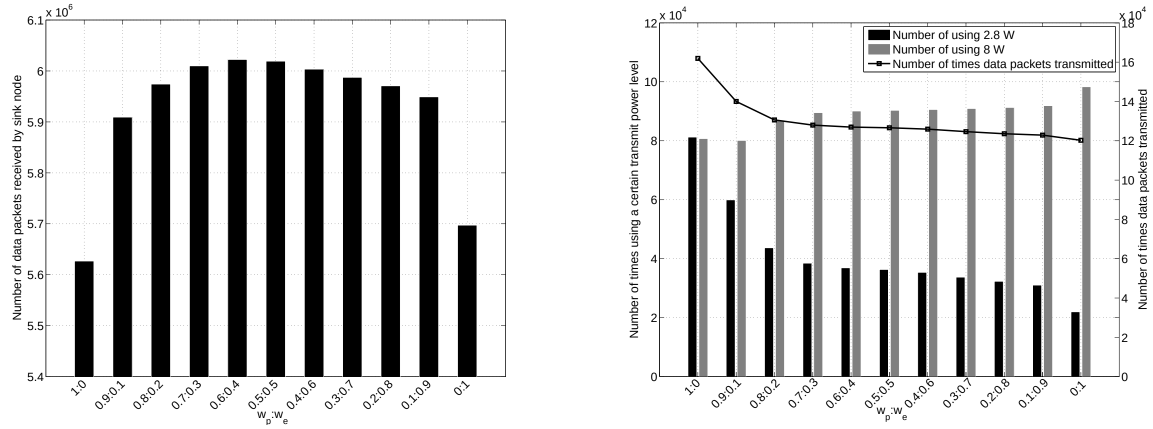

(a) Number of received data packets

(b) Usage frequency of transmitting power levels

Figure 6.5: Performance versus $w_p : w_e$, two transmitting power levels, network size: 15×15

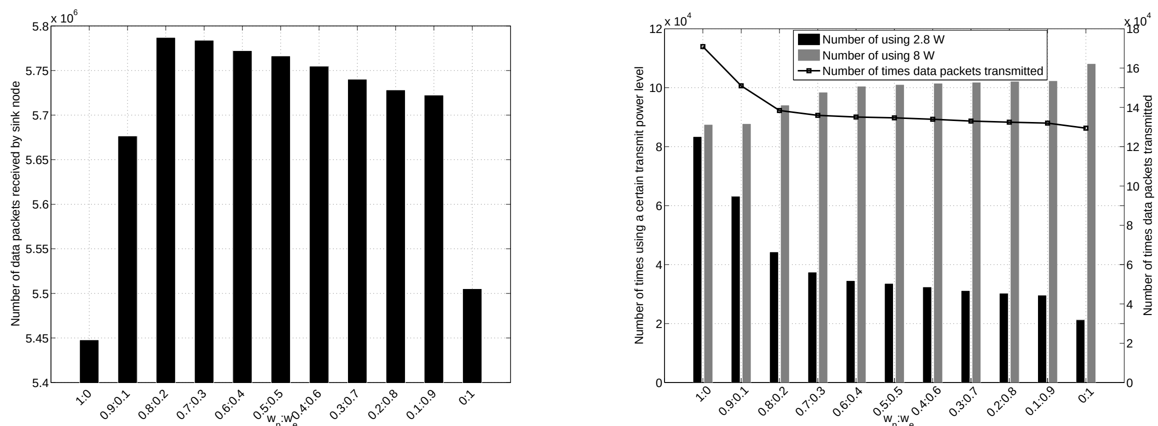

(a) Number of received data packets

(b) Usage frequency of transmitting power levels

Figure 6.6: Performance versus $w_p : w_e$, two transmitting power levels, network size: 17×17

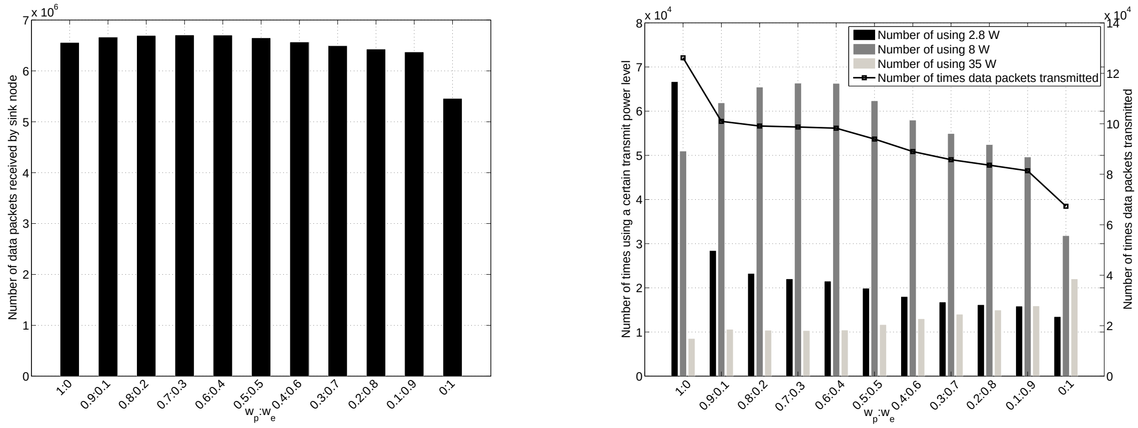

(a) Number of received data packets (b) Usage frequency of transmitting power levels

Figure 6.7: Performance versus $w_p : w_e$, three transmitting power levels, network size: 11×11

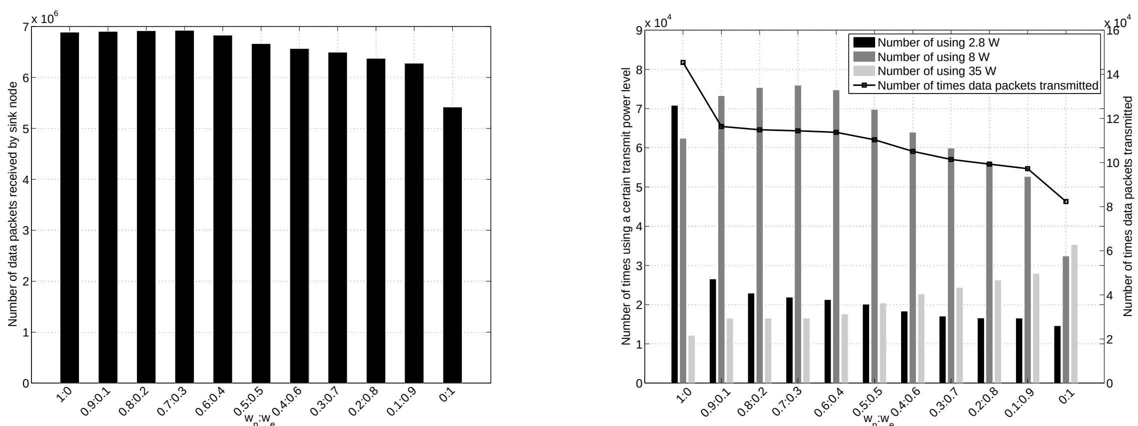

(a) Number of received data packets (b) Usage frequency of transmitting power levels

Figure 6.8: Performance versus $w_p : w_e$, three transmitting power levels, network size: 13×13

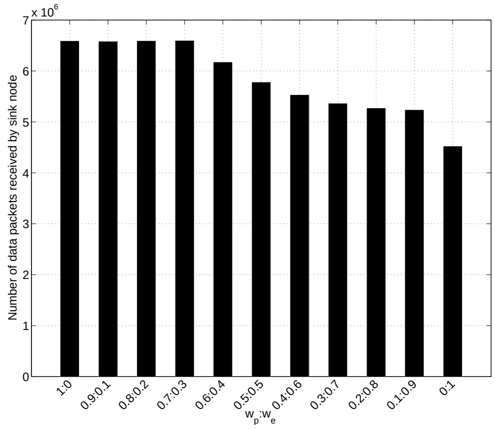

(a) Number of received data packets

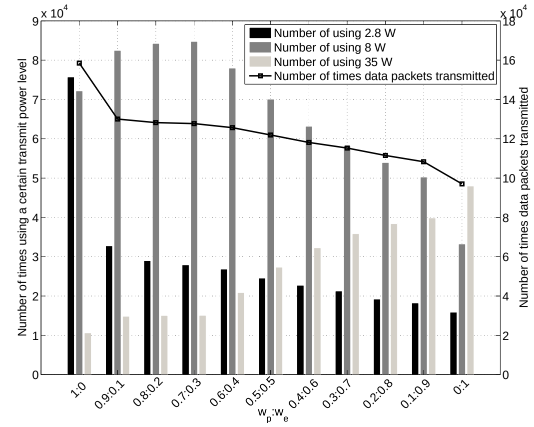

(b) Usage frequency of transmitting power levels

Figure 6.9: Performance versus $w_p : w_e$, three transmitting power levels, network size: 15×15

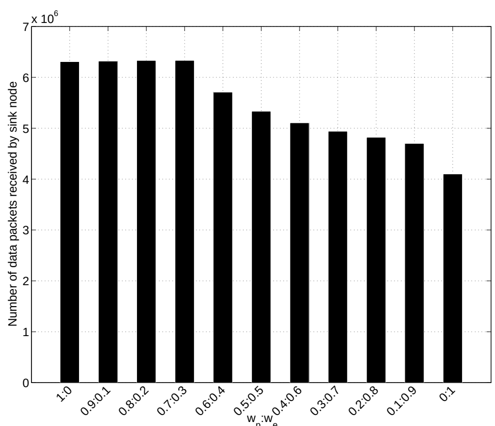

(a) Number of received data packets

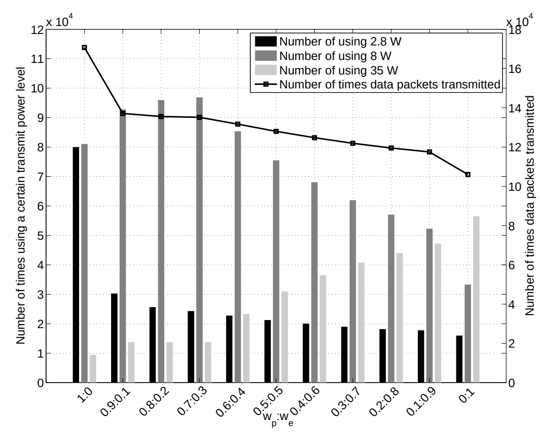

(b) Usage frequency of transmitting power levels

Figure 6.10: Performance versus $w_p : w_e$, three transmitting power levels, network size: 17×17

6.3.3 Performance for Different Network Sizes

We compare the network lifetime with different numbers of transmitting power levels among different network sizes. Here, the network lifetime is obtained by the best ratios of w_p to w_e of the given network size. As shown in Figure 6.11, in different sizes of UWSNs, using three transmitting power levels leads to the longest network lifetime due to its flexibility. In UWSNs with the sink node located in the center of the grid, the number of the one-hop nodes dominates the network lifetime. The reason is that they must share the responsibility of transporting nearly all data to the sink. As shown in Table 6.2, there exists only 8 one-hop nodes when using a single transmitting power level in different network sizes; however, many more one-hop nodes can be utilized when employing higher transmitting power levels. There are 44 one-hop nodes using two transmitting power levels and up to 144 one-hop nodes using three transmitting power levels. Besides, the multiple transmitting power levels provides more choices of paths. Increasing the number of transmitting power levels allows the network to avoid overuse of nodes close to the sink node. On the other hand, nodes would have few choices of paths if only using a single transmitting power level.

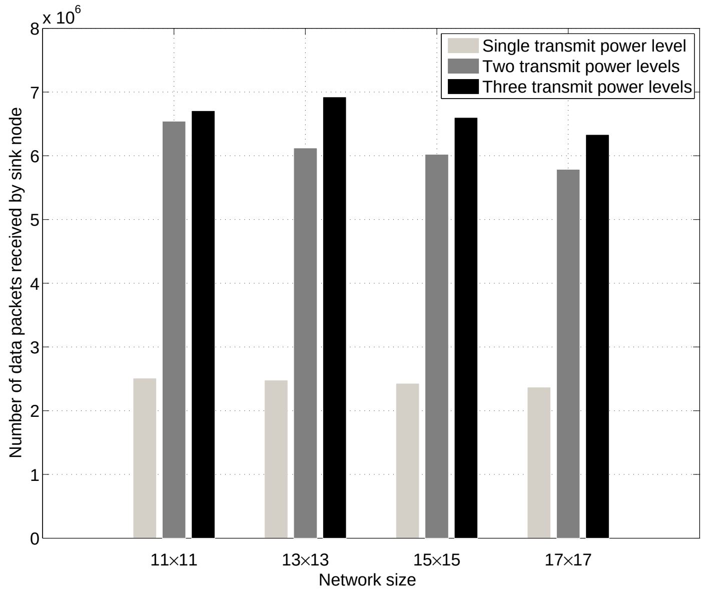

Figure 6.11: Number of received data packets versus network size: different transmitting power levels

Table 6.2: Number of one-hop nodes versus network size (different transmitting power levels)

single transmitting power level (2.8 W)				
	11×11	13×13	15×15	17×17
number of one-hop nodes	8	8	8	8
number of remaining nodes	112	160	216	280
two transmitting power levels (2.8 W and 8 W)				
number of one-hop nodes	44	44	44	44
number of remaining nodes	76	124	180	244
three transmitting power levels (2.8 W, 8 W and 35 W)				
number of one-hop nodes	116	144	144	144
number of remaining nodes	4	24	80	144

For three transmitting power levels, the network lifetime of the 13×13 grid UWSN is the longest among different sizes of UWSNs. It is shown in Table 6.2 that 144 one-hop nodes can transmit their own generated the data and forward the data from 24 other nodes. In 11×11 grid UWSNs, although only 4 nodes need to transmit data via one-hop nodes, the total number of nodes is 120, which means that the total data volume is smaller than that in 13×13 grid UWSNs. The number of received data packets decreases in 15×15 and 17×17 grid UWSNs because more energy is consumed for forwarding.

For the single transmitting power level (8 one-hop nodes) and two transmitting power levels (44 one-hop nodes), we observe that the number of data packets received by the sink node decreases as the network size increases. That is because more data packets are needed to be forwarded when the number of sensor nodes increases. The one-hop nodes tend to exhaust energy quickly in large networks.

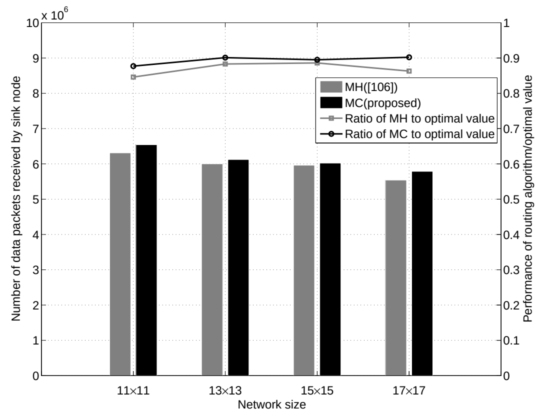

(a) Two transmitting power levels

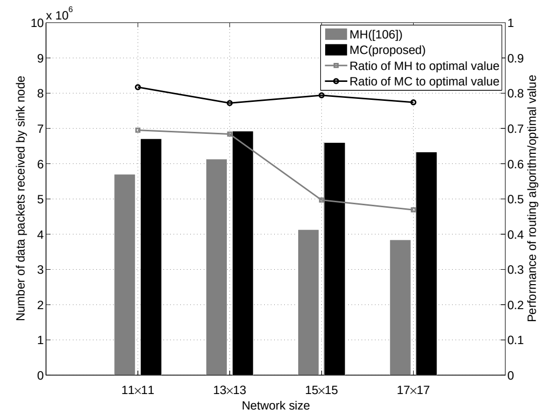

(b) Three transmitting power levels

Figure 6.12: Minimum hops versus minimum cost (proposed algorithm)

We also compare the proposed scheme (i.e., MC in Figures 6.12(a) and 6.12(b)) to the simple minimum hop routing algorithm (i.e., MH in in Figures 6.12(a) and 6.12(b)), reported in [106], for different network sizes. The network lifetime is obtained using the best ratios of w_p to w_e for a given network size. As plotted in Figures 6.12(a) and 6.12(b), the network lifetime utilizing the proposed relay node selection scheme is closer to the optimal value than that of MH, as shown by the ratio of MH and MC to the optimal value in the right Y-axis. In different network sizes, the proposed relay node selection scheme significantly outperforms MH for three transmitting power levels. MH chooses the next-hop nodes that can reach the sink node with the fewest hops. The largest transmitting power, i.e., 35 W, is frequently used for data transmission and, as a results, the battery energy of sensor nodes is quickly depleted after a short time.

6.3.4 Performance for Different Update Periods

Figure 6.13 and Figure 6.14 show the average energy consumption per packet with different update periods in 11×11, 13×13, 15×15, and 17×17 grid UWSNs. We can see that, for two and three transmitting power levels, the performance of the proposed scheme degrades when the updating period becomes longer. The longer update period means less frequent update of the residual energy of sensor nodes. When sensor nodes are not aware of the variation of the residual energy in a timely fashion, the routing decision is not sufficiently adaptive.

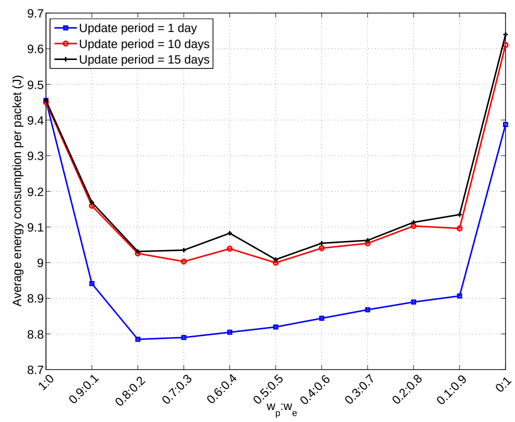

(a) Network size: 11×11

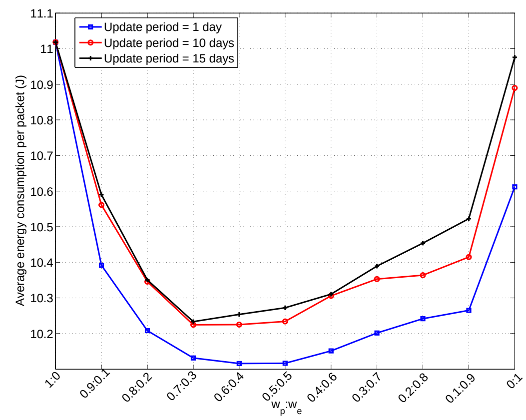

(b) Network size: 13×13

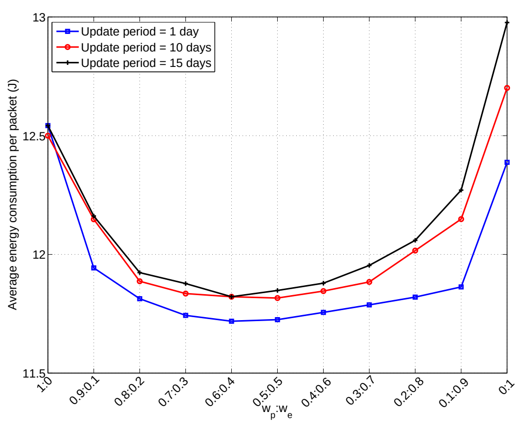

(c) Network size: 15×15

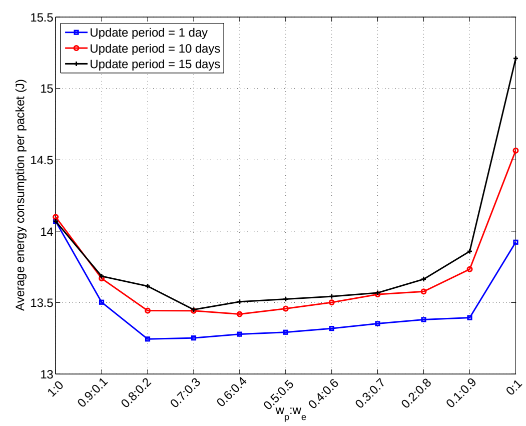

(d) Network size: 17×17

Figure 6.13: Average energy consumption per packet versus different update periods: two transmitting power levels

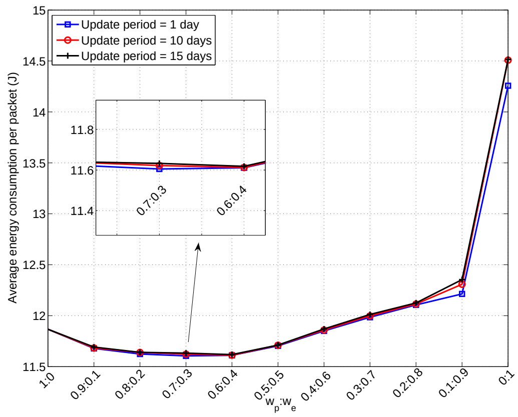

(a) Network size: 11×11

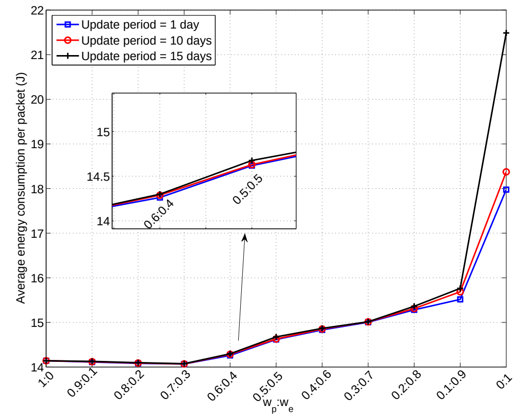

(b) Network size: 13×13

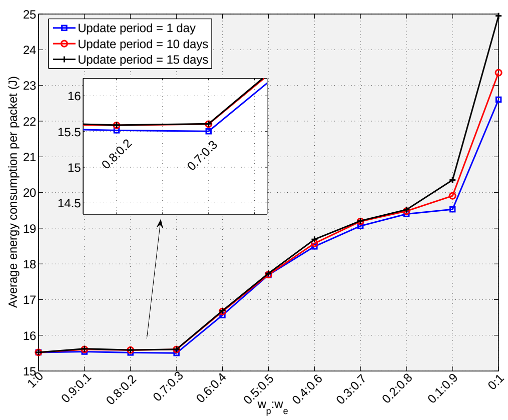

(c) Network size: 15×15

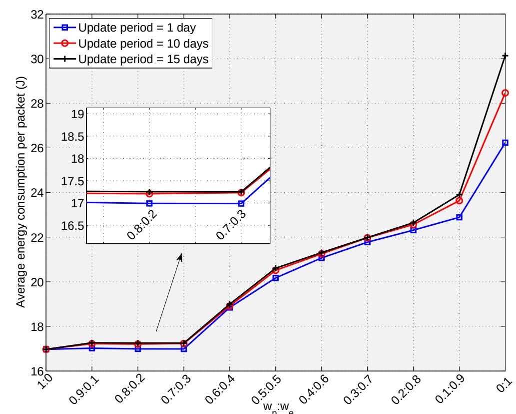

(d) Network size: 17×17

Figure 6.14: Average energy consumption per packet versus different update periods: three transmitting power levels

6.3.5 Performance with Different Energy Assignments

In UWSNs with a square grid topology, the sensor nodes closer to the sink node must forward a larger amount of data than those farther away. Obviously, the network lifetime can be prolonged by providing more energy to the sensor nodes near the sink node. We can estimate the traffic and then reassign the energy for each sensor node. Please note that the total initial energy of all sensor nodes is the *same* as that in the previous cases.

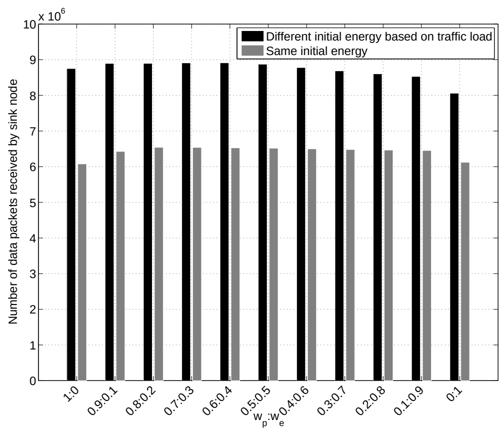

(a) Network size: 11×11

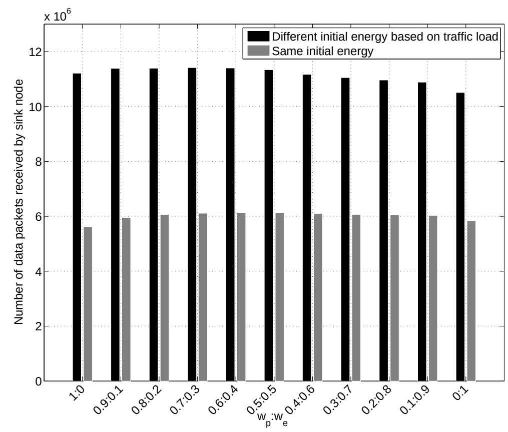

(b) Network size: 13×13

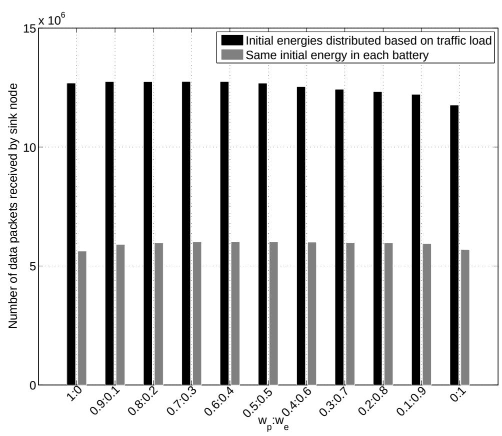

(c) Network size: 15×15

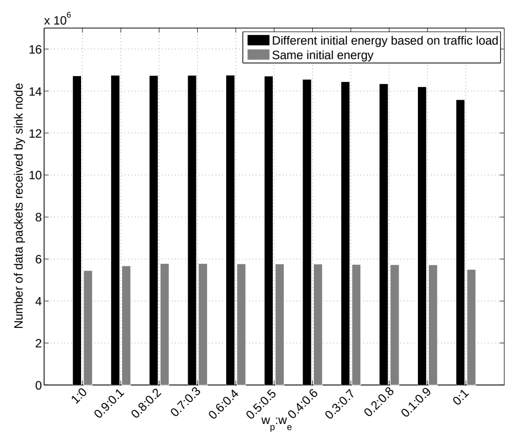

(d) Network size: 17×17

Figure 6.15: Uniform initial energy versus initial energy assignment based on traffic: two transmitting power levels

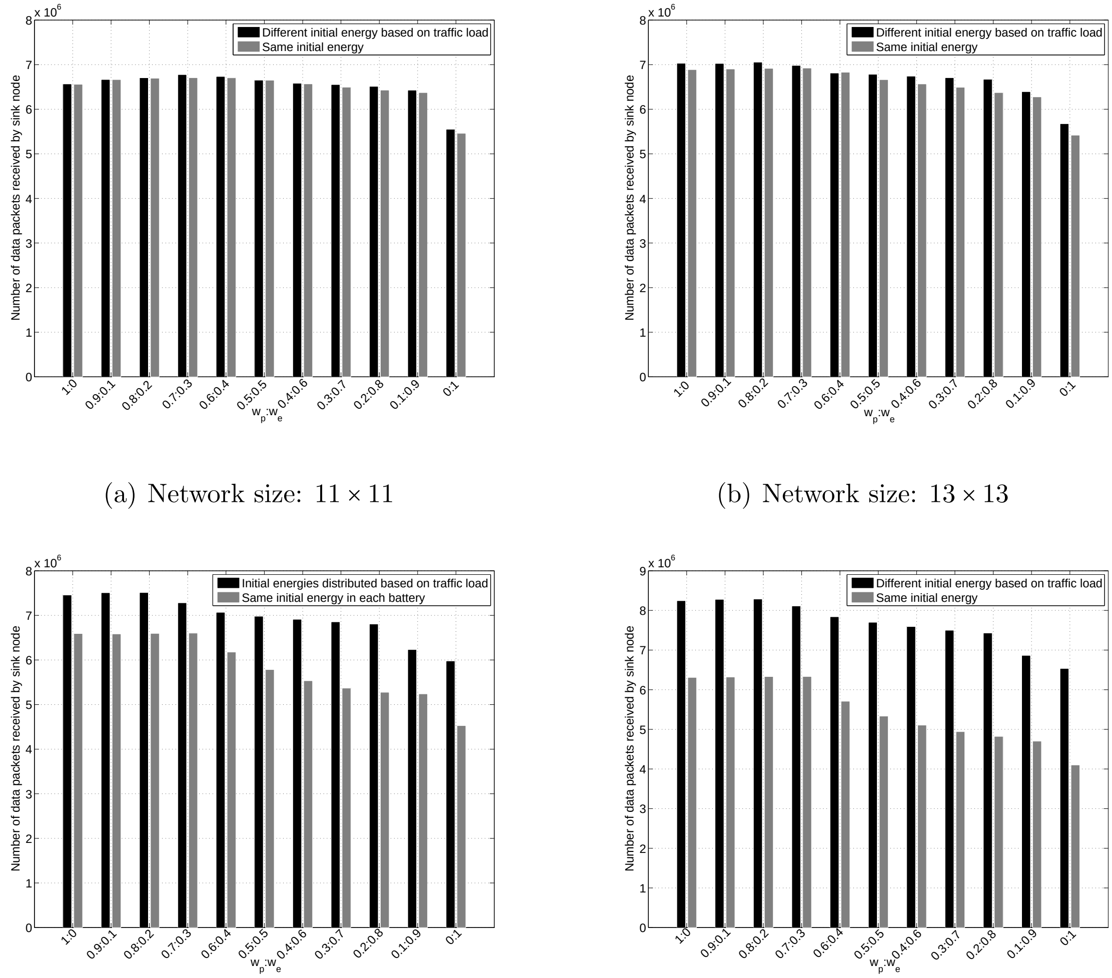

(a) Network size: 11×11

(b) Network size: 13×13

(c) Network size: 15×15

(d) Network size: 17×17

Figure 6.16: Uniform initial energy versus initial energy assignment based on traffic: three transmitting power levels

We compare the number of received data packets using the proposed scheme with uniform and different initial energy assignments in Figure 6.15 and Figure 6.16. Significant improvement can be observed using two transmitting power levels. In this case, the one-hop nodes forward a larger amount of data than those in the three transmit-power-level case, as shown in Table 6.2. Therefore, more battery energy should be allocated to the one-hop nodes for the two transmit-power-level case than three levels. Therefore, the assignment of initial battery energy based on the traffic of sensor nodes can significantly improve the performance of the proposed relay node selection scheme, where the traffic through the one-hop nodes is fairly high in UWSNs.

6.3.6 Comparison of Number of Received Data Packets based on Two Network Lifetime Definitions

As discussed in Section 6.1.3, in UWSNs with a square grid topology where the sensing range is considerably greater than the communication range, the sink node is able to receive packets via other sensor nodes after the first node exhausts energy because we can route data through other areas of the network to reach the sink node. In this section, we compare the number received data packets (network lifetime) under two different definitions: the number of received data packets before the sink node cannot receive any data packet (i.e., 1st definition of network lifetime in Figures 6.17, 6.18, 6.19, and 6.20) and the number of data packets before the first node exhausts energy (i.e., 2nd definition of network lifetime in Figures 6.17, 6.18, 6.19, and 6.20). From Figures 6.17, 6.18, 6.19, and 6.20, we can observe that, in networks of different sizes and using different numbers of transmitting power levels, the number of data packets before the sink node cannot receive any data packet is close to the number of data packets before the first node exhausts energy. There is not a significant difference between these two definitions of network lifetime when using the proposed relay node selection scheme. Therefore, the proposed relay node selection scheme can achieve a novel flow assignment to avoid overusing certain sensor nodes (e.g., one-hop nodes) and to balance the energy consumption among sensor nodes in UWSNs.

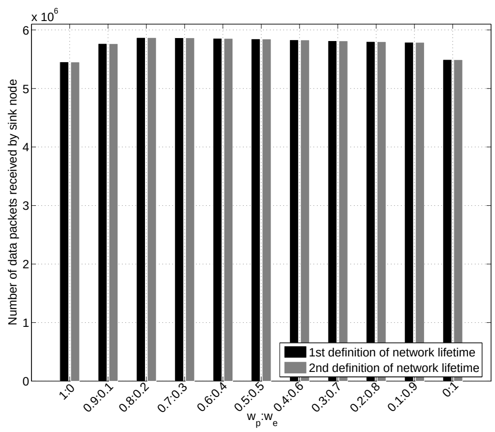

(a) Network size: 11×11

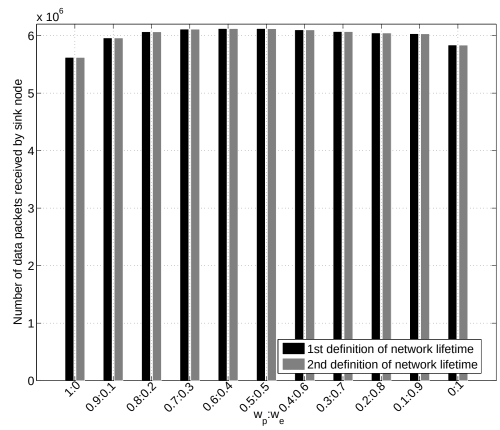

(b) Network size: 13×13

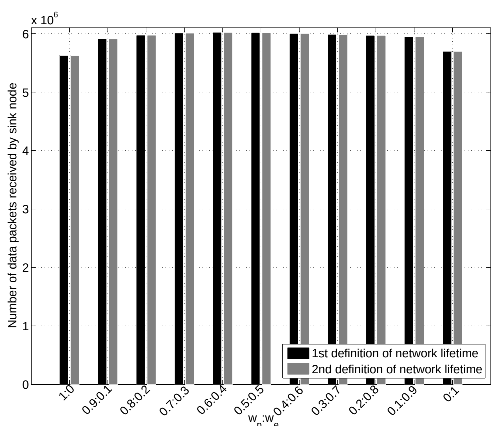

(c) Network size: 15×15

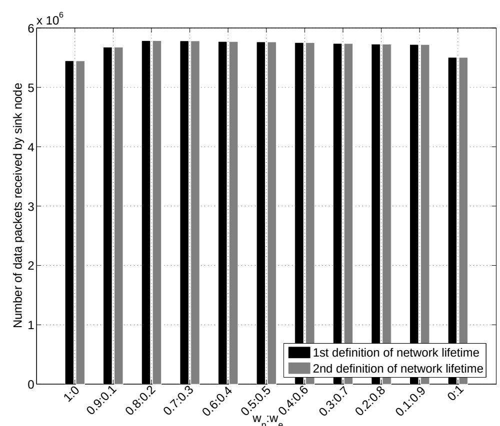

(d) Network size: 17×17

Figure 6.17: Comparison of number of received data packets based on two network lifetime definitions, 2 transmitting power levels, same initial energy

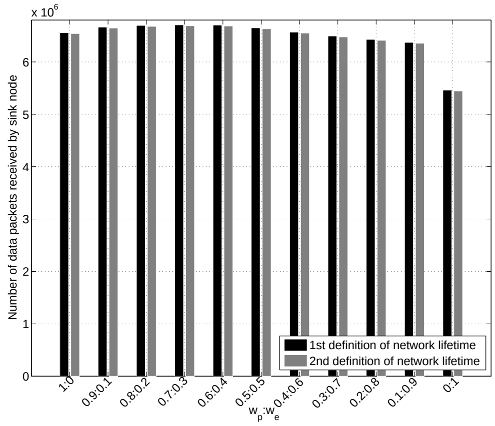

(a) Network size: 11×11

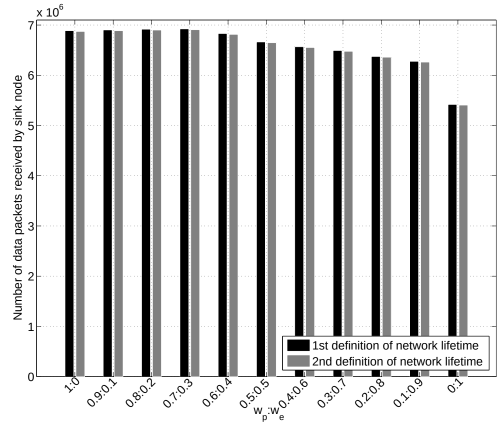

(b) Network size: 13×13

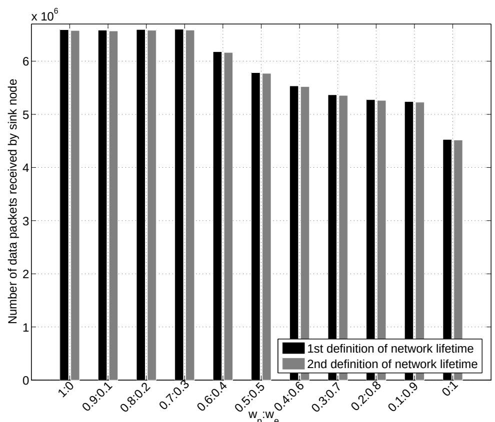

(c) Network size: 15×15

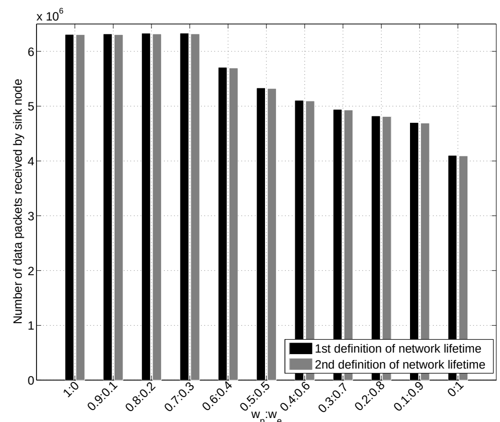

(d) Network size: 17×17

Figure 6.18: Comparison of number of received data packets based on two network lifetime definitions, 3 transmitting power levels, same initial energy

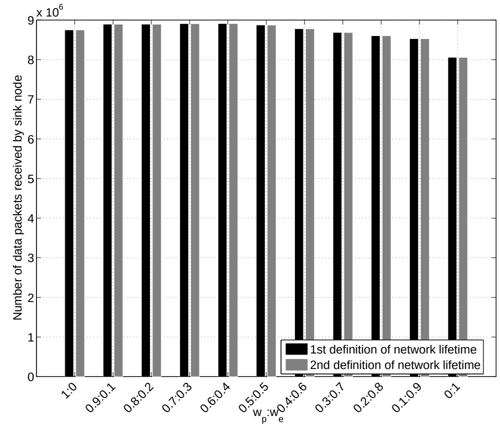

(a) Network size: 11×11

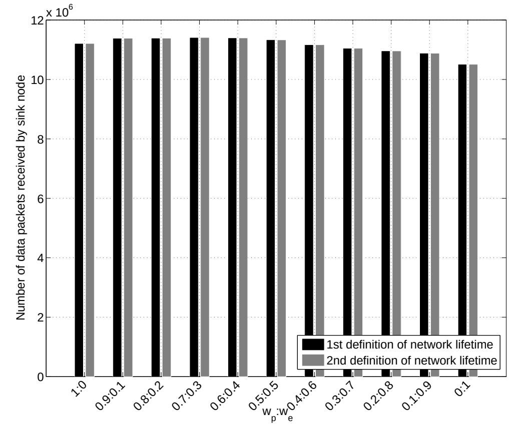

(b) Network size: 13×13

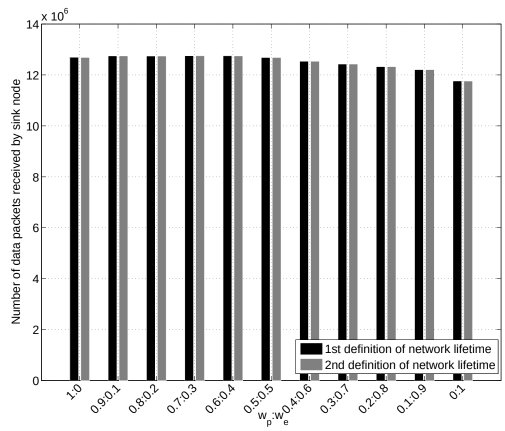

(c) Network size: 15×15

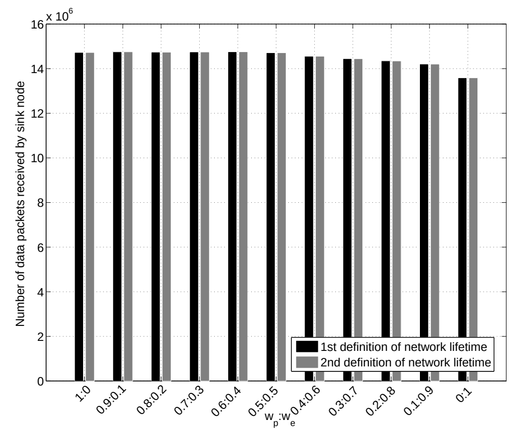

(d) Network size: 17×17

Figure 6.19: Comparison of number of received data packets based on two network lifetime definitions, 2 transmitting power levels, initial energies distributed based on traffic loads

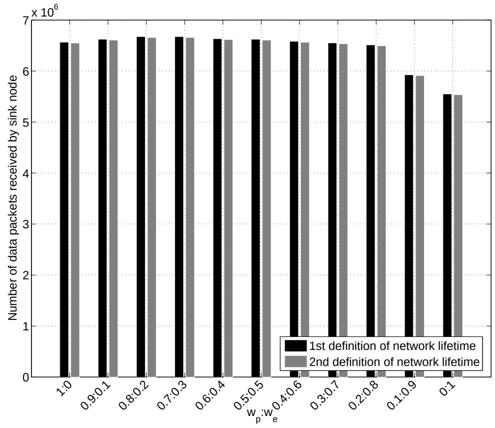

(a) Network size: 11×11

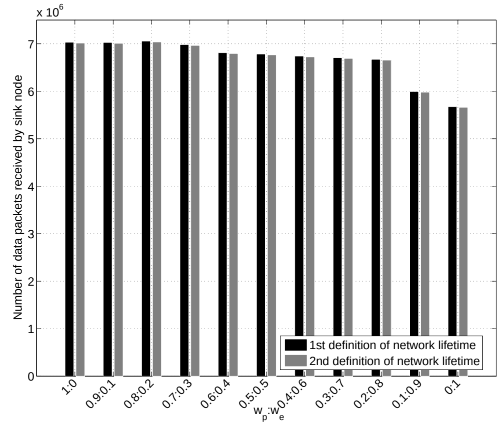

(b) Network size: 13×13

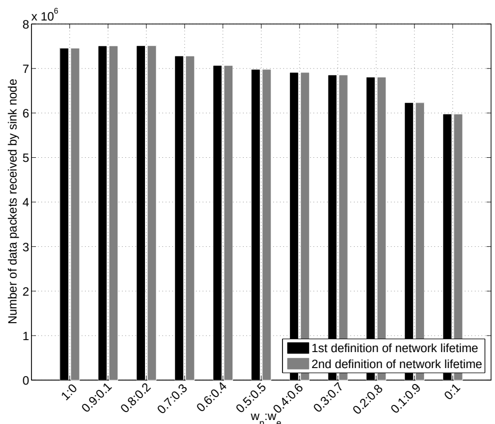

(c) Network size: 15×15

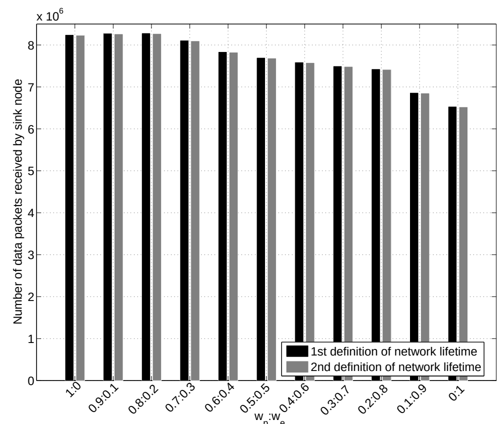

(d) Network size: 17×17

Figure 6.20: Comparison of number of received data packets based on two network lifetime definitions, 3 transmitting power levels, initial energies distributed based on traffic loads

6.3.7 Performance with Faulty Nodes

In this section, we present the performance of the proposed relay node selection scheme when the faulty nodes appear during data transfer in UWSNs. The faulty nodes in this section represents that the sensor node cannot transmit, receive, and forward data packets. The numbers of received data packets by the sink node are corresponding to the best ratios as presented in Section 6.3.2. As shown in Figures 6.21 and 6.22, the number of data packets decreases with the increasing of number of faulty one-hop nodes. The reason is that the sensor nodes (except the one-hop nodes) have to use more hops to report data to the sink node when the faulty one-hop nodes appear. The remaining one-hop nodes (which can transmit, receive, and forward data) must forward a larger amount of data compared with that without faulty one-hop nodes. Additionally, we observe that the number of data packets received by the sink node increases when the number of faulty nodes increases. The reason is that the amount of forwarding data decreases when the number of faulty nodes increases. The one-hop nodes can transmit their own data to the sink node directly and reduce energy consumption.

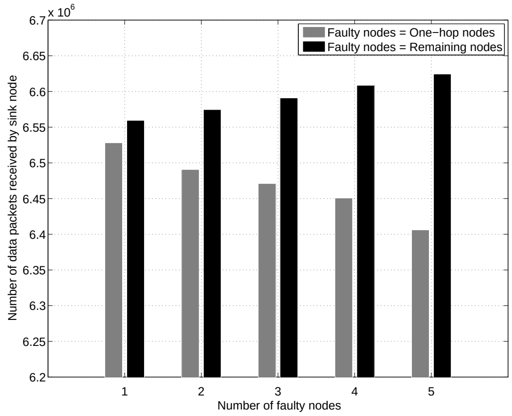

(a) Network size: 11×11

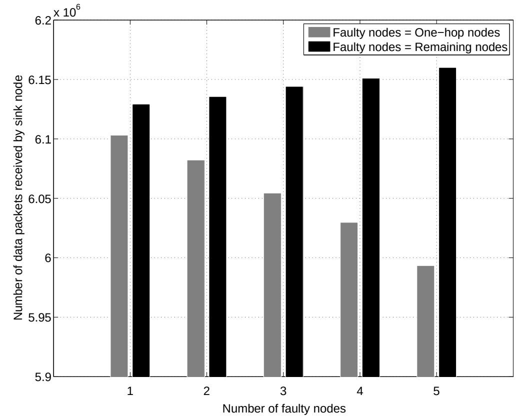

(b) Network size: 13×13

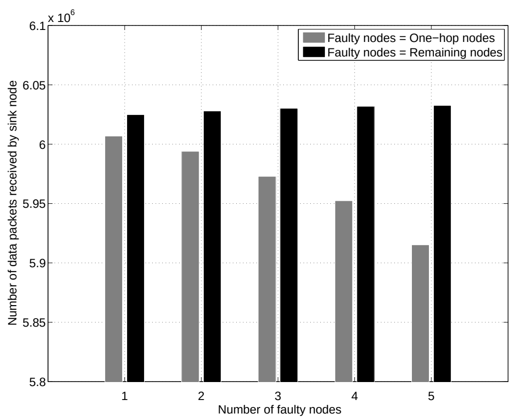

(c) Network size: 15×15

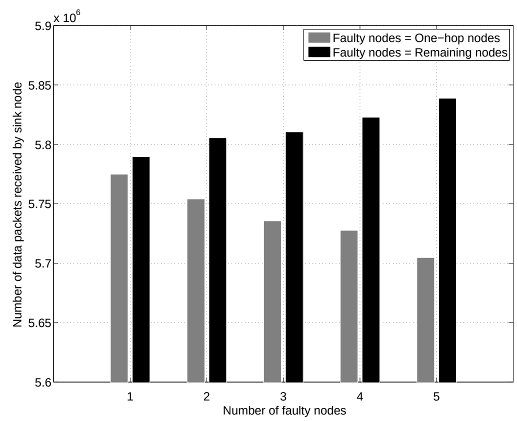

(d) Network size: 17×17

Figure 6.21: Performance versus number of faulty nodes: two transmitting power levels

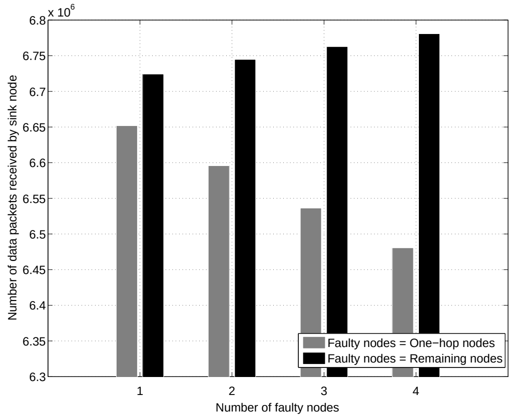

(a) Network size: 11×11

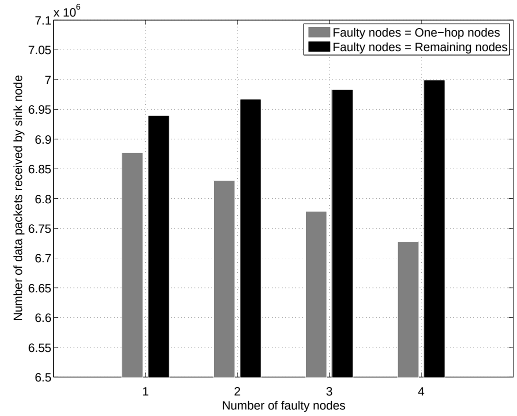

(b) Network size: 13×13

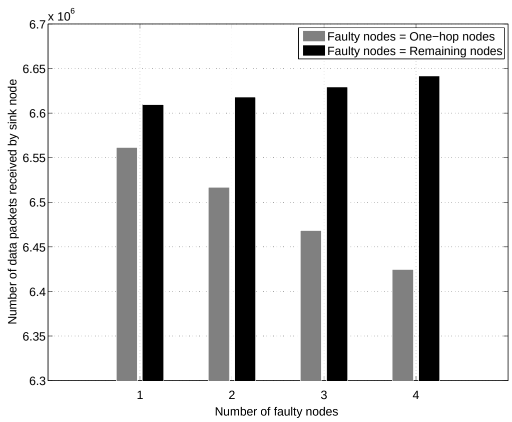

(c) Network size: 15×15

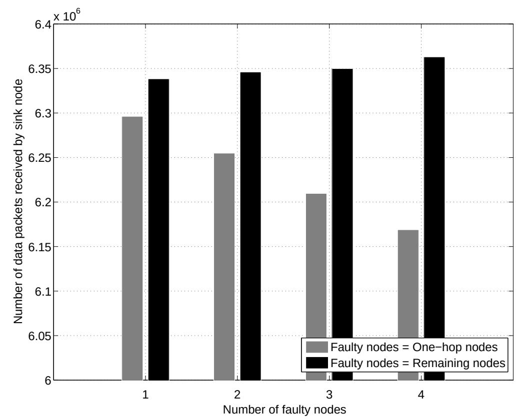

(d) Network size: 17×17

Figure 6.22: Performance versus number of faulty nodes: three transmitting power levels

6.4 Summary

In this chapter, we proposed an energy-efficient relay node selection scheme for UWSNs with a square grid topology for long-term marine environmental monitoring applications.

We formulated the offline relay node selection problem as a linear programming problem, and proposed an online relay node selection scheme that incorporates multiple transmitting power levels and residual energy of downstream nodes. The proposed relay node selection scheme can be a main part of the routing protocol for UWSNs.

The performance evaluation of the our proposed scheme showed that the best ratio of the weight for the power level to the weight for the residual energy can be obtained for different numbers of transmitting power levels and for different network sizes. The best ratio balances the transmitting power level and the residual energy for routing decision. Moreover, the network lifetime can be significantly prolonged using more transmitting power levels and balance energy consumption among sensor nodes. Compared to the routing algorithm based solely on minimum hops, the performance of the proposed relay node selection scheme is closer to the theoretical value obtained from the linear programming problem. Since the initial battery energy and the number of sensor nodes close to the sink node are the performance bottleneck, the network performance is further improved by assigning the initial battery energy to each sensor node based on its location in the network. The proposed relay node selection scheme can more effectively reduce energy consumption if the acoustic modem provides a larger number of transmitting power levels. Furthermore, the same conclusions as presented in this chapter can be achieved by when selecting grids with an even number of sensor nodes, despite the fact that the sink node would be slightly off-center. Not limited to UWSNs with a square grid topology, the proposed scheme also can be used in UWSNs with other regular and irregular topologies.

Chapter 7

Coordination Scheme for Data Gathering in UWSNs using AUV

In previous chapters, we studied the data gathering problem in UWSNs with a square grid topology for long-term marine environmental monitoring applications. The advancement of UWSNs is further augmented by recent engineering activities in the design and deployment of AUVs. The use of AUVs facilitates network deployment and maximizes network coverage. However, AUVs also bring in new challenges for localization and time synchronization, and network connectivity[1]. Data collection with a mobile sink has been studied in recent years, as a significant application issue in WSNs. Unlike the high requirements of network throughput and packet delay in WSNs, energy efficiency is the significant goal of protocol design for UWSNs because of the high transmitting energy consumption and unchangeable

[1]The material in this chapter has been presented at IEEE WCNC'13 [141]

and non-rechargeable batteries of the sensor nodes, as discussed in Sections 2.2.1 and 2.6.

In this chapter, we propose an energy-efficient coordination scheme for data gathering in a UWSN using a single AUV. One problem is that it is difficult to guarantee that the AUV will be able to come out of sleep mode when the AUV is needed for communication with sensor nodes. With different energy consumption requirements and constraints, the AUV operations include sending beacon messages, channel detection, and data reception. In contrast, the underwater sensor nodes operations involve prolonged sleep mode with sporadic data transmission. There, different cycle periods are required for the AUV and sensor nodes. We present the optimal amount of sleeping time for sensor nodes to demonstrate the effectiveness of our scheme when the time is not synchronized between the AUV and sensor nodes. To further conserve energy, we introduce transmitting power control using the received signal strength and study the relationship between the number of power levels and the energy consumption of sensor nodes.

Chapter 7 is organized into four sections. Section 7.1 describes the basic coordination scheme and presents the optimal amount of sleeping time of sensor nodes. In Section 7.2, power control is incorporated in the proposed scheme for the further energy conservation. The performance of the proposed scheme is evaluated in Section 7.3 and conclusions are drawn in Section 7.4.

7.1 Coordination Scheme for Data Collection

An AUV, as a mobile sink with the advantage of being powerful, rechargeable, and controllable, can be used to collect data from sensor nodes located on the seafloor. Energy conservation for underwater sensors is the main goal in this work to design coordination protocols for data collection in UWSN by the AUV. In this Chapter, we consider the scenario where a single AUV is used for data collection in sparsely deployed UWSNs. We assume that the AUV has abundant power supply and no prior time synchronization or schedule synchronization between the AUV and sensor nodes are required (Compared to the sensor node located on the seafloor, the AUV can go to the sea surface autonomously and charge its batteries on the surface ship. Therefore, it is easy to charge the batteries of the AUV). The AUV and sensor nodes operate in different cycle periods and coordinate through signalling packet exchange. We derive the shortest wake-up time of a sensor node, which guarantees successful data transmission when the AUV enters its communication range, meanwhile, reduces the energy consumption of the sensor node.

7.1.1 Problem Definition

In sparsely-distributed UWSNs, sensor nodes are often not within the communication range of each other. Therefore, the network problem can be translated into the communication and coordination problem between the AUV and a sensor node. As sensor nodes and the AUV use different cycle periods, coordination between them is key to this scheme design. Energy consumption is an important issue due to the unchangeable and non-rechargeable batteries of sensor nodes. Therefore, the whole problem is to design a coordination scheme for sensor nodes and the AUV in order to guarantee data packet transmission in an energy efficient way without time synchronization.

7.1.2 Basic Coordination Scheme

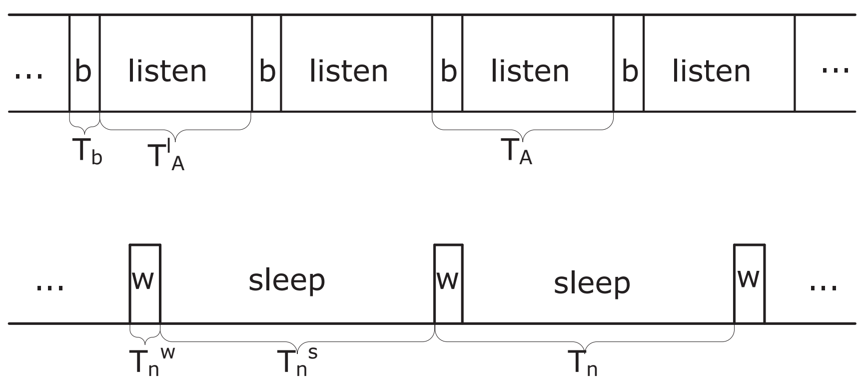

Figure 7.1: Cycle periods of the AUV and sensor nodes in "connection" phase

There are two phases in the proposed coordination scheme, including "connection" phase and "data transmission" phase. Figure 7.1 shows the cycle periods for the AUV and sensor nodes. In "connection" phase, AUV has two states in one cycle period such as sending beacon message ("b" in this figure) and listening to the channel. The duration of one cycle period of the AUV is denoted by T_A. T_b and T^l_A are the transmission time of a beacon message and the listening duration of the AUV in one cycle period, respectively. $T_A = T_b + T^l_A$. Every sensor node also has two states in one cycle period: wake ("w" in Figure 7.2) and sleeping (turn off the transceiver's circuit). In the wake state, the sensor node listens to the channel. T_n is the duration of one cycle period of a sensor node. The wake period of a sensor node in one cycle period is T_n^w. T_n^s is the sleeping period of a sensor node in one cycle period. $T_n = T_n^w + T_n^s$.

When a sensor node is the intended receiver and receives a corresponding beacon message, it will send an acknowledgement for beacon message (ACKB) ("c" in Figure 7.2). Then, the sensor node and the AUV enter "Data transmission" mode without sleeping. After receiving all the data packets, the AUV transmits an acknowledgement (ACK) ("a" in Figure 7.2) to the corresponding sensor node. The "Data transmission" phase is illustrated in Figure 7.2.

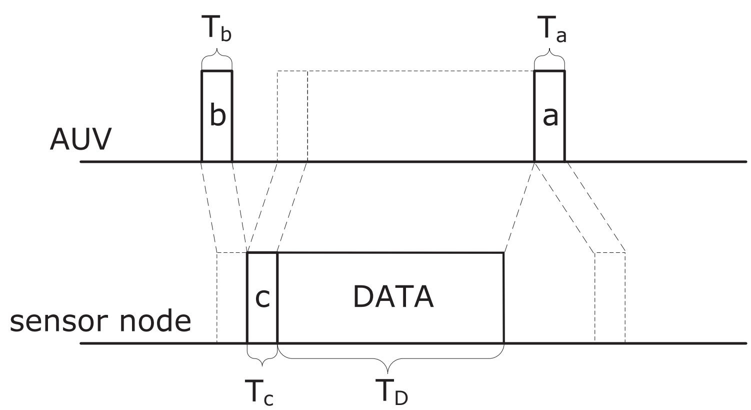

Figure 7.2: An illustration of the coordination scheme

The following discussion are the only required topological information: sensor nodes are sparsely located on the seabed, the AUV has the approximal location information of sensor nodes.

- The AUV collects data packets from each sensor node following the order of the sensor node ID, i.e. $1 \rightarrow 2 \rightarrow 3 \rightarrow 4 \rightarrow 5 \rightarrow \ldots n$;

- A sensor node periodically works as shown in Figure 7.1. It starts with "wake" state to listen to the channel and then sleeps every T_n^s seconds;

- Intuitively, the shortest wake period of the sensor node (T_n^w) should be equal to the duration of the AUV (T_A) to avoid to miss the beacon message. We discuss the optimization strategy $T_n^{s^*}$ in Section 7.1.3;

- A sensor node sends one ACKB to the AUV when it is the intended receiver and then starts to transmit data packets to the AUV. The AUV will circle around the place where it receives the ACKB. The current affects the position of the AUV more or less. We assume that the underwater acoustic communication is in a quiet and homogenous deep seawater. The impact of current on data transmission can be ignored. The sensor node does not enter the sleeping state before finishing data packets transmission.

- Once completing data packets transmission, the sensor node and the AUV restore the original operating cycle periods. Meanwhile, the AUV will change the ID of the intended receiver to the next.

7.1.3 Sleeping Time Optimization

Sensor nodes can consume less energy if they sleep longer. However, it is possible to miss the beacon message from the AUV when it is moving in the communication range of a sensor node if the sensor node oversleeps, which will result in data transmission failure. PL denotes the path length of the AUV in the communication range of a sensor node . In practice, PLs of different sensor nodes are often not equal in sparsely-distributed UWSNs. As shown in Figure 7.3, PL_3 is the maximum path length of AUV and PL_5 is minimum. The dotted line represents the communication range of a sensor node, denoted by r. It is difficult to

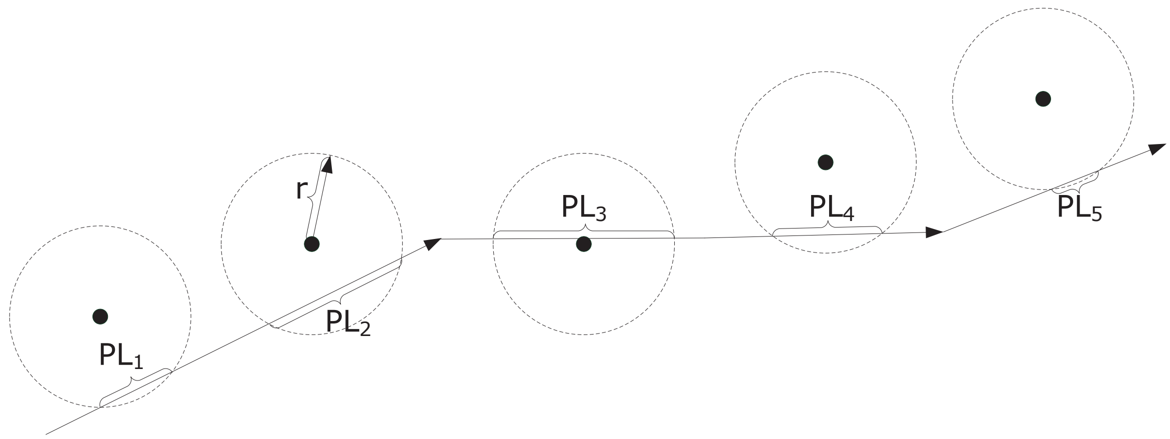

Figure 7.3: An illustration of PLs in different sensor nodes

configure different amounts of sleeping time for different sensor nodes based on different PLs. Therefore, the objective of sleeping time optimization is to find the optimization strategy $T_n^{s^*}$ for all the sensor nodes to maximize the number of sensor nodes that successfully transmit data packets while minimizing energy consumption. In order to simplify the optimization problem, it is assumed that data packets can be successfully transmitted to AUV once a sensor node receives a beacon message without being hindered by underwater acoustic channel conditions.

$\hat{T_n^s}$ is the supposed amount of sleeping time of every sensor node. A utility function, denoted by $U(\hat{T_n^s})$, is introduced to describe our objective, i.e.,

$$T_n^{s^*} = \arg\max\{U(\hat{T_n^s})\}. \tag{7.1}$$

$$U(\hat{T_n^s}) = \sum_{i=1}^{N} \left(B(\hat{T_n^s}) - \beta C(\hat{T_n^s}) \right). \tag{7.2}$$

N is the total number of sensor nodes in sparsely distributed UWSNs. $B(\cdot)$ denotes the benefit of each sensor node by adopting a given amount of sleeping time. $C(\cdot)$ represents the cost of each node when using a given amount of sleeping time in one cycle period. β is a weight coefficient to balance between the cost of energy consumption and the benefit of successfully transmitting data packets. $\mathbb{T}(i)$ is the maximum amount of sleeping time of node i in order to avoid missing data packet transmission.

For each sensor node, we utilize the probability of successfully transmitting data packets to the AUV as this benefit, which can be expressed by:

$$B(\hat{T_n^s}) = \begin{cases} \frac{\mathbb{T}(i)}{\hat{T_n^s}}, & \text{if } \hat{T_n^s} > \mathbb{T}(i) \\ 1, & \text{others} \end{cases} \tag{7.3}$$

$C(\cdot)$ can be expressed by

$$C(\hat{T_n^s}) = \frac{\min\{\hat{T_n^s}\}}{\hat{T_n^s}}. \tag{7.4}$$

$\mathbb{T}(i)$ can be expressed by

$$\mathbb{T}(i) = PL(i)/v_A - T_n^w. \tag{7.5}$$

For one sensor node, $\beta = 1$ denotes that the cost of minimum amount of sleeping time is equal to the benefit of successfully transmitting data packets. Different values of β are investigated and discussed in Section 7.3.

The design of the proposed utility function (Equation 7.2) is not only intuitive, but also indicates that the cost of energy consumption adopting a certain amount of sleeping time of sensor nodes is additive. $B(\cdot)$ and $C(\cdot)$ are the linear components of the utility function. Other possible formulas of the utility function, such as $B(\cdot)/C(\cdot)$, present less physical meaning.

7.2 Further Improvement of the Proposed Coordination Scheme

In the previous section, a sensor node, as a currently intended receiver, will transmit data packets after receiving a beacon message from the AUV with a fixed transmitting power corresponding a fixed communication range. In the underwater acoustic channel, the transmission loss is related to the distance between the sound source and receiver. Therefore, choosing a preferred communication position to transmit data packets with a proper power control can reduce energy consumption. Received signal strength [90, 91], representing the instantaneous channel quality, is introduced in this section to obtain preferred communication positions for different sensor nodes. The quiet and homogenous deep seawater with the symmetric underwater acoustic channel is assumed as the communication environment.

7.2.1 Improvement of the Coordination Scheme

Figure 7.4 shows the "connection" phase of the coordination scheme with power control, where the solid black rectangle stands for the short tone signal (has been implemented on [90, 91]).

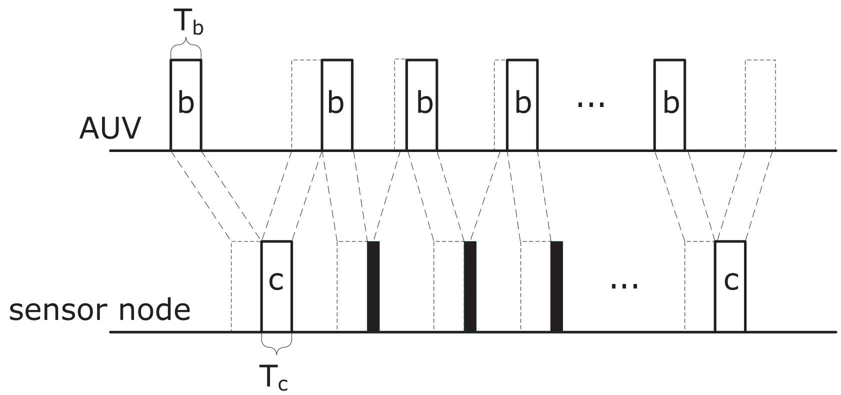

Figure 7.4: An illustration of the coordination scheme with power control

From Figure 7.4, after establishing the connection between the AUV and a sensor node, the sensor node does not immediately transmit the data packets and AUV continuously moves with sending beacon messages, along with a short bit field to indicate its current position. The sensor node will send a short tone signal as a reply [90, 91]. If the AUV does not receive a tone in the time duration of (r/v_s), it will assume that it has missed the preferred communication position with that sensor node. The AUV will then move in the opposite direction and send beacon messages in order to return to the communication range of the sensor node. On the other hand, the sensor node records all the beacon messages to choose the preferred communication position corresponding to the maximum SNR. The second ACKB in Figure 7.4 includes the information of the preferred communication position. The AUV moves to the preferred communication position after receiving the ACKB. The AUV circles around the preferred communication position until finishing the data transmission. The following steps are same as in the coordination scheme presented in Section 7.1.

7.2.2 Transmitting Power Control

7.2.2.1 Underwater Acoustic Channel Model

In this chapter, we utilize the underwater acoustic channel model as discussed in Chapter 3 where the semi-empirical formula (Equation 3.11) is used for transmission loss calculation. The transmitting power level can be calculated by Equation 4.1, 4.2, 4.3, 4.4, and 4.5.

7.2.2.2 Step Size between Two Consecutive Transmitting power Levels

Assuming the step of transmission range, denoted by ϵ in meters, ϵ can be expressed by

$$\epsilon = (d_{max} - d_{min})/(N_{tp} - 1), \tag{7.6}$$

where d_{max} and d_{min} denote the maximum transmission distance and the minimum transmission distance, respectively. N_{tp} represents the number of transmitting power levels. Based on the above formulas, the sensor node is able to select a proper transmitting power based on the corresponding transmission loss and the distance between the sensor node and the AUV. A larger number of transmitting power levels can conserve more energy. However, a limited number of transmitting power levels is better for practical implementation. We evaluate the performance of different transmitting power levels in the next section.

7.3 Performance Evaluation

7.3.1 Simulation Scenario and Parameters

All the sensor nodes are sparsely distributed in deep seawater, which are located on the seafloor. The noise level η_0 is assumed as 50 dB re 1 μ Pa^2 for the quiet deep seawater and DT of the acoustic modem is 30 dB [47, 48, 125]. The maximum communication radius of the sensor nodes is 1,000 m with the transmitting power of 20 W. The reason is similar as we discuss in Chapter 3 and Section 4.1.1. The velocity of the AUV is assumed to be 1 m/s, which is a common speed of the majority of AUVs [8, 25, 26]. The AUV collects data packets, which is conducted once a month or once every several weeks. The sensor nodes collect and report the environmental and seismic data to the AUV. In this chapter, we assume that there are 50 sensor nodes deployed in sparsely-distributed UWSNs. The power consumption specification of the Micro-modem produced by WHOI [30] is applied to calculate the energy consumption of sensor nodes. In this scenario, there are 50 sensor nodes deployed on the seafloor. The transmission range of a sensor node is 1,000 m and the longest path length of the AUV in the transmission range of a sensor node is 2,000 m. Several trials with different Monte Carlo runs have been conducted. We find that the averaged simulation results have small variances after 10,000 Monte Carlo runs. Therefore, we believe that 10,000 Monte Carlo runs is adequate in this scenario (Figure 7.6 shows an example with error bars when PL $\in [1800, 2000]$ with $\beta = 1$). Table 7.1 summarizes the simulation parameters.

Table 7.1: Simulation parameters in Chapter 7

Parameters	Value
maximum transmitting power level $\max p_t$	20 W
receiving power level p_r	3 W
listening power level p_l	0.08 W
sleeping power level p_s	0 W
data rate	5000 b/s
size of a beacon message L_b or an ACK L_c	32 B
size of a data packets	1200 B
center frequency of the acoustic modem f	30 kHz
velocity of the AUV v_A	1 m/s
velocity of sound v_s	1500 m/s

7.3.2 Simulation Results on Optimization Strategy T_n^{s*}

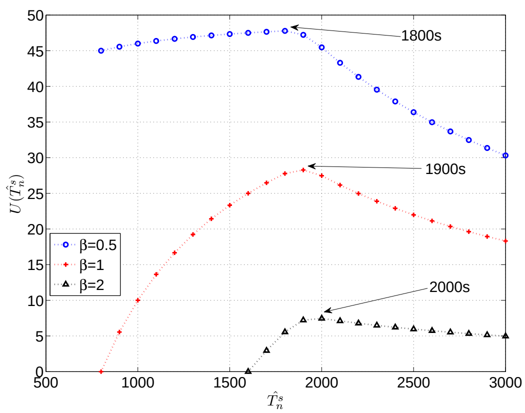

(a) PL ∊ [1800, 2000] m

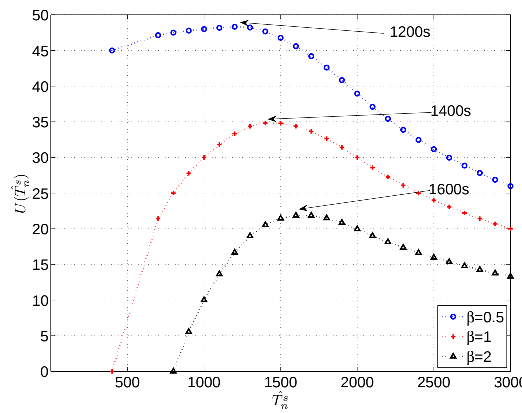

(b) PL ∊ [1200, 2000] m

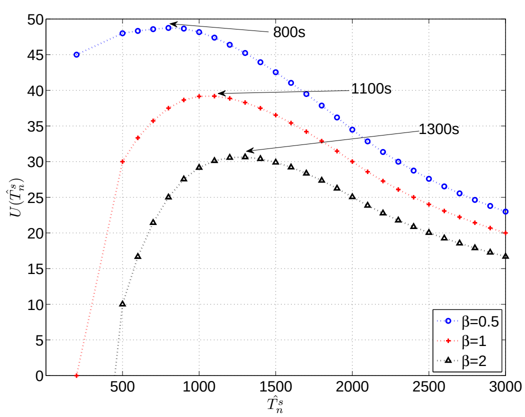

(c) PL ∊ [800, 2000] m

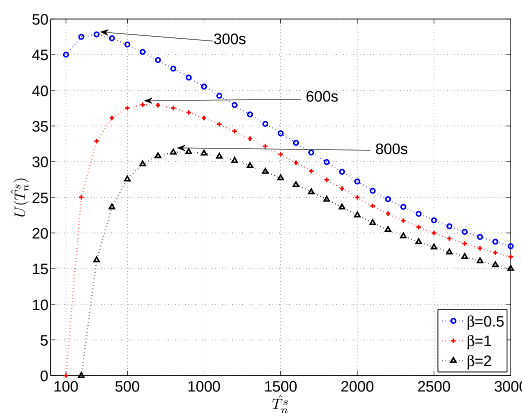

(d) PL ∊ [200, 2000] m

Figure 7.5: Sleeping time optimization in different ranges of PLs

Figure 7.5 shows the value of the utility function under different ranges of PLs and different values of β. The range of PLs, for example, is expressed by PL $\in [1800, 2000]$ m in Figure 7.5(a), which means that the maximum and minimum path length of AUV is 2000

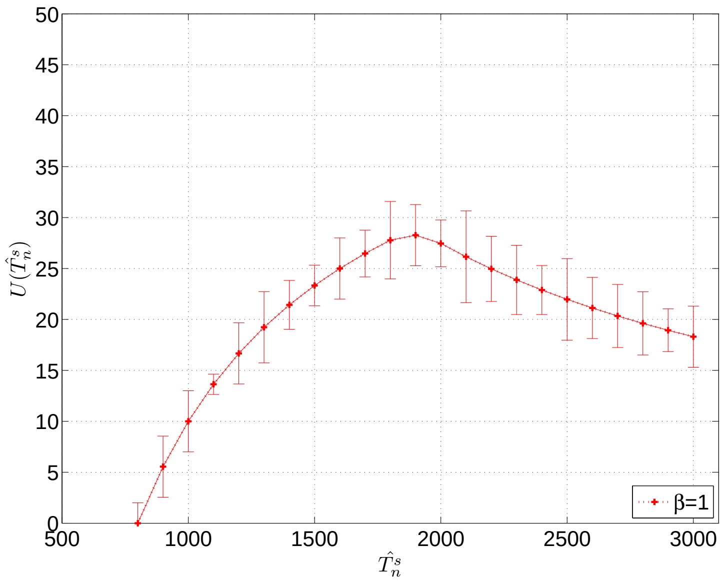

Figure 7.6: Sleeping time optimization, PL ∈ [1800, 2000] m, β=1

m and 1800 m. From Figure 7.5(a) to Figure 7.5(d), we can obtain optimal amounts of sleeping time in one cycle period for each sensor node in different ranges of PLs. We take T_A = 1.4357 s as AUV's cycle period with considering the maximum propagation delay of the beacon message. When the range of PLs increases, the amount of sleeping time of sensor nodes decreases as shown from Figure 7.5(a) to Figure 7.5(d). The sensor nodes can obtain more sleeping time to consume less energy without time synchronization if the AUV has relative accurate location information of sensor nodes and a novel navigation system. On the contrary, low location accuracy results in the short amount of sleeping time of sensor nodes and more energy consumption. For example, from Figure 7.5(a), if the AUV knows the location of sensor nodes within several hundred meters, we determine that sensor nodes can turn off their acoustic transceivers for 1900 s (when β = 1) and turn them on for only

1.5 s before turning them off again.

We also compare the impact of the value of β on the amount of sleeping time. $\beta = 1$ means that the cost of adopting the minimum amount of sleeping time is equal to the benefit of successfully establishing connection between the AUV and a sensor node. $\beta = 0.5$ and $\beta = 2$ means adopting the minimum amount of sleeping time is less and more important than successfully establishing connection between the AUV and a sensor node, respectively. From Figure 7.5(a) to Figure 7.5(d), a given range of PLs, we can obtain optimal amounts of sleeping time under different values of β. A sensor node sleeps shorter when $\beta = 0.5$ than the case of $\beta = 2$ because successfully establishing a connection becomes more important than energy conservation (i.e., the larger amount of sleeping time). For example, from Figure 7.5(a), a sensor node only sleeps 1800 s in one cycle period in the case of $\beta = 0.5$. On the other hand, the amount of sleeping time is 2000 s in the case of $\beta = 2$.

7.3.3 Simulation Results on Energy Consumption of Coordination Scheme

In this section, all the simulation results are averaging the value over 10,000 Monte Carlo runs. The optimization strategy T_n^{s*} derived in the previous part is applied in this part when $\beta = 1$. Under different ranges of PLs, Figure 7.7 presents the average energy consumption per sensor node with different numbers of data packets per sensor nodes. From these results, for a given range of PLs, under different numbers of data packets per sensor nodes, we observe that more energy can be conserved using power control compared with the fixed transmitting

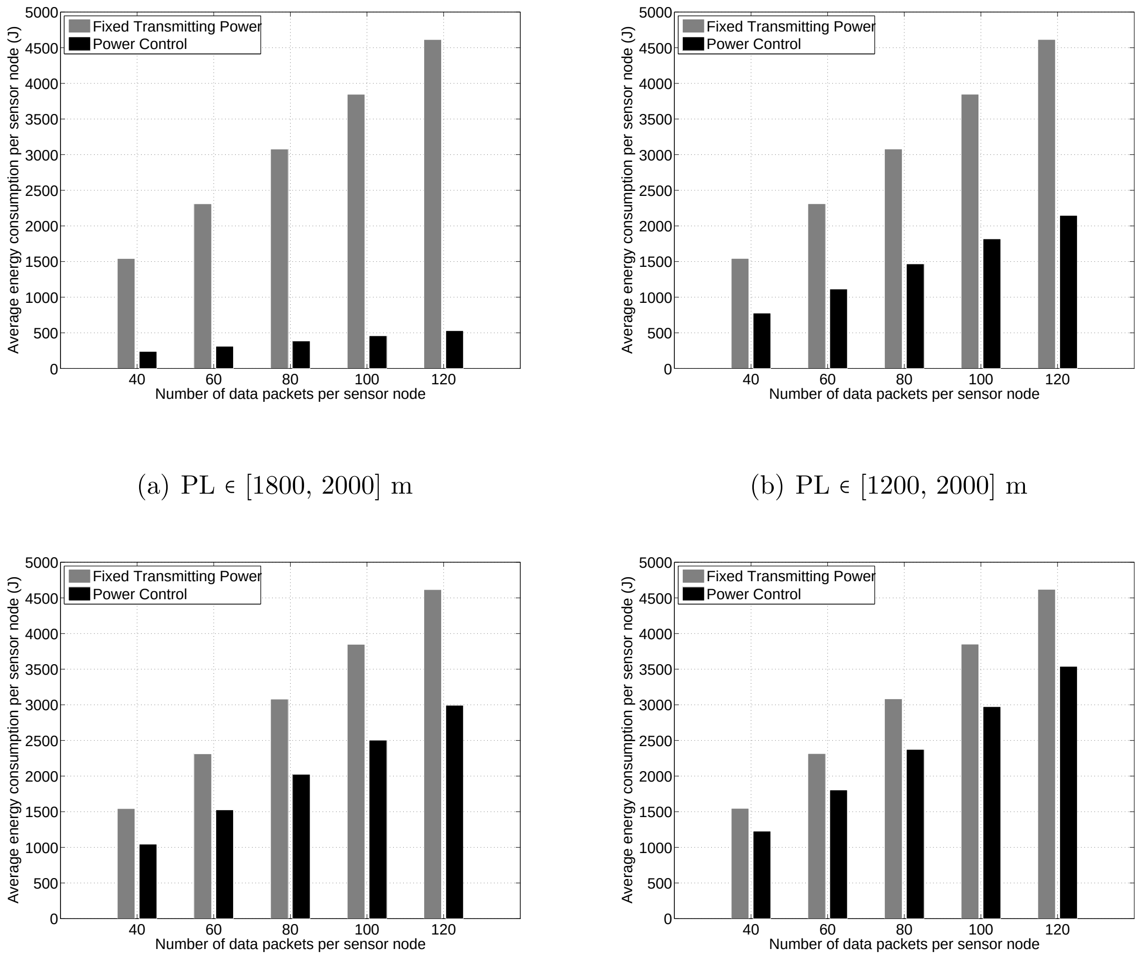

(a) PL ∊ [1800, 2000] m

(b) PL ∊ [1200, 2000] m

(c) PL ∊ [800, 2000] m

(d) PL ∊ [200, 2000] m

Figure 7.7: Average energy consumption per sensor node versus number of data packets per sensor node

power. From Figure 7.7(a) and Figure 7.7(b), a sensor node has more opportunities to choose relatively small transmitting power levels to send data packets to the AUV because the AUV can be close to the sensor nodes with the relatively high accuracy of location information. However, sensor nodes must frequently choose larger transmitting power levels to deliver data packets leading to increased of energy consumption because the AUV is sometimes farther away from the sensor nodes when a low location accuracy navigation system is employed, as shown in Figure 7.7(c) and Figure 7.7(d). Furthermore, in the coordination scheme with power control, the growth ratio of average energy consumption of each sensor node with the number of data packets is lower than that without power control because power control can conserve a large amount of energy. It should be noted that the data transmission accounts for a large part of the energy consumption.

7.3.4 Simulation Results on Power Control with Different Power Levels

Figure 7.8 shows the difference in the average energy consumption of each sensor node with different power levels and different ranges of PLs. Each sensor node has 50 data packets to transmit. With increase in the number of power levels, the sensor nodes are able to conserve more energy. For a given number of power levels, the average energy consumption per sensor node under different ranges of PLs shows a similar tendency. Larger number of power levels can improve the energy consumption. However, fewer power levels can decrease the complexity of implementation.

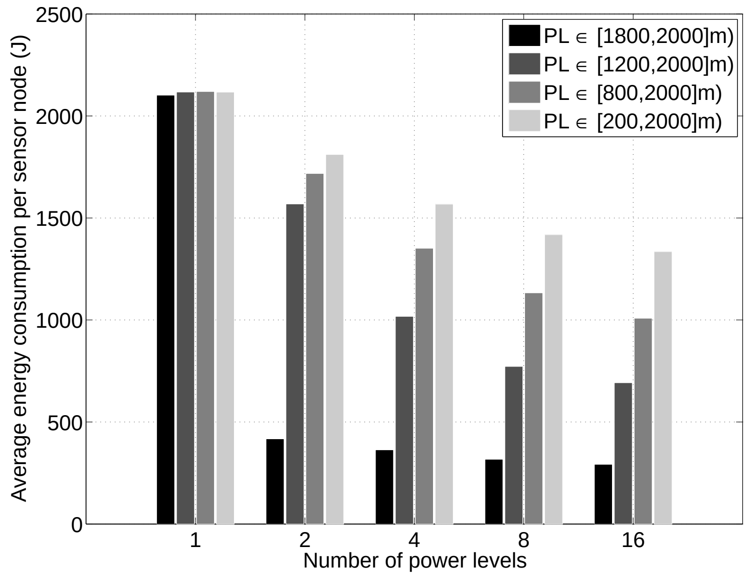

Figure 7.8: Average energy consumption per sensor node versus number of power levels

7.4 Summary

Energy consumption is a significant issue when designing high-level schemes for UWSNs due to harsh marine communication conditions and limitations of the battery energy of sensor nodes. AUVs, as mobile sinks, can collect data from UWSNs. In this chapter, we proposed a coordination scheme for data collection using a single AUV in a sparsely-distributed UWSN. In this coordination scheme, the AUV and sensor nodes required different cycle periods without time synchronization. For sensor nodes, the shortest wake time and the optimal amount of sleeping time were determined by considering the path length of the AUV within the communication range of a sensor node. The simulation results showed that the coordination scheme conserves more energy when a navigation system with high location accuracy is employed. Moreover, sensor nodes consume less energy using the coordination scheme with transmitting power control compared to the scheme with fixed transmitting power level. A typical set of parameters associated with the Micro-modem was applied in our simulation, but power consumption parameters from different acoustic modems can also be used in the proposed scheme, which would lead to similar conclusions.

Chapter 8

Conclusion and Future Work

In long-term marine monitoring applications, energy efficiency is a critical and challenging issue in designing network protocols for UWSNs. This dissertation presents schemes corresponding to different aspects of UWSNs, aiming at energy-efficient data transmission and prolonging network lifetime. Subsequent sections provide a summary of research contributions and conclusions, and suggestions for future work.

8.1 Summary of Thesis

The main research contributions of this thesis are summarized as follows.

Comprehensive Study of Underwater Acoustic Channel Models

In Chapter 3, we reviewed the properties of acoustic signal propagation in seawater in terms of sound speed profile, geometric spreading loss, and absorption loss. As well, we studied and compared different underwater acoustic channel models including the normal mode model and the ray-theoretical model. The ray-theoretical model and the semi-empirical formula are used to investigate transmission loss of acoustic signals. Our results indicate that, in shallow water scenarios, the transmission loss from the ray-theoretical model is very close to the transmission loss predicted by the semi-empirical formula with $\mathcal{K} = 1.5$. For deep sea conditions, the transmission loss is close to that predicted by the semi-empirical formula with $\mathcal{K} = 2$ (corresponding to the spherical spreading loss). In general, the semi-empirical formula provides a conservative estimate of the transmission loss for the link budget in underwater acoustic communication [123]. The analysis of the transmission loss of acoustic signals provides a theoretical basis on underwater channel conditions when developing new schemes and techniques for UWSNs.

Energy-Efficient Asynchronous Wake-up Scheme for UWSNs

For long-term environmental monitoring applications, we proposed an asynchronous wake-up scheme to reduce energy consumption during idle listening, which provides a point-to -point, energy-efficient approach to exchanging data [131]. Based on combinatorial designs, the proposed wake-up coordination scheme achieves energy efficiency without compromising network connectivity. Additionally, the proposed scheme can be extended using Kronecker product, which can outperform existing schemes, such as EACDS and MACDS. We further studied the sink node utilization ratio and the network scalability for large size networks. Simulation results show that the proposed wake-up scheme achieves its goal by effectively reducing the energy consumption for idle listening. The results are consistent for different network sizes when compared with other CDS-based coordination schemes. By incorporating multiple sink nodes, we can effectively handle higher traffic intensity and support larger network sizes.

Balance Network Robustness and Energy Consumption of Sensor Nodes

We addressed the link failure problem caused by the deployment error of sensor nodes in 2D UWSNs with a square grid topology [135]. We formulated the deployment error of UWSNs as a mathematical model, and studied the network robustness problem based on this model. We investigated on how to balance the robustness of UWSNs and the energy consumption of sensor nodes using the parameter α, which is defined as the ratio of the transmission range of a sensor node to the shortest distance between two closest adjacent sensor nodes. We found that the optimal value of α can be obtained to satisfy different requirements of robustness and energy consumption in UWSNs.

Energy-Efficient Relay Node Selection Scheme for UWSNs

For long-term marine monitoring applications, we proposed a relay node selection scheme that can achieve an end-to-end, energy-efficient approach to transmit data in UWSNs. We formulated the relay node selection problem as a linear programming problem, and proposed a relay node selection scheme, which incorporates multiple transmitting power levels and residual energy of sensor nodes. The performance evaluation showed that the best ratio of the weight for the power level to the weight for the residual energy can be obtained for different numbers of transmitting levels and for different network sizes. Moreover, the network lifetime can be significantly prolonged using more transmitting levels. Compared to the conventional minimum hop routing algorithm, the performance of the proposed relay node selection scheme is closer to the theoretical results obtained from the linear programming formulation. It was shown that the network performance can be further improved (*a.k.a.* balanced) by reassigning the initial battery power to each sensor node based on its traffic load.

An Energy-Efficient Data Collection Scheme using AUVs in UWSNs

In sparsely-distributed UWSNs, we proposed a coordination scheme for data collection using a single AUV instead of the surface node. In the proposed coordination scheme [141], the AUV and sensor nodes operate asynchronously using different duty cycles. For sensor nodes, the shortest wake-up time and the optimal amount of sleeping time were determined by considering of the path length of the AUV in the communication range of a sensor node. Moreover, further energy conservation can be achieved by the transmitting power control, and where proper transmitting power level for data transmission can be calculated by the passive sonar equation. In the performance evaluation, we compared the average energy consumption of each sensor node under different ranges of the path length of the AUV. The coordination scheme can conserve more energy when the AUV is equipped with a navigation system with high location accuracy. Moreover, sensor nodes will consume less energy when transmitting power control is utilized, when compared with schemes using fixed transmitting power levels.

Extendability of the Proposed Schemes

In this thesis, all proposed schemes are based on sensor nodes located on the seafloor, which can be extended to UWSNs with other regular or irregular topologies. Furthermore, we used a set of power consumption parameters for two common acoustic modems, i.e., Micro-modem and EvoLogics modem, but the proposed schemes can easily be extended to other acoustic modems, leading to the conclusions with similar trends as presented in corresponding chapters. Additionally, selecting grids with an even number of total sensor nodes would lead to approximately the same conclusions as presented in corresponding chapter, despite the fact that the sink node would be slightly off-center.

8.2 Future Research

In this dissertation, we have studied different approaches to improve energy efficiency in data transmission in UWSNs. Next, we present and discuss some future research directions and ideas.

Extension of the Asynchronous Wake-up Scheme

For long-term marine environmental monitoring applications, we have proposed an asynchronous wake-up scheme for UWSNs with a square grid topology. The proposed asynchronous wake-up scheme can be extended to other topologies. For example, the hexagonal grid topology has been widely used in terrestrial cellular communications because fewer cells (hexagonal cells) are required to cover a given geographic region compared to other topologies. Using the proposed asynchronous wake-up scheme in UWSNs with a hexagonal grid topology, the balancing between the network coverage and the overall budget of the underwater network can be achieved by considering different network applications, the cost of sensor nodes, and the collected data volume.

Traffic load is another consideration when designing network protocols. In this dissertation, the traffic load is low and the data generation rate is constant, which is required by the long-term marine monitoring application. It would be informative to further test the proposed asynchronous wake-up scheme under higher traffic loads and variable data generation rates. In delay sensitive applications, the optimal length of one cycle period of each sensor node can be decided by jointly considering the requirements of packet latency and data generation rates.

Relay Node Selection Scheme

We have proposed a relay node selection scheme for UWSNs with a square grid topology. In the proposed relay node selection scheme, we proposed a routing metric jointly considering the transmitting power levels and the residual energy of sensor nodes to improve energy-efficiency in data transmission and prolong network lifetime. The proposed relay node selection method can be extended to applications with higher traffic loads, however, the packet collision condition must be carefully considered to reduce the possibility of energy wastage caused by data retransmission. Several existing TDMA-based schemes can be utilized.

Coordinated Data Collection Scheme using AUVs

In this dissertation, to reduce energy consumption of sensor nodes, we present a coordination scheme that uses a single AUV to collect data from sparsely-distributed UWSNs. This work can be extended to densely-distributed UWSNs. However, in densely-distributed UWSNs, new schemes can be designed to avoid packet collision and reduce energy consumption for retransmission. For example, TDMA-based MAC protocols can be modified for underwater communication conditions. Furthermore, though rechargeable, energy supple in AUV is still limited. Therefore, effective tour (path) planning of the AUV requires further research. Intuitively, the tour planning problem of the AUV can be formulated as the travelling salesman problem. The balancing between the amount of data collected from sensor nodes and the energy consumption of the AUV can be studied for different application requirements. Another future direction of research is the data collection problem using multiple AUVs. Multiple AUVs can be deployed in sparsely-distributed UWSNs with large coverage area to avoid overusing a single AUV. In this scenario, the coordination among multiple AUVs should be researched, aiming at reducing the overlapping area where any two AUVs collect data from sensor nodes.

Field Experiment and Proposed Schemes Implementation

Unlike terrestrial wireless channel models, there is no consensus on the statistical characterization of the underwater acoustic channel model due to its temporal and spatial variability. Therefore, it is worthwhile to obtain the realistic underwater acoustic channel model through sea trials and experiments in Newfoundland region. It would be a significant step toward in the research to implement the proposed schemes on the commercial acoustic modems and evaluate the performance of the proposed schemes by field experiments.

References

[1] I. F. Akyildiz, D. Pompili, and T. Melodia, “Underwater acoustic sensor networks: research challenges,” *Ad Hoc Networks*, vol. 3, pp. 257–279, May 2005.

[2] M. Chitre, S. Shahabudeen, and M. Stojanovic, “Underwater acoustic communications and networking: Recent advances and future challenges,” *Marine Technology Society Journal*, vol. 42, pp. 103–116, Spring 2008.

[3] M. Erol-Kantarci, H. Mouftah, and S. Oktug, “A survey of architectures and localization techniques for underwater acoustic sensor networks,” *IEEE Communications Surveys & Tutorials*, vol. 13, pp. 487–502, Third 2011.

[4] J. Catipovic, D. Brady, and S. Etchemendy, “Development of underwater acoustic modems and networks,” *Oceanography*, vol. 6, no. 3, pp. 112–119, 1993.

[5] J. Rice, K. Amundsen, and K. Scussel, “Seaweb 2002 experiment quick-look report,” *SPAWAR Systems Center*, Aug. 2002.

[6] J. Rice, B. Creber, C. Fletcher, P. Baxley, K. Rogers, K. McDonald, D. Rees, M. Wolf, S. Merriam, R. Mehio, J. Proakis, K. Scussel, D. Porta, J. Baker, J. Hardiman,

and D. Green, "Evolution of seaweb underwater acoustic networking," in *Proc. of MTS/IEEE Conference and Exhibition for Ocean Engineering, Science and Technology (OCEANS)*, vol. 3, (Providence, RI), pp. 2007–2017, Sept. 2000.

[7] Teledyne Benthos, "Product catalog 2010 (telesonar): Wireless subsea communications." http://www.comm-tec.com/Prods/mfgs/Benthos/Brochures/Telesonar%20Product%20Catalog.pdf, 2010.

[8] G. Hollinger, S. Choudhary, P. Qarabaqi, C. Murphy, U. Mitra, G. Sukhatme, M. Stojanovic, H. Singh, and F. Hover, "Underwater data collection using robotic sensor networks," *IEEE Journal on Selected Areas in Communications*, vol. 30, pp. 899–911, Jun. 2012.

[9] L. Vieira, U. Lee, and M. Gerla, "Phero-trail: a bio-inspired location service for mobile underwater sensor networks," *IEEE Journal on Selected Areas in Communications*, vol. 28, pp. 553–563, May 2010.

[10] A. Caiti, K. Grythe, J. Hovem, S. Jesus, A. Lie, A. Munafo, T. Reinen, A. Silva, and F. Zabel, "Linking acoustic communications and network performance: Integration and experimentation of an underwater acoustic network," *IEEE Journal of Oceanic Engineering*, vol. 38, pp. 758–771, Oct. 2013.

[11] A. Caiti, P. Felisberto, T. Husoy, S. Jesus, I. Karasalo, R. Massimelli, T. Reinen, and A. Silva, "UAN-underwater acoustic network," in *Proc. of MTS/IEEE Conference and*

Exhibition for Ocean Engineering, Science and Technology (OCEANS), (Santander, Spain), pp. 1–7, Jun. 2011.

[12] A. Caiti, V. Calabro, G. Dini, A. Duca, and A. Munafo, "AUVs as mobile nodes in acoustic communication networks: Field experience at the uan10 experiment," in *Proc. of MTS/IEEE Conference and Exhibition for Ocean Engineering, Science and Technology (OCEANS)*, (Santander, Spain), pp. 1–6, Jun. 2011.

[13] F. Ulaby, *Fundamentals of electromagnetics*. Upper Saddle River, NJ: Pearson/Prentice Hall, 2007.

[14] R. Boules, "Absorption losses in seawater for a rectangular electromagnetic pulse," in *IEEE International Symposium on Electromagnetic Compatibility*, (Cherry Hill, NJ, USA), pp. 220–221, Aug. 1991.

[15] L. Liu, S. Zhou, and J. Cui, "Prospects and problems of wireless communication for underwater sensor networks," *Wireless Communications and Mobile Computing*, vol. 8, pp. 977–994, Jul. 2008.

[16] S. Tang, Y. Dong, and X. Zhang, "Impulse response modeling for underwater wireless optical communication links," *IEEE Transactions on Communications*, vol. 62, pp. 226–234, Jan. 2014.

[17] M. Doniec, M. Angermann, and D. Rus, "An end-to-end signal strength model for underwater optical communications," *IEEE Journal of Oceanic Engineering*, vol. 38, pp. 743–757, Oct. 2013.

[18] C. Gabriel, M. Khalighi, S. Bourennane, P. Leon, and V. Rigaud, "Monte-carlo-based channel characterization for underwater optical communication systems," *IEEE/OSA Journal of Optical Communications and Networking*, vol. 5, pp. 1–12, Jan. 2013.

[19] L. Berkhovskikh and Y. Lysanov, *Fundamentals of Ocean Acoustics*. New York, NY: Springer, 2 ed., 1991.

[20] F. Jensen, W. Kuperman, M. Porter, and H. Schmidt, *Computational Ocean Acoustics*. New York, NY: Springer, 2000.

[21] R. Urick, *Principles of Underwater Sound*. New York, NY: McGraw Hill, 3 ed., 1983.

[22] A. Al-Shamma'a, A. Shaw, and S. Saman, "Propagation of electromagnetic waves at mhz frequencies through seawater," *IEEE Transactions on Antennas and Propagation*, vol. 52, pp. 2843–2849, Nov. 2004.

[23] M. Stojanovic and J. Preisig, "Underwater acoustic communication channels: Propagation models and statistical characterization," *IEEE Communications Magazine*, vol. 47, pp. 84–89, Jan. 2009.

[24] P. Qarabaqi and M. Stojanovic, "Statistical characterization and computationally efficient modeling of a class of underwater acoustic communication channels," *IEEE Journal of Oceanic Engineering*, vol. 38, pp. 701–717, Oct. 2013.

[25] I. Vasilescu, K. Kotay, D. Rus, M. Dunbabin, and P. Corke, "Data collection, storage, and retrieval with an underwater sensor network," in *Proc. of International Conference*

on Embedded Networked Sensor Systems, (San Diego, California, USA), pp. 154–165, Nov. 2005.

[26] M. Dunbabin, P. Corke, I. Vasilescu, and D. Rus, "Data muling over underwater wireless sensor networks using an autonomous underwater vehicle," in *Proc. of IEEE International Conference on Robotics and Automation*, (Orlando, FL, USA), pp. 2091–2098, May 2006.

[27] M. Stojanovic, "Recent advances in high-speed underwater acoustic communications," *IEEE Journal of Oceanic Engineering*, vol. 21, pp. 125–136, Apr. 1996.

[28] Z. Zvonar, D. Brady, and J. Catipovic, "Adaptive detection for shallow-water acoustic telemetry with cochannel interference," *IEEE Journal of Oceanic Engineering*, vol. 21, pp. 528–536, Oct. 1996.

[29] R. Vaccaro, "The past, present, and the future of underwater acoustic signal processing," *IEEE Signal Processing Magazine*, vol. 15, pp. 21–51, Jul. 1998.

[30] S. Singh, M. Grund, B. Bingham, R. Eustice, H. Singh, and L. Freitag, "Underwater acoustic navigation with the WHOI micro-modem," in *Proc. of MTS/IEEE Conference and Exhibition for Ocean Engineering, Science and Technology (OCEANS)*, (Boston, MA, USA), pp. 1–4, Sept. 2006.

[31] Teledyne Benthos, "Acoustic modem." http://www.benthos.com/index.php/product_dashboard/acoustic_modems, 2014.

[32] M. Stojanovic, J. Catipovic, and J. Proakis, "Adaptive multichannel combining and equalization for underwater acoustic communications," *Journal of the Acoustical Society of America*, vol. 94, pp. 1621–1631, Sept. 1993.

[33] S. Cho, H. C. Song, and W. Hodgkiss, "Successive interference cancellation for underwater acoustic communications," *IEEE Journal of Oceanic Engineering*, vol. 36, pp. 490–501, Oct. 2011.

[34] M. Stojanovic, J. Catipovic, and J. Proakis, "Phase-coherent digital communications for underwater acoustic channels," *IEEE Journal of Oceanic Engineering*, vol. 19, pp. 100–111, Jan. 1994.

[35] M. Stojanovic and L. Freitag, "Multichannel detection for wideband underwater acoustic cdma communications," *IEEE Journal of Oceanic Engineering*, vol. 31, pp. 685–695, Jul. 2006.

[36] J. Huang, S. Zhou, J. Huang, C. Berger, and P. Willett, "Progressive inter-carrier interference equalization for ofdm transmission over time-varying underwater acoustic channels," *IEEE Journal of Selected Topics in Signal Processing*, vol. 5, pp. 1524–1536, Dec. 2011.

[37] C. Polprasert, J. Ritcey, and M. Stojanovic, "Capacity of OFDM systems over fading underwater acoustic channels," *IEEE Journal of Oceanic Engineering*, vol. 36, pp. 514–524, Oct. 2011.

[38] K. Pelekanakis and A. Baggeroer, "Exploiting space-time-frequency diversity with MIMO-OFDM for underwater acoustic communications," *IEEE Journal of Oceanic Engineering*, vol. 36, pp. 502–513, Oct. 2011.

[39] N. Chirdchoo, W.-S. Soh, and K. C. Chua, "ALOHA-based mac protocols with collision avoidance for underwater acoustic networks," in *Proc. of IEEE International Conference on Computer Communications (INFOCOM)*, (Anchorage, AK, USA), pp. 2271–2275, May 2007.

[40] J. Ahn, A. Syed, B. Krishnamachari, and J. Heidemann, "Design and analysis of a propagation delay tolerant aloha protocol for underwater networks," *Ad Hoc Networks*, vol. 9, pp. 752–766, Jul. 2011.

[41] L. Jin and D. D. Huang, "A slotted CSMA based reinforcement learning approach for extending the lifetime of underwater acoustic wireless sensor networks," *Computer Communications*, vol. 36, pp. 1094–1099, May 2013.

[42] B. Peleato and M. Stojanovic, "Distance aware collision avoidance protocol for ad-hoc underwater acoustic sensor networks," *IEEE Communications Letters*, vol. 11, pp. 1025–1027, Dec. 2007.

[43] S. Basagni, C. Petrioli, R. Petroccia, and M. Stojanovic, "Optimized packet size selection in underwater wireless sensor network communications," *IEEE Journal of Oceanic Engineering*, vol. 37, pp. 321–337, Jul. 2012.

[44] A. Syed, W. Ye, and J. Heidemann, "Comparison and evaluation of the T-Lohi mac for underwater acoustic sensor networks," *IEEE Journal on Selected Areas in Communications*, vol. 26, pp. 1731–1743, Dec. 2008.

[45] D. Pompili, T. Melodia, and I. Akyildiz, "Three-dimensional and two-dimensional deployment analysis for underwater acoustic sensor networks," *Ad Hoc Networks*, vol. 7, pp. 778–790, Jun. 2009.

[46] J. Partan, J. Kurose, and B. N. Levine, "A survey of practical issues in underwater networks," *ACM SIGMOBILE Mobile Computing and Communications Review*, vol. 11, pp. 23–33, Oct. 2007.

[47] M. Stojanovic, "Design and capacity analysis of cellular-type underwater acoustic networks," *IEEE Journal of Oceanic Engineering*, vol. 33, pp. 171–181, Apr. 2008.

[48] J. Jornet, M. Stojanovic, and M. Zorzi, "On joint frequency and power allocation in a cross-layer protocol for underwater acoustic networks," *IEEE Journal of Oceanic Engineering*, vol. 35, pp. 936–947, Oct. 2010.

[49] M. Isik and O. Akan, "A three dimensional localization algorithm for underwater acoustic sensor networks," *IEEE Transactions on Wireless Communications*, vol. 8, pp. 4457–4463, Sept. 2009.

[50] D. Pompili, T. Melodia, and I. Akyildiz, "Deployment analysis in underwater acoustic wireless sensor networks," in *Proc. of ACM International Workshop on Underwater Networks (WUWNet)*, (Los Angeles, CA, USA), pp. 48–55, Sept. 2006.

[51] D. Pompili, T. Melodia, and I. Akyildiz, “Distributed routing algorithms for underwater acoustic sensor networks,” *IEEE Transactions on Wireless Communications*, vol. 9, pp. 2934–2944, Sept. 2010.

[52] M. Zorzi, P. Casari, N. Baldo, and A. Harris, “Energy-efficient routing schemes for underwater acoustic networks,” *IEEE Journal on Selected Areas in Communications*, vol. 26, pp. 1754–1766, Dec. 2008.

[53] U. Lee, P. Wang, Y. Noh, F. Vieira, M. Gerla, and J. Cui, “Pressure routing for underwater sensor networks,” in *Proc. of IEEE International Conference on Computer Communications (INFOCOM)*, (San Diego, CA, USA), pp. 1–9, Mar. 2010.

[54] Y. Noh, U. Lee, P. Wang, B. C. Choi, and M. Gerla, “VAPR: Void-aware pressure routing for underwater sensor networks,” *IEEE Transactions on Mobile Computing*, vol. 12, pp. 895–908, May 2013.

[55] Z. Zhou and J. Cui, “Energy efficient multi-path communication for time-critical applications in underwater sensor networks,” in *Proc. of ACM international symposium on Mobile ad hoc networking and computing (MobiHoc)*, (Hong Kong, China), pp. 221–230, May 2008.

[56] C. Jones, K. M. Sivalingam, P. Agrawal, and J. Chen, “A survey of energy efficient network protocols for wireless networks,” *Wireless Networks*, vol. 7, pp. 343–358, Sept. 2001.

[57] A. Harris, M. Stojanovic, and M. Zorzi, “Idle-time energy savings through wake-up modes in underwater acoustic networks,” *Ad Hoc Networks*, vol. 7, pp. 770–777, Jun. 2009.

[58] W. Ye, J. Heidemann, and D. Estrin, “Medium access control with coordinated adaptive sleeping for wireless sensor networks,” *IEEE/ACM Transcation on Networking*, vol. 12, pp. 493–506, Jun. 2004.

[59] T. van Dam and K. Langendoen, “An adaptive energy-efficient MAC protocol for wireless sensor networks,” in *Proc of ACM Embedded networked Sensor Systems conference (SenSys)*, (Los Angeles, CA), pp. 171–180, Nov. 2003.

[60] R. Diamant and L. Lampe, “Underwater localization with time-synchronization and propagation speed uncertainties,” *IEEE Transactions on Mobile Computing*, vol. 12, pp. 1257–1269, Jul. 2013.

[61] B. Liu, H. Chen, Z. Zhong, and H. Poor, “Asymmetrical round trip based synchronization-free localization in large-scale underwater sensor networks,” *IEEE Transactions on Wireless Communications*, vol. 9, pp. 3532–3542, Nov. 2010.

[62] B. Choi and X. Shen, “Adaptive asynchronous sleep scheduling protocols for delay tolerant networks,” *IEEE Transactions on Mobile Computing*, vol. 10, pp. 1283–1296, Sept. 2011.

[63] C. Chao, J. Sheu, and I. Chou, "An adaptive quorum-based energy conserving protocol for IEEE 802.11 ad hoc networks," *IEEE Transactions on Mobile Computing*, vol. 5, pp. 560–570, Jul. 2006.

[64] R. Zheng, J. C. Hou, and L. Sha, "Asynchronous wakeup for ad hoc networks," in *Proc. of ACM international symposium on mobile ad hoc networking & computing (MobiHoc)*, pp. 35–45, Jun. 2003.

[65] F. Hu, Y. Malkawi, S. Kumar, and Y. Xiao, "Vertical and horizontal synchronization services with outlier detection in underwater acoustic networks," *Wireless Communications and Mobile Computing*, vol. 8, pp. 1165–1181, Nov. 2008.

[66] WHOI, "Whoi: Who we are." http://www.whoi.edu/main/about, 2013.

[67] Interntional Transducer Corporation, "Model ITC-1001 spherical omnidirectional tranducer." http://pdf.directindustry.com/pdf/international-transducer/itc-1001/25344-402773.html, 2010.

[68] Evologics, "S2CR 18/34 acoustic modem." http://www.evologics.de/en/products/acoustics/s2cm_series.html, 2005.

[69] D. Pompili and I. Akyildiz, "Overview of networking protocols for underwater wireless communications," *IEEE Communications Magazine*, vol. 47, pp. 97–102, Jan. 2009.

[70] J. Chang and L. Tassiulas, "Maximum lifetime routing in wireless sensor networks," *IEEE/ACM Transcation on Networking*, vol. 12, pp. 609–619, Aug. 2004.

[71] R. Madan and S. Lall, "Distributed algorithms for maximum lifetime routing in wireless sensor networks," *IEEE Transcation on Wireless Communications*, vol. 5, pp. 2185–2193, Aug. 2006.

[72] M. Chitre, "A high-frequency warm shallow water acoustic communications channel model and measurements," *The Journal of the Acoustical Society of America*, vol. 122, pp. 2580–2586, Nov. 2007.

[73] M. Chitre, J. Potter, and O. Heng, "Underwater acoustic channel characterisation for medium-range shallow water communications," in *Proc. of MTS/IEEE Conference and Exhibition for Ocean Engineering, Science and Technology (OCEANS)*, vol. 1, (Kobe, Japan), pp. 40–45, Nov. 2004.

[74] T. Yang, "Measurements of temporal coherence of sound transmissions through shallow water," *The Journal of the Acoustical Society of America*, vol. 120, pp. 2595–2614, Nov. 2006.

[75] W. Yang and T. Yang, "High-frequency channel characterization for m-ary frequency-shift-keying underwater acoustic communications," *The Journal of the Acoustical Society of America*, vol. 120, pp. 2615–2626, Jan. 2006.

[76] I. Udovydchenkov, R. Stephen, T. F. Duda, S. Bolmer, P. Worcester, M. Dzieciuch, J. Mercer, R. Andrew, and B. Howe, "Bottom interacting sound at 50 km range in a deep ocean environment," *The Journal of the Acoustical Society of America*, vol. 132, pp. 2224–2231, Oct. 2012.

[77] T. Shimura, H. Ochi, and H. Song, "Experimental demonstration of multiuser communication in deep water using time reversal," *The Journal of the Acoustical Society of America*, vol. 134, pp. 3223–3229, Oct. 2013.

[78] H. Song, H. Song, M. Brown, and R. Andrew, "Diversity-based acoustic communication with a glider in deep water," *The Journal of the Acoustical Society of America*, vol. 135, pp. 1023–1026, Mar. 2014.

[79] G. Palou and M. Stojanovic, "Underwater acoustic MIMO-OFDM: An experimental analysis," in *Proc. of MTS/IEEE Conference and Exhibition for Ocean Engineering, Science and Technology (OCEANS)*, (Biloxi, MS), pp. 1–8, Oct. 2009.

[80] P. Carrascosa and M. Stojanovic, "Adaptive channel estimation and data detection for underwater acoustic MIMO-OFDM systems," *IEEE Journal of Oceanic Engineering*, vol. 35, pp. 635–646, Jul. 2010.

[81] T. Kang, H. Song, W. Hodgkiss, and J. S. Kim, "Long-range multi-carrier acoustic communications in shallow water based on iterative sparse channel estimation," *The Journal of the Acoustical Society of America*, vol. 128, pp. 372–377, Dec. 2010.

[82] W. Hodgkiss, "Program introduction and requirements document for the Kauai Acomms MURI 2008 KAM08 experiment," *Project report*, pp. 1–24, 2008.

[83] H. Song and W. Hodgkiss, "Efficient use of bandwidth for underwater acoustic communication," *The Journal of the Acoustical Society of America*, vol. 134, pp. 905–908, Aug. 2013.

[84] M. Stojanovic, J. Proakis, and J. Catipovic, "Performance of high rate adaptive equalization on a shallow water acoustic channel," *Journal of the Acoustical Society of America*, vol. 100, pp. 2213–2219, Oct. 1996.

[85] R. Ahmed, "An experimental study of OFDM in a software defined acoustic testbed," *Project report*, pp. 1–79, 2010.

[86] Interntional Transducer Corporation, "Model ITC-1001 deep water omnidirectional transducer." http://www.channeltechgroup.com/publication/view/model-itc-1007-deep-water-omnidirectional-transducer/, 2010.

[87] Kongsberg, "cNODE mini transponder instruction manual," *Techique report*, pp. 1–79, 2011.

[88] K. Kebkal, R. Bannasch, and A. Kebkal, "Estimation of phase error limits for psk-modulated sweep-spread carrier signal," in *Proc. of MTS/IEEE Conference and Exhibition for Ocean Engineering, Science and Technology (OCEANS)*, vol. 2, (Kobe, Japan), pp. 748–756, Nov 2004.

[89] DSPComm, "AquaComm: Underwater wireless modem." http://www.dspcomm.com/products_aquacomm.html, 2009.

[90] USC, "SNUSE: Sensor networks for undersea seismic experimentation." http://www.isi.edu/ilense/snuse/index.html, 2008.

[91] J. Wills, W. Ye, and J. Heidemann, "Low-power acoustic modem for dense underwater sensor networks," in *Proc. of ACM International Workshop on Underwater Networks (WUWNet)*, (Los Angeles, CA, USA), pp. 79–85, Sept. 2006.

[92] Sonardyne Inc., "BlueComm underwater optical modem." http://www.sonardyne.com/images/stories/system_sheets/product_leaflets/bluecomm.pdf, 2014.

[93] E. Gallimore, J. Partan, I. Vaughn, S. Singh, J. Shusta, and L. Freitag, "The whoi micromodem-2: A scalable system for acoustic communications and networking," in *Proc. of MTS/IEEE Conference and Exhibition for Ocean Engineering, Science and Technology (OCEANS)*, (Seattle, WA), pp. 1–7, Sept. 2010.

[94] J. Landt, "The history of RFID," *IEEE Potentials*, vol. 24, pp. 8–11, Oct. 2005.

[95] R. Weinstein, "RFID: a technical overview and its application to the enterprise," *IT Professional*, vol. 7, pp. 27–33, May 2005.

[96] R. Jurdak, A. Ruzzelli, and G. O'Hare, "Radio sleep mode optimization in wireless sensor networks," *IEEE Transactions on Mobile Computing*, vol. 9, pp. 955–968, Jul. 2010.

[97] J. Polastre, J. Hill, and D. Culler, "Versatile low power media access for wireless sensor networks," in *Proc. of International Conference on Embedded Networked Sensor Systems*, (Baltimore, MD, USA), pp. 95–107, Nov. 2004.

[98] IEEE, "IEEE 802.15.4 MAC/PHY standard for low-rate wireless personal area networks." http://www.ieee802.org/15/pub/TG4.html, 2010.

[99] C. Lee, D. Kim, and J. Kim, "An energy efficient active RFID protocol to avoid overhearing problem," *IEEE Sensors Journal*, vol. 14, pp. 15–24, Jan. 2014.

[100] Z. Zhou, Z. Peng, J. Cui, and Z. Jiang, "Handling triple hidden terminal problems for multichannel MAC in long-delay underwater sensor networks," *IEEE Transactions on Mobile Computing*, vol. 11, pp. 139–154, Jan. 2012.

[101] UC-Berkeley, "UC Berkeley Mote." http://www.webs.cs.berkeley.edu/tos, 2005.

[102] M. Park and V. Rodoplu, "UWAN-MAC: An energy-efficient MAC protocol for underwater acoustic wireless sensor networks," *IEEE Journal of Oceanic Engineering*, vol. 32, pp. 710–720, Jul. 2007.

[103] D.Stinson, *Combinatorial designs: constructions and analysis.* New York, NY: Springer, 2004.

[104] I. Anderson, *Combinatorial designs and tournaments.* Oxford, England: Oxford University Press, 1998.

[105] D. Bernstein, *Matrix mathematics: theory, facts, and formulas.* Princeton, New Jersey: Princeton University Press, 2008.

[106] V. Park and M. Corson, "A highly adaptive distributed routing algorithm for mobile wireless networks," in *Proc. of IEEE International Conference on Computer Communications (INFOCOM)*, vol. 3, (Kobe, Japan), pp. 1405–1413, Apr. 1997.

[107] C. Toh, "Maximum battery life routing to support ubiquitous mobile computing in wireless ad hoc networks," *IEEE Communications Magazine*, vol. 39, pp. 138–147, Jun. 2001.

[108] M. Gatzianas and L. Georgiadis, "A distributed algorithm for maximum lifetime routing in sensor networks with mobile sink," *IEEE Transcation on Wireless Communications*, vol. 7, pp. 984–994, Mar. 2008.

[109] J. Jornet, M. Stojanovic, and M. Zorzi, "Focused beam routing protocol for underwater acoustic networks," in *Proc. of ACM international workshop on Underwater Networks (WUWNet)*, (San Francisco, California, USA), pp. 75–82, Sept. 2008.

[110] S. Basagni, C. Petrioli, R. Petroccia, and M. Stojanovic, "Optimized packet size selection in underwater wireless sensor network communications," *IEEE Journal of Oceanic Engineering*, vol. 37, pp. 321–337, Jul. 2012.

[111] A. Mohapatra, N. Gautam, and R. Gibson, "Combined routing and node replacement in energy-efficient underwater sensor networks for seismic monitoring," *IEEE Journal of Oceanic Engineering*, vol. 38, pp. 80–90, Jan. 2013.

[112] P. Xie, Z. Zhou, N. Nicolaou, A. See, H. Cui, and Z. Shi, "Efficient vector-based forwarding for underwater sensor networks," *EURASIP Journal on Wireless Communications and Networking*, vol. 2010, Jun. 2010.

[113] LinkQuest Inc., "LinkQest." http://www.link-quest.com/, 2009.

[114] T. Hu and Y. Fei, "QELAR: A machine-learning-based adaptive routing protocol for energy-efficient and lifetime-extended underwater sensor networks," *IEEE Transactions on Mobile Computing*, vol. 9, pp. 796–809, Jun. 2010.

[115] C. Huang, P. Ramanathan, and K. Saluja, "Routing TCP flows in underwater mesh networks," *IEEE Journal on Selected Areas in Communications*, vol. 29, pp. 2022–2032, Dec. 2011.

[116] J. Luo and J. Hubaux, "Joint mobility and routing for lifetime elongation in wireless sensor networks," in *Proc. of IEEE International Conference on Computer Communications (INFOCOM)*, vol. 3, pp. 1735–1746, Mar. 2005.

[117] S. Gao, H. Zhang, and S. Das, "Efficient data collection in wireless sensor networks with path-constrained mobile sinks," *IEEE Transactions on Mobile Computing*, vol. 10, pp. 592–608, Apr. 2011.

[118] G. Xing, T. Wang, W. Jia, and M. Li, "Rendezvous design algorithms for wireless sensor networks with a mobile base station," in *Proc. of ACM International Symposium on Mobile Ad Hoc Networking and Computing (MobiHoc)*, (Hong Kong, China), pp. 231–240, May 2008.

[119] L. Song and D. Hatzinakos, "Architecture of wireless sensor networks with mobile sinks: Sparsely deployed sensors," *IEEE Transactions on Vehicular Technology*, vol. 56, pp. 1826–1836, Jul. 2007.

[120] C. Petres, Y. Pailhas, P. Patron, Y. Petillot, J. Evans, and D. Lane, "Path planning for autonomous underwater vehicles," *IEEE Transactions on Robotics*, vol. 23, pp. 331–341, Apr. 2007.

[121] I. Vasilescu, K. Kotay, D. Rus, M. Dunbabin, and P. Corke, "Data collection, storage, and retrieval with an underwater sensor network," in *Proc. of International Conference on Embedded Networked Sensor Systems*, (San Diego, California, USA), pp. 154–165, Nov. 2005.

[122] I. Kulkarni and D. Pompili, "Task allocation for networked autonomous underwater vehicles in critical missions," *IEEE Journal on Selected Areas in Communications*, vol. 28, pp. 716–727, Jun. 2010.

[123] R. Su, R. Venkatesan, and C. Li, "Acoustic propagation properties of underwater communication channels and their influence on the medium access control protocols," in *Proc. of IEEE International Conference on Communications (ICC)*, (Ottawa, ON), pp. 5015–5019, Jun. 2012.

[124] "Rays." `http://oalib.hlsresearch.com/Rays/`, 2015.

[125] P. C. Etter, *Underwater Acoustic Modeling and Simulation.* Boca Raton, FL: CRC Press, 3 ed., 2003.

[126] J. Cybulski, F. Ingenito, and A. Newman, "Normal-mode solutions for arbitrary sound speed profiles," *The Journal of the Acoustical Society of America*, vol. 48, pp. 91–91, Apr. 1970.

[127] E. Eby, "Geometric theory of ray tracing," *The Journal of the Acoustical Society of America*, vol. 47, pp. 273–275, Jun. 1969.

[128] E. Westwood and P. Vidmar, "Eigenray finding and time series simulation in a layered-bottom ocean," *The Journal of the Acoustical Society of America*, vol. 81, pp. 912–924, Apr. 1987.

[129] M. Porter, "Acoustics toolbox." http://oalib.hlsresearch.com/Modes/AcousticsToolbox/, 2010.

[130] United State Department of Commerce, "National oceanic and atmospheric administration." http://www.noaa.gov/, 2013.

[131] R. Su, R. Venkatesan, and C. Li, "An energy-efficient asynchronous wake-up scheme for underwater acoustic sensor networks," *Wireless Communications and Mobile Computing*, to appear, 2016.

[132] E. Sozer, M. Stojanovic, and J. Proakis, "Underwater acoustic networks," *IEEE Journal of Oceanic Engineering*, vol. 25, pp. 72–83, Jan. 2000.

[133] J. Proakis and M. Salehi, *Digital Communications*. New York: McGraw-Hill, 5 ed., 2007.

[134] S. Alam and Z. Haas, "Coverage and connectivity in three-dimensional underwater sensor networks," *Wireless Communications and Mobile Computing*, vol. 8, pp. 995–1009, Jul. 2008.

[135] R. Su, R. Venkatesan, and C. Li, "Balancing between robustness and energy consumption for underwater acoustic sensor networks," in *Proc. of IEEE Wireless Communications and Networking Conference (WCNC)*, (New Orleans, LA), Mar. 2015.

[136] M. Ilyas and I. Mahgoub, *Handbook of Sensor Networks: Compact Wireless and Wired Sensing Systems.* Boca Raton, FL: CRC Press, 1 ed., 2004.

[137] H. Karl and A. Willig, *Protocols and Architectures for Wireless Sensor Networks.* New York: John Wiley & Sons, 1 ed., 2007.

[138] R. Su, R. Venkatesan, and C. Li, "An energy-efficient relay node selection scheme for uwsns," *submitted to Wireless Communications and Mobile Computing*, 2015.

[139] K. G. Kebkal and R. Bannasch, "Sweep-spread carrier for underwater communication over acoustic channels with strong multipath propagation," *The Journal of the Acoustical Society of America*, vol. 112, pp. 2043–2052, Nov. 2002.

[140] S. Zhou and Z. Wang, *OFDM for Underwater Acoustic Communications.* New York: John Wiley & Sons, 2014.

[141] R. Su, R. Venkatesan, and C. Li, "A new node coordination scheme for data gathering in underwater acoustic sensor networks using autonomous underwater vehicle," in *Proc.*

of IEEE Wireless Communications and Networking Conference (WCNC), (Shanghai, China), pp. 4370–4374, Apr. 2013.